CHARMONIUM ABSORPTION AND CHARMED HADRON PRODUCTION IN

HADRONIC REACTIONS

A Dissertation

by

WEI LIU

Submitted to the Office of Graduate Studies of
Texas A&M University
in partial fulfillment of the requirements for the degree of

DOCTOR OF PHILOSOPHY

December 2004

Major Subject: Physics

CHARMONIUM ABSORPTION AND CHARMED HADRON PRODUCTION IN

HADRONIC REACTIONS

A Dissertation

by

WEI LIU

Submitted to Texas A&M University
in partial fulfillment of the requirements
for the degree of

DOCTOR OF PHILOSOPHY

Approved as to style and content by:

Che-Ming Ko
(Chair of Committee)

Siu Ah Chin
(Member)

Christopher N. Pope
(Member)

Joseph B. Natowitz
(Member)

Edward S. Fry
(Head of Department)

December 2004

Major Subject: Physics

ABSTRACT

Charmonium Absorption and Charmed Hadron Production in Hadronic Reactions.

(December 2004)

Wei Liu, B.E., Tongji University;

M.S., Peking University

Chair of Advisory Committee: Dr. Che-Ming Ko

A gauged SU(4) flavor symmetric hadronic Lagrangian with empirical hadron masses is constructed to study charmonium absorption and charmed hadron production in hadronic reactions. For the coupling constants, empirical values are used if available. Otherwise, they are determined from known coupling constants using the SU(4) relations. To take into account the finite sizes of hadrons, form factors are introduced at strong interaction vertices with empirical cutoff parameters. For $J/\psi$ absorption by nucleons, we have included both two- and three-body final states and find that with a cutoff parameter of 1 GeV at interaction vertices involving charm hadrons, the cross section is at most 5 mb and is consistent with that extracted from $J/\psi$ production from both photo- and proton-nucleus reactions. We have also evaluated the cross sections for charmed hadron production from pion and rho meson interactions with nucleons. With the same cutoff parameter of 1 GeV at interaction vertices, we find that these cross sections have values of a few tenths of mb and are dominated by the $s$-channel nucleon pole diagram. For charmed hadron production from proton-proton reactions, their cross sections including both two- and three-body final states are about 1 $\mu$b at center-of-mass energy of 11.5 GeV, which is comparable to the measured inclusive cross section in these reactions. Including photon as a U(1) gauge particle, we have extended the model to study charmed hadron production in

photon-proton reactions with both two- and three-body final states included. For form factors, an overall one is introduced in each process in order to maintain the gauge invariance of the total amplitude. Fitting the cutoff parameter in the form factor to the measured total cross section for charmed hadron production in photon-proton reactions at a center-of-mass energy of 6 GeV, the ratio of the cross sections for two-body and three-body final states is consistent with available experimental data. This result is further compared with predictions from the leading-order perturbative QCD calculation. Knowledge of the cross sections for charmonium absorption by hadrons and for charmed hadron production in hadronic reactions is essential for understanding charm production in heavy ion collisions at the Relativistic Heavy Ion Collider (RHIC), where a quark-gluon plasma is expected to be formed during the initial hot dense stage.

To My daughter, My wife, and My parents

ACKNOWLEDGMENTS

I feel very fortunate to have had the opportunity to study and carry out research at the Cyclotron Institute, Texas A&M University. I would like to thank all the people at the institute for their continual help, patience, support, and friendship.

I would like to especially thank Dr. Che-Ming Ko for suggesting the problem addressed in this dissertation. His advice, guidance and encouragement were invaluable for the completion of this work.

I would like to thank Dr. Su Houng Lee, Dr. Zi-wei Lin, Tiegang Di, Changhui Li, Dr. Liewen Chen, and Dr. Vincenzo Grevo for their kindness in helping me with the questions I encountered during my study.

My thanks also go to Dr. Xiaodong Tang, Lijun Qin, Xinfeng Chen, Changbo Fu, Yongjun Zhai, and Yong Peng for their help, friendship and encouragement, which have made my study here full of happiness.

TABLE OF CONTENTS

LIST OF FIGURES

FIGURE                                                                       Page

CHAPTER I

INTRODUCTION

Collisions between energetic nuclei from the Relativistic Heavy Ion Collider (RHIC) at the Brookhaven National Laboratory make it possible to create in the laboratory a hot dense matter that consists of the constituent quarks and gluons inside nucleons. This so-called quark-gluon plasma (QGP) is believed to have existed during the first microsecond after the Big Bang. One of the proposed signatures for the quark-gluon plasma is the suppression of the yield of $J/\psi$, which is a charm-anticharm quark bound state, resulting from Debye screening of the color force in the quark-gluon plasma [1]. Extensive experimental and theoretical efforts have been devoted to study this phenomenon at the Super Proton Synchrotron (SPS) at the European Laboratory for Particle Physics (CERN) [2, 3, 4, 5, 6]. However, available experimental data on $J/\psi$ suppression in colliding systems ranging from $pA$ to S+U are consistent with the scenario that charmoniums are absorbed by target and projectile nucleons with a cross section of about 7 mb [5]. Only in data from Pb+Pb collisions at $P_{\text{lab}} = 158$ GeV/$c$ in the NA50 experiment is there a large additional $J/\psi$ suppression in events with high transverse energies, which requires the introduction of other absorption mechanisms. While there are suggestions that this anomalous suppression may be due to the formation of QGP [7, 8], other more conventional mechanisms based on $J/\psi$ absorption by comoving hadrons have also been proposed as a possible explanation [9, 10]. Since the latter depends on the values of $J/\psi$ absorption cross sections by hadrons, which are not known empirically, it is important to have a better knowledge of the interactions between charmonium states and hadrons in order to understand

---

The journal model is Physical Review C.

the nature of the observed anomalous charmonium suppression.

Knowledge of $J/\psi$ absorption cross sections by hadrons is also useful in estimating the contribution of $J/\psi$ production from charmed mesons in the hadronic matter formed in relativistic heavy ion collisions. Since the charmed meson to $J/\psi$ ratio in proton-proton collisions increases with energy, it has been shown that $J/\psi$ production from the hadronic matter may not be negligible in heavy ion collisions at the Large Hadronic Collider energies [11, 12]. To use $J/\psi$ suppression as a signature for the formation of QGP in these collisions thus requires the understanding of both $J/\psi$ absorption and production in hadronic matter.

Another signature suggested for the formation of QGP is enhanced production of dileptons in the intermediate mass region (1.5 GeV$< M_{ll} < $ 3 GeV) from quark-antiquark annihilation and quark-gluon interactions [13]. These dileptons are well above the masses of light vector mesons ($\rho$, $\omega$, and $\phi$), so that contributions from low energy hadronic processes like $\pi\pi$ annihilation are sufficiently suppressed. They are also below the mass of $J/\psi$ resonance, so that contributions from hard processes like the Drell-Yan annihilation, which prevail in the high energy region (M$>$ 4 GeV), increase rather slowly toward smaller masses. Intermediate mass dilepton spectra have been measured in central heavy ion collisions at SPS energy in the dimuon channel [14], and their yield were 2~3 times more than that based on the extrapolation of known sources from proton-induced collisions, given by primordial Drell-Yan annihilation as well as semileptonic decays of associated produced $D, \bar{D}$ mesons. To conclude that this enhancement is exclusively related to the QGP effects, it is, however, important to understand other possible mechanisms that can contribute to the production of intermediate mass dileptons, such as enhanced production of $c\bar{c}$ pairs, rescattering of D meson in hot/dense matter [15] which might generate a transverse momentum broadening to increase the $\mu^+\mu^-$ phase space, and enhancement of D

meson production from secondary $\pi N$ interactions in the hadronic matter [16].

Various approaches have been used in evaluating the cross section for charmonium absorption by hadrons. In one approach, the quark-exchange model has been used. An earlier study based on this model by Martins, Blaschke, and Quack [17] has shown that the $J/\psi$ absorption cross section $\sigma_{\pi\psi}$ by pions has a peak value of about 7 mb at $E_{\rm kin} \equiv \sqrt{s} - m_\pi - m_\psi \simeq 0.8$ GeV, but a more recent study by Wong, Swanson, and Barnes [18] gives a peak value of only $\sigma_{\pi\psi} \sim 1$ mb at the same $E_{\rm kin}$ region. In the perturbative QCD approach, Kharzeev and Satz [19] have studied the dissociation of charmonium bound states by energetic gluons inside hadrons. They have predicted that the dissociation cross section increases monotonously with $E_{\rm kin}$ and has a value of only about 0.1 mb around $E_{\rm kin} \sim 0.8$ GeV. In the third approach, meson-exchange models based on hadronic effective Lagrangians have been used. With only pseudoscalar-pseudoscalar-vector-meson couplings (PPV couplings), Matinyan and Müller [20] have found $\sigma_{\pi\psi} \simeq 0.3$ mb at $E_{\rm kin} = 0.8$ GeV. In a later study, Haglin [21] has included also the three-vector-meson couplings (VVV couplings) and four-point couplings (or contact terms), and obtained much larger values of $J/\psi$ absorption cross sections. A similar magnitude for the $J/\psi - \pi$ absorption cross section has also been obtained in the QCD sum rules [22]. Large discrepancies in the magnitude of $\sigma_{\pi\psi}$ (as well as $\sigma_{\rho\psi}$) thus exist among the predictions from these three approaches, and further theoretical studies are needed. In another effective Lagrangian approach study [23], a meson-exchange model as in Ref. [21] has been used but the VVV and four-point couplings in the effective Lagrangian are treated differently and also the effect of form factors at interaction vertices has been taken into account. It is then found that the $J/\psi$ absorption cross sections remain appreciable after including form factors at the interaction vertices. The values for $\sigma_{\pi\psi}$ and $\sigma_{\rho\psi}$ are roughly 7 mb and 3 mb, respectively, and are comparable to those used in phenomenological studies of

$J/\psi$ absorption by comoving hadrons in relativistic heavy ion collisions [9, 10, 24].

Since the cross sections for $J/\psi$ absorption by pion and rho meson cannot be directly measured, it is useful to find the empirical information which can constrain their values. One such constraint is the cross section for $J/\psi$ absorption by nucleon, as this process can be viewed as $J/\psi$ absorption by the virtual pion and rho meson cloud of the nucleon. From $J/\psi$ production in photo-nucleus reactions, the cross section of $J/\psi$ absorption by nucleon can be extracted, and its magnitude has been found to be about 4 mb [25]. The $J/\psi - N$ absorption cross section has also been extracted from proton-nucleus collisions at proton energies from 200 to 800 GeV, and the empirical value is about 7 mb [5]. In this dissertation, we use an effective Lagrangian to evaluate the $J/\psi$ absorption cross section by nucleon and find that its magnitude is consistent with these empirical information.

Because of their large masses, open charm mesons are expected to be mostly produced in the initial preequilibrium stage of relativistic heavy ion collisions. They have thus been suggested as possible probes of the initial dynamics in these collisions. Previous studies have been concentrated on the production of charm quarks from the preequilibrium partonic matter [26, 27]. In these studies, it has been found that charm quark production is sensitive to not only the rapidity and space correlations of initial minijet partons but also their energy loss in the dense partonic matter. For charmed meson production from nonpartonic matter, the only study is the one [16] based on the Hadron-String Dynamics (HSD) [28] using hadronic cross sections obtained from the Quark-Gluon String Model (QGSM) [29]. Allowing scatterings between the leading quark and diquark in a baryonic string with the quark and antiquark in a mesonic string and taking their cross sections to be the same as in meson-baryon scatterings, this study shows that charm production is appreciable even with a small cross section of a few $\mu$b as predicted by the QGSM. The factor of two enhancement obtained in

this study for charmed mesons over that produced from the primary nucleon-nucleon collisions offers a possible explanation for the observed enhancement of intermediate mass dileptons seen in heavy ion collisions at SPS [30].

The QGSM model treats charmed meson production from pion-nucleon scattering as a process involving the exchange of the vector charm meson Regge trajectory in $t$-channel. Contributions from the $s$ and $u$ channels are neglected. Although the $u$ channel is expected to be small as it involves nonplanar diagrams, which are known to be negligible in the large $N_c$ limit, the $s$ channel contribution may not be small because of the planarity of associated diagrams. To study the relative importance of the $s$, $t$, and $u$ channel contributions to charmed meson production in pion-nucleon scattering, we shall use the effective hadronic Lagrangian based on the flavor SU(4) symmetry but with empirical hadron masses. We find that the magnitude of the cross section for charmed meson production from pion-nucleon scattering depends sensitively on the value of the cutoff parameter at interaction vertices. Using a cutoff parameter of 1 GeV as used previously in studying $J/\psi$ absorption [23, 31] and charmed meson scattering [32, 33], we find that the $t$ channel process involving vector charmed meson exchange indeed gives a small cross section as in QGSM and the $u$ channel contribution is negligible. The contribution from the $s$ channel is, however, appreciable, leading to a few tenth of mb for the production cross section of charmed meson from pion-nucleon scattering. Furthermore, the model allows us to study the cross section for charm production from the interaction of nucleons with rho mesons, which are abundant in the initial stage of the hadronic matter in heavy ion collisions and also have a lower threshold for charmed meson production.

To test our model we also use the same hadronic Lagrangian to evaluate charmed hadron production from proton-proton collisions. Motivated by future experiments at proposed accelerator facility at the German Heavy Ion Research Center [34], there

are already studies on these reactions based on the meson-exchange model [35, 36]. However, effects due to off-shellness of exchanged mesons have been neglected in these studies. As in our studies of $J/\psi$ absorption by nucleon [31] and photoproduction of $J/\psi$ on nucleons [37], we do not make the on-shell approximation in evaluating the charmed meson production cross section from proton-proton collisions.

We further generalize the effective hadronic Lagrangian to include the photon and to study charmed hadron production from photon-proton reactions near threshold. Both two-body ($\bar{D}\Lambda_c$, $\bar{D}^*\Lambda_c$) and three-body ($D\bar{D}N$, $D\bar{D}^*N$, $D^*\bar{D}N$, $D^*\bar{D}^*N$) final states are included. To take into account finite hadron sizes without violating the gauge invariance, the total amplitude of each process is multiplied by an overall form factor of monopole form. With cutoff parameter in the form factor adjusted to fit the measured total cross section for charmed hadron production from photon-proton reactions at center-of-mass energy of 6 GeV [38], we find that the relative contribution of two-body to three-body final states is consistent with that seen in experimental data. We have also made predictions for charmed hadron production cross section from photon-proton reactions both near threshold and at high energies. As expected, two-body final states dominate near threshold while three-body final states become important at high energies. However, the total cross sections at high energies are much smaller than those measured experimentally or given by the LO perturbative QCD as more complicated final states are not included in the hadronic approach.

Our results provide an independent test and confirmation of the usefulness of hadronic models for determining the production and scattering cross sections of charmed hadrons at low energies. The effective hadronic Lagrangian used in the present study will be useful for evaluating the cross sections for other reactions involving heavy flavored hadrons. These reactions can be studied at both the Japanese Hadron facility [39] and at the GSI future accelerator [34], where both open and hid-

den charmed hadrons can be copiously produced in proton- and antiproton-nucleus reactions near threshold.

The dissertation is arranged as follows. The effective hadronic Lagrangian is presented and discussed in Chapter II, which also includes a brief discussion on the form factors that will be used in the following chapters. In Chapter III, we evaluate the cross section for $J/\psi$ absorption by nucleons, which is relevant to $J/\psi$ suppression in relativistic heavy ion collisions. The cross sections for open charm production from secondary scatterings, i.e., meson-nucleon and nucleon-nucleon collisions, are evaluated in Chapter IV . The results on charm photoproduction on nucleons are given in Charter V. Finally, the summary and conclusion are presented in Chapter VI.

CHAPTER II

EFFECTIVE LAGRANGIAN

Since it is still difficult to study strong interaction phenomena at non-perturbative regime using the QCD, effective theories are usually employed. In this chapter, we introduce an effective Lagrangian that is based on the SU(4) flavor symmetry. To take into account the symmetry breaking effects, we use empirical hadrons masses and coupling constants if they are available. Otherwise, they are determined from the known ones using the SU(4) relations. We also introduce form factors at the strong interaction vertices to take take into account the effect due to final hadron sizes. To include the electromagnetic interaction, photon is introduced into the effective Lagrangian as a U(1) gauge particle. In the following, we first start from the more familiar SU(3)invariant effective Lagrangian for hadronic interactions involving hadrons that are made of light $u$, $d$, and strange $s$ quarks.

A.   Effective Lagrangian with SU(3) flavor symmetry

In the case of SU(3) flavor symmetry, the hadronic Lagrangian for octet pseudoscalar mesons and baryons can be written as

$$
\begin{aligned}
\mathcal{L}_{\text{eff}} &= iTr(\bar{B}\slashed{\partial}B) + Tr[(\partial_\mu P)(\partial^\mu P^\dagger)] \\
&\quad + g'Tr[\alpha_D(\bar{B}\gamma_5 B + B\gamma_5\bar{B})P + (1-\alpha_D)P(\bar{B}\gamma_5 B - B\gamma_5\bar{B})], \quad (2.1)
\end{aligned}
$$

where $P$ and $B$ denote, respectively, the $3 \times 3$ matrix representation of pseudoscalar meson and baryons

$$
B = \begin{pmatrix} \frac{\Sigma^0}{\sqrt{2}} + \frac{\Lambda}{\sqrt{6}} & \Sigma^+ & p \\ \Sigma^- & -\frac{\Sigma^0}{\sqrt{2}} + \frac{\Lambda}{\sqrt{6}} & n \\ \Xi^- & \Xi^0 & -\sqrt{\frac{2}{3}}\Lambda \end{pmatrix}, \tag{2.2}
$$

$$
P = \frac{1}{\sqrt{2}} \begin{pmatrix} \frac{\pi^0}{\sqrt{2}} + \frac{\eta}{\sqrt{6}} & \pi^+ & K^\dagger \\ \pi^- & -\frac{\pi^0}{\sqrt{2}} + \frac{\eta}{\sqrt{6}} & K^0 \\ K^- & \bar{K}^0 & -\sqrt{\frac{2}{3}}\eta \end{pmatrix}. \tag{2.3}
$$

In Eq.(2.1), $g'$ is the universal pseudoscalar coupling between pseudoscalar mesons and baryons, and the parameter $\alpha_D$ is given by $D/(D+F)$ with $D$ and $F$ denoting, respectively, the coupling constants for the $D$-type $\mathrm{Tr}(\{B, \bar{B}\}P)$ and $F$-type $\mathrm{Tr}([B, \bar{B}]P)$ interaction Lagrangians.

Vector mesons are introduced to the hadronic model by treating them as gauge particles, i.e., replacing the partial derivative $\partial_\mu$ in Eq.(2.1) with the covariant derivative

$$
D_\mu = \partial_\mu - \frac{i}{2}g[V_\mu, \ ], \tag{2.4}
$$

where V denotes the matrix representation of vector mesons, i.e.,

$$
V = \frac{1}{\sqrt{2}} \begin{pmatrix} \frac{\rho^0}{\sqrt{2}} + \frac{\omega}{\sqrt{6}} & \rho^\dagger & K^{*+} \\ \rho^- & -\frac{\rho^0}{\sqrt{2}} + \frac{\omega}{\sqrt{6}} & K^{*0} \\ K^{*-} & \bar{K}^{*0} & -\sqrt{\frac{2}{3}}\omega \end{pmatrix}, \tag{2.5}
$$

and $g$ is the universal coupling between vector mesons with baryons and pseudoscalar mesons.

Expanding the above interaction Lagrangian using the explicit representations of $P$, $V$, and $B$, we obtain the following $\pi NN$ and $\rho NN$ interaction Lagrangians:

$$\begin{aligned}
\mathcal{L}_{\pi NN} &= -ig_{\pi NN}\bar{N}\gamma_5\vec{\tau}N \cdot \vec{\pi}, \\
\mathcal{L}_{\rho NN} &= g_{\rho NN}\bar{N}\gamma_\mu\vec{\tau}N \cdot \vec{\rho},
\end{aligned} \tag{2.6}$$

In the above, $\vec{\tau}$ is the Pauli matrices; $N$, $\vec{\pi}$, and $\vec{\rho}$ denote, respectively, the nucleon isospin doublet, pion and rho meson isospin triplets. The coupling constants $g_{\pi NN}$ and $g_{\rho NN}$ are given by

$$g_{\pi NN} = \frac{1}{2\alpha_D}g', \quad g_{\rho NN} = \frac{g}{4}, \quad \text{and} g_{KN\Lambda} = \frac{3-2\alpha_D}{\sqrt{3}}g_{\pi NN}. \tag{2.7}$$

From the empirical values $g_{\pi NN} = 13.5$, $g_{\rho NN} = 3.25$ and $\alpha_D = D/(D+F) = 0.64$ [40], we obtain $g' = 17.28$ and $g = 13.0$. Other coupling constants can then be related to these two through the SU(3) relations.

## B.  Effective Lagrangian with SU(4) flavor symmetry

The above SU(3) effective Lagrangian can be generalized to SU(4) in order to include hadrons consisting of the charm quark. In this case, both the 15-plet pseudoscalar mesons and 15-plet vector mesons can be expressed by by $4 \times 4$ matrix, and their interaction Lagrangians can still be written in forms similar to those in the SU(3) case. This is, however, different for the interaction Lagrangian of the 20-plet baryons with either pseudoscalar or vector mesons as they cannot be expressed in simple matrix form. Instead, we use the tensor notation to express the meson-baryon interaction Lagrangians.

### 1. Meson-meson interactions

The free Lagrangian for pseudoscalar and vector mesons in the limit of SU(4) invariance can be written as

$$\mathcal{L}_0 = \text{Tr} \left( \partial_\mu P^\dagger \partial^\mu P \right) - \frac{1}{2}\text{Tr} \left( F_{\mu\nu}^\dagger F^{\mu\nu} \right) , \tag{2.8}$$

where $F_{\mu\nu} = \partial_\mu V_\nu - \partial_\nu V_\mu$, and $P$ and $V$ denote, respectively, the properly normalized $4 \times 4$ pseudoscalar and vector meson matrices in SU(4) [23]:

$$P = \frac{1}{\sqrt{2}} \begin{pmatrix} \frac{\pi^0}{\sqrt{2}} + \frac{\eta}{\sqrt{6}} + \frac{\eta_c}{\sqrt{12}} & \pi^+ & K^+ & \bar{D}^0 \\ \pi^- & -\frac{\pi^0}{\sqrt{2}} + \frac{\eta}{\sqrt{6}} + \frac{\eta_c}{\sqrt{12}} & K^0 & D^- \\ K^- & \bar{K}^0 & -\sqrt{\frac{2}{3}}\eta + \frac{\eta_c}{\sqrt{12}} & D_s^- \\ D^0 & D^+ & D_s^+ & -\frac{3\eta_c}{\sqrt{12}} \end{pmatrix} ,$$

$$V = \frac{1}{\sqrt{2}} \begin{pmatrix} \frac{\rho^0}{\sqrt{2}} + \frac{\omega'}{\sqrt{6}} + \frac{J/\psi}{\sqrt{12}} & \rho^+ & K^{*+} & \bar{D}^{*0} \\ \rho^- & -\frac{\rho^0}{\sqrt{2}} + \frac{\omega'}{\sqrt{6}} + \frac{J/\psi}{\sqrt{12}} & K^{*0} & D^{*-} \\ K^{*-} & \bar{K}^{*0} & -\sqrt{\frac{2}{3}}\omega' + \frac{J/\psi}{\sqrt{12}} & D_s^{*-} \\ D^{*0} & D^{*+} & D_s^{*+} & -\frac{3J/\psi}{\sqrt{12}} \end{pmatrix} . \tag{2.9}$$

To obtain the couplings between pseudoscalar mesons and vector mesons, we introduce the minimal substitution

$$\partial_\mu P \rightarrow \mathcal{D}_\mu P = \partial_\mu P - \frac{ig}{2}\left[V_\mu, P\right] ,$$

$$F_{\mu\nu} \rightarrow \partial_\mu V_\nu - \partial_\nu V_\mu - \frac{ig}{2}\left[V_\mu, V_\nu\right] , \tag{2.10}$$

as in the SU(3) case. The effective Lagrangian is then given by

$$\begin{aligned} \mathcal{L} &= \mathcal{L}_0 + \frac{ig}{2}\text{Tr}\left(\partial^\mu P\left[P^\dagger, V_\mu^\dagger\right] + \partial^\mu P^\dagger\left[P, V_\mu\right]\right) - \frac{g^2}{4}\text{Tr}\left(\left[P^\dagger, V_\mu^\dagger\right]\left[P, V^\mu\right]\right) \\ &+ \frac{ig}{2}\text{Tr}\left(\partial^\mu V^\nu\left[V_\mu^\dagger, V_\nu^\dagger\right] + \partial_\mu V_\nu^\dagger\left[V^\mu, V^\nu\right]\right) + \frac{g^2}{8}\text{Tr}\left(\left[V^\mu, V^\nu\right]\left[V_\mu^\dagger, V_\nu^\dagger\right]\right) \end{aligned} \tag{2.11}$$

The hermiticity of $P$ and $V$ reduces this to

$$
\begin{aligned}
\mathcal{L} &= \mathcal{L}_0 + ig\mathrm{Tr}\left(\partial^\mu P\left[P, V_\mu\right]\right) - \frac{g^2}{4}\mathrm{Tr}\left(\left[P, V_\mu\right]^2\right) \\
&+ ig\mathrm{Tr}\left(\partial^\mu V^\nu\left[V_\mu, V_\nu\right]\right) + \frac{g^2}{8}\mathrm{Tr}\left(\left[V_\mu, V_\nu\right]^2\right) .
\end{aligned} \tag{2.12}
$$

Since the SU(4) symmetry is explicitly broken by hadron masses, terms involving hadron masses are added to Eq.(2.12) using the experimentally determined values.

We note that similar interaction Lagrangians for meson-meson interactions were obtained in [21] based on the SU(4) chiral Lagrangian with vector mesons introduced through the covariant derivative.

## 2. Meson-baryon interactions

In the SU(4) quark model, baryons belong to the 20-plet states. These states can be conveniently expressed by tensors $\phi_{\mu\nu\lambda}$ [41], where $\mu$, $\nu$, and $\lambda$ run from 1 to 4, that satisfy the conditions

$$
\phi_{\mu\nu\lambda} + \phi_{\nu\lambda\mu} + \phi_{\lambda\mu\nu} = 0, \quad \phi_{\mu\nu\lambda} = \phi_{\nu\mu\lambda}. \tag{2.13}
$$

For baryons without charm quarks, i.e., belonging to SU(3) octet, they are given by

$$
\begin{aligned}
p &= \phi_{112}, \quad n = \phi_{221}, \quad \Lambda = \sqrt{\frac{2}{3}}(\phi_{321} - \phi_{312}), \\
\Sigma^+ &= \phi_{113}, \quad \Sigma^0 = \sqrt{2}\phi_{123} \quad \Sigma^- = \phi_{223}, \\
\Xi^0 &= \phi_{331}, \quad \Xi^- = \phi_{332}.
\end{aligned} \tag{2.14}
$$

For baryons with one charm quark, they are

$$
\begin{aligned}
\Sigma_c^{++} &= \phi_{114}, \quad \Sigma_c^+ = \phi_{124}, \quad \Sigma_c^0 = \phi_{224}, \\
\Xi_c^+ &= \phi_{134}, \quad \Xi_c^0 = \phi_{234},
\end{aligned}
$$

$$\Xi_c^{+\prime} = \sqrt{\frac{2}{3}}(\phi_{413} - \phi_{431}), \quad \Xi_c^{0\prime} = \sqrt{\frac{2}{3}}(\phi_{423} - \phi_{432}),$$

$$\Lambda_c^+ = \sqrt{\frac{2}{3}}(\phi_{421} - \phi_{412}), \quad \Omega_c^0 = \phi_{334}. \tag{2.15}$$

For baryons with two charm quarks, they are

$$\Xi_{cc}^{++} = \phi_{441}, \quad \Xi_{cc}^+ = \phi_{442}, \quad \Omega_{cc}^+ = \phi_{443}. \tag{2.16}$$

Mesons in the SU(4) quark model belong to the 15-plet. In the tensor notations, pseudoscalar and vector mesons are expressed by $P_\beta^\alpha$ and $V_\beta^\alpha$, respectively. For pseudoscalar mesons, we have

$$\pi^+ = P_1^2, \quad \pi^- = P_2^1, \quad \pi^0 = \frac{1}{\sqrt{2}}(P_1^1 - P_2^2),$$

$$K^+ = P_1^3, \quad K^0 = P_2^3, \quad K^- = P_3^1, \quad \bar{K}^0 = P_3^2,$$

$$D^+ = P_4^2, \quad D^0 = P_4^1, \quad D^- = P_2^4, \quad \bar{D}^0 = P_1^4,$$

$$D_s^+ = P_4^3, \quad D_s^- = P_3^4,$$

$$\eta = \frac{1}{\sqrt{6}}(P_1^1 + P_2^2 - 2P_3^3),$$

$$\eta_c = \frac{1}{\sqrt{12}}(P_1^1 + P_2^2 + P_3^3 - 3P_4^4). \tag{2.17}$$

Similarly, we have for vector mesons

$$\rho^+ = V_1^2, \quad \rho^- = V_2^1, \quad \rho^0 = \frac{1}{\sqrt{2}}(V_1^1 - V_2^2),$$

$$K^{*+} = V_1^3, \quad K^{*0} = V_2^3, \quad K^{*-} = V_3^1, \quad \bar{K}^{*0} = V_3^2,$$

$$D^{*+} = V_4^2, \quad D^{*0} = V_4^1, \quad D^{*-} = V_2^4, \quad \bar{D}^{*0} = V_1^4,$$

$$D_s^{*+} = V_4^3, \quad D_s^{*-} = V_3^4,$$

$$\omega = \frac{1}{\sqrt{6}}(V_1^1 + V_2^2 - 2V_3^3),$$

$$J/\psi = \frac{1}{\sqrt{12}}(V_1^1 + V_2^2 + V_3^3 - 3V_4^4). \tag{2.18}$$

In tensor notations, the SU(4) invariant interaction Lagrangians between baryons and pseudoscalar mesons as well as between baryons and vector mesons can be written, respectively, as

$$
\begin{aligned}
\mathcal{L}_{PBB} &= g_p(a\phi^{*\alpha\mu\nu}\gamma_5 P^\beta_\alpha \phi_{\beta\mu\nu} + b\psi^{*\alpha\mu\nu}\gamma_5 P^\beta_\alpha \phi_{\beta\nu\mu}), \\
\mathcal{L}_{VBB} &= g_v(c\phi^{*\alpha\mu\nu}\gamma \cdot V^\beta_\alpha \phi_{\beta\mu\nu} + d\phi^{*\alpha\mu\nu}\gamma \cdot V^\beta_\alpha \phi_{\beta\nu\mu}),
\end{aligned}
\tag{2.19}
$$

where $g_p$ and $g_v$ are the universal baryon-pseudoscalar-meson and baryon-vector-meson coupling constants, and $a$, $b$, $c$, and $d$ are constants.

Writing explicitly, we obtain the following interaction Lagrangians,

$$
\begin{aligned}
\mathcal{L}_{PBB} &= g_p\left[\frac{1}{\sqrt{2}}\left(a - \frac{5}{4}b\right)\bar{N}\gamma_5\vec{\tau}\cdot\vec{\pi}N \frac{3\sqrt{6}}{8}(b-a)(\bar{N}\gamma_5 K\Lambda \bar{N}\gamma_5 \bar{D}\Lambda_c) + \cdots\right], \\
\mathcal{L}_{VBB} &= g_v\left[\frac{1}{\sqrt{2}}\left(c - \frac{5}{4}d\right)\bar{N}\gamma_\mu\rho^\mu N \frac{3\sqrt{6}}{8}(d-c)(\bar{N}\gamma_\mu K^{*\mu}\Lambda + \bar{N}\gamma_\mu \bar{D}^{\mu*}\Lambda_c)\right. \\
&\quad + \left.\frac{\sqrt{3}}{4}\left(-c + \frac{3}{2}d\right)\bar{\Lambda}_c\gamma_\mu\psi^\mu\Lambda_c + \cdots\right].
\end{aligned}
\tag{2.20}
$$

From the previous subsection on the SU(3) effective Lagrangian, we have the following relation between $g_{\pi NN}$ and $g_{KN\Lambda}$ coupling constants in the interaction Lagrangians $\mathcal{L}_{\pi NN} = -ig_{\pi NN}\bar{N}\gamma_5\vec{\tau}N\cdot\vec{\pi}$ and $\mathcal{L}_{KN\Lambda} = ig_{KN\Lambda}\bar{N}\gamma_5\Lambda\bar{K}$:

$$
g_{KN\Lambda} = \frac{3 - 2\alpha_D}{\sqrt{3}}g_{\pi NN},
\tag{2.21}
$$

where $\alpha_D = D/(D + F) \approx 0.64$ [40] is related to the $D$- and $F$-type couplings. Comparisons with the SU(4) relations in Eq. (2.20) then gives

$$
\frac{b}{a} = \frac{3 - 8\alpha_D}{6 - 10\alpha_D}.
\tag{2.22}
$$

Similarly, the $g_{\rho NN}$ and $g_{K^*N\Lambda}$ coupling constants in the interaction Lagrangians

involving vector mesons, given by

$$\mathcal{L}_{\rho NN} = g_{\rho NN} \bar{N} (\gamma^\mu \vec{\tau} \cdot \vec{\rho}_\mu + \frac{\kappa_\rho}{2m_N} \sigma^{\mu\nu} \vec{\tau} \cdot \partial_\mu \vec{\rho}_\nu) N \qquad (2.23)$$

and

$$\mathcal{L}_{K^*N\Lambda} = g_{K^*N\Lambda} \bar{N} \gamma_\mu \Lambda \bar{K}^*, \qquad (2.24)$$

are related by

$$g_{K^*N\Lambda} = -\sqrt{3} g_{\rho NN}. \qquad (2.25)$$

Comparing with the SU(4) relations in Eq. (2.20) then leads to

$$\frac{d}{c} = \frac{1}{2}. \qquad (2.26)$$

Using Eqs. (2.22) and (2.26) in Eq.(2.20), we then have

$$
\begin{aligned}
g_{DN\Lambda_c} &= \frac{3 - 2\alpha_D}{\sqrt{3}} g_{\pi NN}, \\
g_{\psi\Lambda_c\Lambda_c} &= -\frac{g_{\rho NN}}{\sqrt{6}}, \quad g_{D^*N\Lambda_c} = -\sqrt{3} g_{\rho NN}.
\end{aligned} \qquad (2.27)
$$

### 3. The electromagnetic interaction

The electromagnetic interaction can be included in the effective Lagrangian by introducing the $U_{\mathrm{EM}}(1)$ gauge transformation, i.e.,

$$
\begin{aligned}
\delta A_\mu &= \frac{1}{e} \partial_\mu \epsilon, \\
\delta P &= i\epsilon [Q, P], \\
\delta V_\mu &= i\epsilon [Q, V_\mu] + \frac{1}{g} Q \partial_\mu \epsilon,
\end{aligned} \qquad (2.28)
$$

where $A_\mu$ is the $U_{\mathrm{EM}}(1)$ gauge field, $e$ is the unit of electric charge, $\epsilon(x)$ is the $U(1)$ gauge parameter, and the quark charge matrix $Q = \mathrm{diag}(\frac{2}{3}, -\frac{1}{3}, -\frac{1}{3}, \frac{2}{3})$. The La-

grangians for meson-meson Eq.(2.12) and meson-baryon Eq.(2.19) interactions then vary under U(1) transformation according to

$$\delta\mathcal{L} = \delta\mathcal{L}_{PPV} + \delta\mathcal{L}_{PVPV} + \delta\mathcal{L}_{VVV} + \delta\mathcal{L}_{VVVV} + \delta\mathcal{L}_{PBB} + \delta\mathcal{L}_{PBB}, \qquad (2.29)$$

where

$$
\begin{aligned}
\delta\mathcal{L}_{PPV} &= iTr[(\partial^\mu P P - P \partial^\mu P)Q]\partial_\mu \epsilon, \\
\delta\mathcal{L}_{PVPV} &= -\frac{g}{2}Tr([P,V^\mu][P,Q])\partial_\mu \epsilon, \\
\delta\mathcal{L}_{VVV} &= iTr(\partial^\mu V^\nu [Q,V_\nu]\partial_\mu \epsilon) + iTr(\partial^\mu V^\nu [V_\mu,Q]\partial_\nu \epsilon) + iTr(\partial^\mu \partial^\nu \epsilon Q[V_\mu,V_\nu]), \\
\delta\mathcal{L}_{VVVV} &= \frac{g}{2}Tr([Q,V_\nu][V^\mu,V^\nu])\partial_\mu \epsilon, \\
\delta\mathcal{L}_{BBM} &= \bar{\Phi}\gamma^\mu \Phi \partial_\mu \epsilon. \qquad (2.30)
\end{aligned}
$$

To ensure gauge invariance of the total Lagrangian, we need to add the following additional interaction Lagrangians between the photon and the pseudoscalar as well as the vector mesons:

$$
\begin{aligned}
\mathcal{L}_{\gamma PP} &= -ieTr([\partial^\mu P, P]Q)A_\mu, \\
\mathcal{L}_{\gamma PPV} &= \frac{eg}{2}Tr([P,V^\mu][P,Q])A_\mu, \\
\mathcal{L}_{\gamma VV} &= -ieTr(\partial^\mu V^\nu [Q,V_\nu]A_\mu) - ieTr(\partial^\mu V^\nu [V_\mu,Q]A_\nu) - ieTr(\partial^\mu A^\nu Q[V_\mu,V_\nu]), \\
\mathcal{L}_{\gamma VVV} &= -\frac{eg}{2}Tr([Q,V_\nu][V^\mu,V^\nu])A_\mu, \\
\mathcal{L}_{\gamma BB} &= -\bar{\Phi}\gamma^\mu \Phi A_\mu. \qquad (2.31)
\end{aligned}
$$

C.  Form factors

To take into account the finite size of hadrons, form factors need to be introduced at the interaction vertices. In principle, form factors can be determined from the quark wave functions of the interacting hadrons. In practice, they are parameterized in

terms of the momentum of the off-shell particle at the interaction vertex. Although form factors at interaction vertices involving only light hadrons have been used extensively, very little is known about those involving charmonium and charmed hadrons. In this dissertation, we shall use the common monopole type for the form factors at both types of interaction vertices, and they will be discussed explicitly when they appear in our calculations.

CHAPTER III

*J/ψ* ABSORPTION BY NUCLEON*

Using the effective Lagrangian introduced in previous chapter, we have evaluated the cross section for $J/\psi$ absorption by nucleon in a meson-exchange model that includes not only pseudoscalar-pseudoscalar-vector-meson couplings but also three-vector-meson and four-point contact couplings. The result will be compared with the empirical one extracted from $J/\psi$ production in photo-nucleus and proton-nucleus reactions.

A.   $J/\psi$ absorption by nucleon via pion and rho meson exchange

Possible processes for $J/\psi$ absorption by nucleon involving its virtual pion and rho meson cloud are $J/\psi N \to D^*\bar{D}N(\bar{D}^*DN)$, $J/\psi N \to D\bar{D}N$, and $J/\psi N \to D^*\bar{D}^*N$, as shown by the diagrams in Fig. 1. From the effective Lagrangians of Chapter II, the interaction Lagrangian densities that are needed for evaluating their amplitudes can be derived, and they are given by

$$
\begin{aligned}
\mathcal{L}_{\pi NN} &= -ig_{\pi NN}\bar{N}\gamma_5\vec{\tau}N\cdot\vec{\pi}, \\
\mathcal{L}_{\rho NN} &= g_{\rho NN}\bar{N}(\gamma^\mu\vec{\tau}\cdot\vec{\rho}_\mu + \frac{\kappa_\rho}{2m_N}\sigma^{\mu\nu}\vec{\tau}\cdot\partial_\mu\vec{\rho}_\nu)N, \\
\mathcal{L}_{\pi DD^*} &= ig_{\pi DD^*}D^{*\mu}\vec{\tau}\cdot(\bar{D}\partial_\mu\vec{\pi} - \partial_\mu\bar{D}\vec{\pi}) + \text{H.c.}, \\
\mathcal{L}_{\rho DD} &= ig_{\rho DD}(D\vec{\tau}\partial_\mu\bar{D} - \partial_\mu D\vec{\tau}\bar{D})\cdot\vec{\rho}^\mu, \\
\mathcal{L}_{\rho D^*D^*} &= ig_{\rho D^*D^*}[(\partial_\mu D^{*\nu}\vec{\tau}\bar{D}^*_\nu - D^{*\nu}\vec{\tau}\partial_\mu\bar{D}^*_\nu)\cdot\vec{\rho}^\mu \\
&\quad + (D^{*\nu}\vec{\tau}\cdot\partial_\mu\vec{\rho}^\nu - \partial_\mu D^{*\nu}\vec{\tau}\cdot\vec{\rho}_\nu)\bar{D}^{*\mu} + D^{*\mu}(\vec{\tau}\cdot\vec{\rho}^\nu\partial_\mu\bar{D}^*_\nu - \vec{\tau}\cdot\partial_\mu\vec{\rho}^\nu\bar{D}^*_\nu)],
\end{aligned}
$$

Fig. 1. $J/\psi$ absorption by nucleon via pion and rho meson exchanges.

$$\mathcal{L}_{\psi DD} = ig_{\psi DD}\psi^\mu[D\partial_\mu\bar{D}) - (\partial_\mu D)\bar{D}],$$

$$\mathcal{L}_{\psi D^*D^*} = ig_{\psi D^*D^*}[\psi^\mu(\partial_\mu D^{*\nu}\bar{D}^*_\nu - D^{*\nu}\partial_\mu\bar{D}^*_\nu)$$

$$+ (\partial_\mu\psi^\nu D^*_\nu - \psi^\nu\partial_\mu D^*_\nu)\bar{D}^{*\mu} + D^{*\mu}(\psi^\nu\partial_\mu D^*_\nu - \partial_\mu\psi^\nu\bar{D}^*_\nu),$$

$$\mathcal{L}_{\pi\psi DD^*} = -g_{\pi\psi DD^*}\psi^\mu(D^*_\mu\vec{\tau}\bar{D} + D\vec{\tau}\bar{D}^*_\mu)\cdot\vec{\pi},$$

$$\mathcal{L}_{\rho\psi DD} = g_{\rho\psi DD}\psi^\mu D\vec{\tau}\bar{D}\cdot\vec{\rho}_\mu,$$

$$\mathcal{L}_{\rho\Psi D^*D^*} = g_{\rho\Psi D^*D^*}(\psi^\nu D^*_\nu\vec{\tau}\bar{D}^*_\mu + \psi^\nu D^*_\mu\vec{\tau}\bar{D}^*_\nu - 2\psi_\mu D^{*\nu}\vec{\tau}\bar{D}^*_\nu)\cdot\vec{\rho}^\mu. \tag{3.1}$$

As defined in Chapter II, $\vec{\tau}$ are Pauli spin matrices, and $\pi$ and $\rho$, denote the pion and rho meson isospin triplet, respectively,, while $D = (D^0, D^+)$ and $D^* = (D^{*0}, D^{*+})$ denote the pseudoscalar and vector charmed meson doublets, respectively. The $J/\psi$

is denoted by $\psi$ while $N$ represents the nucleon.

For the coupling constants, we use the empirical values $g_{\pi NN} = 13.5$ [42], $g_{\rho NN} = 3.25$, and $\kappa_\rho = 6.1$ [43], and $g_{\pi DD^*} = 4.4$ [20]. From the vector dominance model, we have $g_{\rho DD} = g_{\rho D^* D^*} = 2.52$ and $g_{\psi DD} = g_{\psi D^* D^*} = 7.64$ [23], as shown in Appendix A. For the four-point coupling constants, we relate their values to the three-point coupling constants using the SU(4) relations [23], i.e.,

$$g_{\pi\psi DD^*} = g_{\pi DD^*} g_{\psi DD}, \ \ g_{\rho\psi DD} = 2 g_{\rho DD} g_{\psi DD}, \ \ g_{\rho\psi D^* D^*} = g_{\rho D^* D^*} g_{\psi D^* D^*}. \tag{3.2}$$

The amplitudes for the first two processes in Fig. 1 are given by

$$
\begin{aligned}
M_1 &= -i g_{\pi NN} \bar{N}(p_3) \gamma_5 N(p_1) \frac{1}{t - m_\pi^2} (M_{1a} + M_{1b} + M_{1c}), \\
M_2 &= g_{\rho NN} \bar{N}(p_3) \left[ \gamma^\mu + i \frac{\kappa_\rho}{2 m_N} \sigma^{\alpha\mu} (p_1 - p_3)_\alpha \right] N(p_1) \frac{1}{t - m_\rho^2} \\
&\quad \times \left[ -g_{\mu\nu} + \frac{(p_1 - p_3)_\mu (p_1 - p_3)_\nu}{m_\rho^2} \right] (M_{2a}^\nu + M_{2b}^\nu + M_{2c}^\nu), \tag{3.3}
\end{aligned}
$$

where $p_1$ and $p_3$ are the four momenta of the initial and final nucleons, respectively. In the above, $M_{1a}$, $M_{1b}$, and $M_{1c}$ are the amplitudes for the subprocess $\pi\psi \to D^* \bar{D}$ in the top three diagrams of Fig. 1, while $M_{2a}^\nu$, $M_{2b}^\nu$, and $M_{2c}^\nu$ are the amplitudes for the subprocesses $\rho\psi \to D\bar{D}$ in the middle three diagrams. The amplitude for the third process has a similar expression as that for the second process with $M_{2a}^\nu$, $M_{2b}^\nu$, and $M_{2c}^\nu$ replaced, respectively, by $M_{3a}^\nu$, $M_{3b}^\nu$, and $M_{3c}^\nu$, which are the amplitudes for the subprocess $\rho\Psi \to D^* \bar{D}^*$ in the bottom three diagrams. Expressions for these amplitudes can be found in Ref. [23].

The cross sections for these processes with three particles in the final state can be expressed in terms of the off-shell cross sections of the subprocesses described by the amplitudes $M_1$, $M_2$, and $M_3$. Following the method of Ref. [44] for the reaction $NN \to N\Lambda K$, the spin and isospin averaged differential cross sections for the first

two processes in Fig. 1 can be written as

$$
\begin{aligned}
\frac{d\sigma_{\psi N \to N D^* \bar{D}}}{dt ds_1} &= \frac{g_{\pi NN}^2}{16\pi^2 s p_i^2} k\sqrt{s_1}(-t)\frac{F_{\pi NN}^2(t)}{(t - m_\pi^2)^2}\sigma_{\pi\psi \to D^* \bar{D}}(s_1, t), \\
\frac{d\sigma_{\psi N \to N D \bar{D}}}{dt ds_1} &= \frac{3g_{\rho NN}^2}{32\pi^2 s p_i^2} k\sqrt{s_1}\frac{F_{\rho NN}^2(t)}{(t - m_\rho^2)^2}\left[4(1+\kappa_\rho)^2(-t - 2m_N^2)\right. \\
&+ \left.\kappa_\rho^2\frac{(4m_N^2 - t)^2}{2m_N^2} + 4(1+\kappa_\rho)\kappa_\rho(4m_N^2 - t)\right]\sigma_{\rho\psi \to D\bar{D}}(s_1, t), \quad (3.4)
\end{aligned}
$$

and the differential cross section for $J/\psi N \to D^*\bar{D}^* N$ is similar to that for $J/\psi N \to D\bar{D}N$ with $\sigma_{\rho\psi \to D\bar{D}}(s_1, t)$ replaced by $\sigma_{\rho\psi \to D^*\bar{D}^*}(s_1, t)$.

In the above, $p_i$ is the center-of-mass momentum of $J/\psi$ and $N$, $t$ is the squared four momentum transfer, and $s_1$ and $k$ are, respectively, the squared invariant mass and center-of-mass momentum of $\pi$ and $J/\psi$ in the process $J/\psi N \to D^*\bar{D}N$ or $\rho$ and $J/\psi$ in the processes $J/\psi N \to D\bar{D}N$ and $J/\psi N \to D^*\bar{D}^*N$. We have also introduced form factors $F_{\pi NN}$ and $F_{\rho NN}$ at the $\pi NN$ and $\rho NN$ vertices, respectively. As in Ref.[44], both are taken to have the monopole form, i.e.,

$$
F_1(t) = \frac{\Lambda^2 - m^2}{\Lambda^2 - t}, \quad (3.5)
$$

where $m$ is the mass of exchanged pion or rho meson, and $\Lambda$ is a cutoff parameter. Following Refs.[42, 43], we take $\Lambda_{\pi NN} = 1.3$ GeV and $\Lambda_{\rho NN} = 1.4$ GeV.

The cross sections $\sigma_{\pi\psi \to D^*\bar{D}}(s_1, t)$, $\sigma_{\rho\psi \to D\bar{D}}(s_1, t)$, and $\sigma_{\rho\psi \to D^*\bar{D}^*}(s_1, t)$ are the spin and isospin averaged differential cross sections for the subprocesses $\pi\psi \to D^*\bar{D}$, $\rho\psi \to D\bar{D}$, and $\rho\Psi \to D^*\bar{D}^*$ with off-shell pion or rho meson. Explicit expressions for these cross sections can be obtained from Ref. [23] by replacing the square of pion or rho meson masses by $t$. In evaluating these cross sections, we also introduce form factors at the interaction vertices. Following Ref.[23], the form factors at three-point $t$ channel and $u$ channel vertices, i.e., $\pi DD^*$, $\rho DD$, $\rho D^*D^*$, $\psi DD$, and $\psi D^*D^*$ that

involve heavy virtual charmed mesons, are taken to have the following form:

$$F_2(\mathbf{q}^2) = \frac{\Lambda^2}{\Lambda^2 + \mathbf{q}^2}, \tag{3.6}$$

instead of the monopole form of Eq. (3.5). In the above, $\mathbf{q}$ is the three momentum transfer in the center-of-mass of $\psi$ and pion or rho meson.

The form factor at four-point vertices, i.e., $\pi\psi DD^*$, $\rho\psi DD$, and $\rho\psi D^*D^*$, are taken to be

$$f_4 = \left(\frac{\Lambda_1^2}{\Lambda_1^2 + <\mathbf{q}^2>}\right)\left(\frac{\Lambda_2^2}{\Lambda_2^2 + <\mathbf{q}^2>}\right), \tag{3.7}$$

where $\Lambda_1$ and $\Lambda_2$ are the two different cutoff parameters at the three-point vertices present in processes with the same initial and final particles, and $< \mathbf{q}^2 >$ is the average value of the squared three momentum transfers in $t$ and $u$ channels.

Using the same value of 1 GeV for cutoff parameters in the form factors involving charmed mesons as in Refs. [23, 45], we have evaluated the cross sections for $J/\psi$ absorption by nucleon, and they are shown in Fig. 2 as functions of total center-of-mass energy. It is seen that all cross sections are less than 2 mb. Furthermore, the cross section for $J/\psi N \rightarrow D^*\bar{D}N$ and $J/\psi N \rightarrow \bar{D}^*DN$ (solid curve) due to pion exchange is larger than those for $J/\psi N \rightarrow D\bar{D}N$ (dashed curve) and $J/\psi N \rightarrow D^*\bar{D}^*N$ (dotted curve) that are due to rho meson exchange.

Our result for $\sigma_{J/\psi N \rightarrow D\bar{D}N}$ is order-of-magnitude smaller than that of Ref. [46], where this processes is viewed as the elastic scattering of a nucleon with one of the charmed mesons from the decay of $J/\psi$. The latter cross section is then assumed to have a constant value of 20 mb. Compared to our approach, they have neglected both the energy dependence and the off-shell effect of the subprocess involved in $J/\psi - N$ absorption to three-body final state. Also contributing to this large difference in the cross section is the value of cutoff parameter, 3.1 GeV in Ref.[46] versus 1 GeV
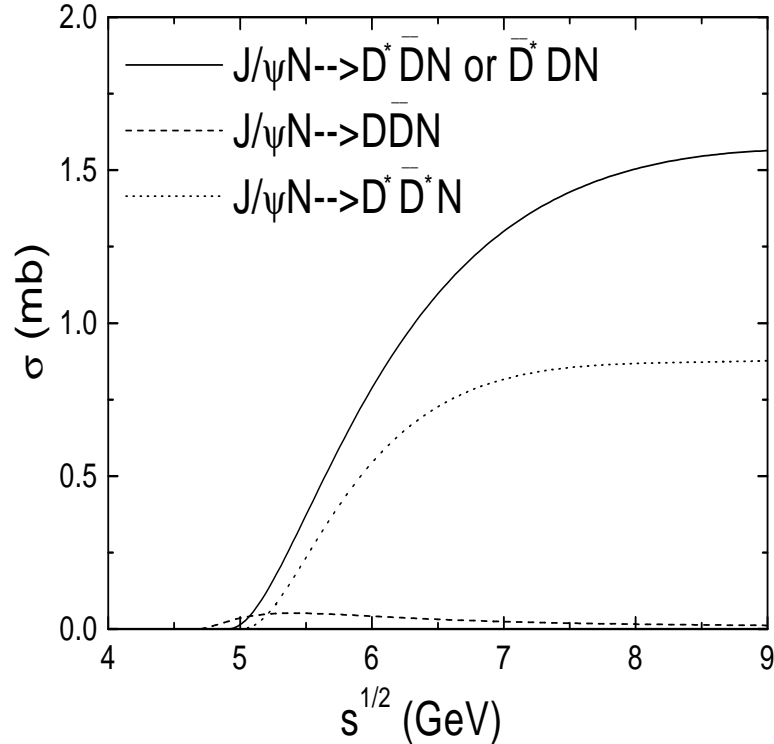
Fig. 2. Cross section for $J/\psi$ absorption by nucleon due to the virtual pion and rho meson cloud of the nucleon as a function of center-of-mass energy.

used here, and the different momentum dependence, i.e., four momentum transfer in Ref.[46] while three momentum transfer in the present study. We note that the more important processes $J/\Psi \rightarrow D^*\bar{D}N(\bar{D}^*DN)$ and $J/\Psi \rightarrow D^*\bar{D}^*N$ are not considered in Ref.[46].

B. $J/\psi$ absorption by nucleon via charmed hadron exchange

Besides absorption by the virtual pion and rho meson cloud of a nucleon, $J/\psi$ can also be absorbed by the nucleon via charmed hadron exchange in the reaction $J/\psi N \rightarrow \bar{D}\Lambda_c$ and $J/\psi N \rightarrow \bar{D}^*\Lambda_c$ shown by the diagrams in Fig. 3. These processes involve
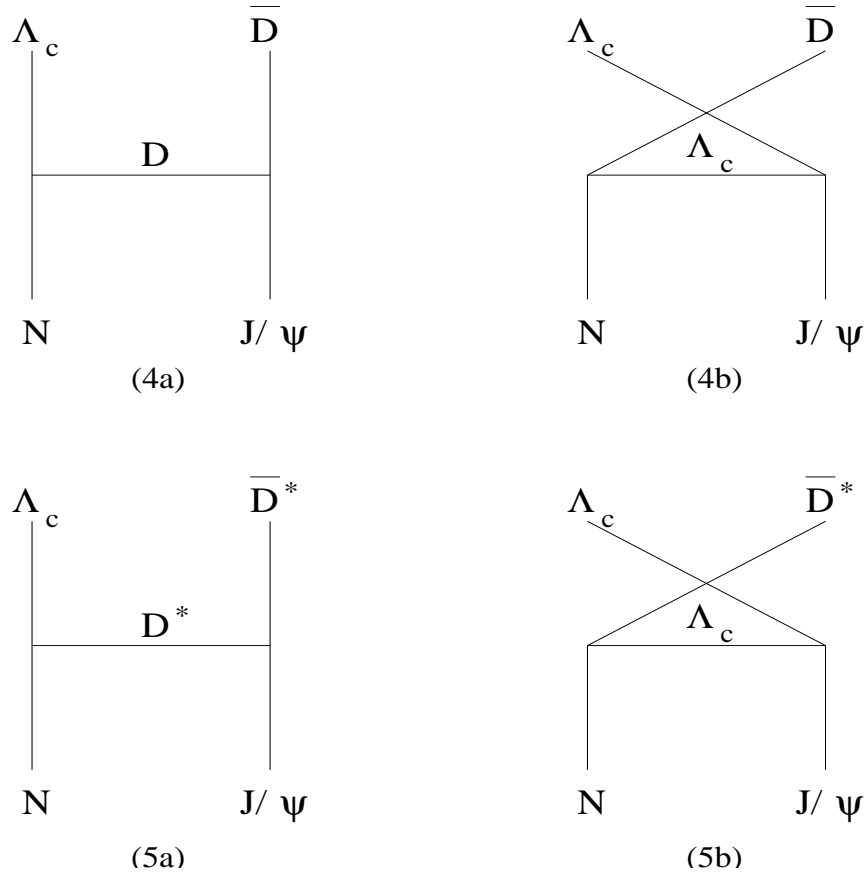
Fig. 3. $J/\psi$ absorption by nucleon via charmed hadron exchange.

the following interaction Lagrangians:

$$
\begin{aligned}
\mathcal{L}_{DN\Lambda_c} &= ig_{DN\Lambda_c}(\bar{N}\gamma_5\Lambda_c\bar{D} + D\bar{\Lambda}_c\gamma_5 N), \\
\mathcal{L}_{D^*N\Lambda_c} &= g_{D^*N\Lambda_c}(\bar{N}\gamma_\mu\Lambda_c\bar{D}^{*\mu} + D^{*\mu}\bar{\Lambda}_c\gamma_\mu N), \\
\mathcal{L}_{\Psi\Lambda_c\Lambda_c} &= g_{\psi\Lambda_c\Lambda_c}\bar{\Lambda}_c\gamma^\mu\psi_\mu\Lambda_c,
\end{aligned}
\tag{3.8}
$$

where $\Lambda_c$ denotes the charmed baryon, that resulting from the effective Lagrangian of Chapter II. The coupling constants $g_{DN\Lambda_c}$, $g_{D^*N\Lambda_c}$, and $g_{\psi\Lambda_c\Lambda_c}$ can be related to known coupling constants $g_{\pi NN}$ and $g_{\rho NN}$ using the SU(4) symmetry shown in Chapter II. Using $g_{\pi NN} = 13.5$ and $g_{\rho NN} = 3.25$, we then have $g_{DN\Lambda_c} = 13.5$,

$g_{D^*N\Lambda_c} = -5.6$, and $g_{\psi\Lambda_c\Lambda_c} = -1.4$.

The amplitudes for these processes are given by

$$
\begin{aligned}
M_{4a} &= M_{4a}^\mu \varepsilon_{2\mu}, \quad M_{4b} = M_{4b}^\mu \varepsilon_{2\mu}, \\
M_{5a} &= M_{5a}^{\mu\nu} \varepsilon_{2\mu} \varepsilon_{4\nu}, \quad M_{5b} = M_{5b}^{\mu\nu} \varepsilon_{2\mu} \varepsilon_{4\nu}.
\end{aligned}
\tag{3.9}
$$

with $\varepsilon_{2\mu}$ and $\varepsilon_{4\mu}$ being the polarization vectors of $J/\psi$ and $D^*$, respectively, and

$$
\begin{aligned}
M_{4a}^\mu &= 2ig_{\psi DD}g_{DN\Lambda_c}\frac{1}{t-m_D^2}p_4^\mu \bar{\Lambda}_c(p_3)\gamma_5 N(p_1), \\
M_{4b}^\mu &= ig_{DN\Lambda_c}g_{\psi\Lambda_c\Lambda_c}\bar{\Lambda}_c(p_3)\gamma^\mu \frac{\slashed{q}+m_{\Lambda_c}}{u-m_{\Lambda_c}^2}\gamma_5 N(p_1), \\
M_{5a}^{\mu\nu} &= -g_{D^*N\Lambda_c}g_{\psi D^*D^*}\bar{\Lambda}_c(p_3)\gamma^\alpha N(p_1)\left[g_{\alpha\beta}-\frac{(p_1-p_3)_\alpha(p_1-p_3)_\beta}{m_{D^*}^2}\right] \\
&\quad \times \frac{1}{t-m_{D^*}^2}[2p_2^\nu g^{\beta\mu}-(p_2+p_4)^\beta g^{\mu\nu}+2p_4^\mu g^{\beta\nu}], \\
M_{5b}^{\mu\nu} &= g_{D^*N\Lambda_c}g_{\psi\Lambda_c\Lambda_c}\bar{\Lambda}_c(p_3)\gamma^\mu \frac{\slashed{q}+m_{\Lambda_c}}{u-m_{\Lambda_c}^2}\gamma^\nu N(p_1).
\end{aligned}
\tag{3.10}
$$

In the above, $q = p_1 - p_4$, and $s = (p_1 + p_2)^2$ and $t = (p_1 - p_3)^2$ are the standard Mendelstam variables.

The spin and isospin averaged differential cross sections for these two-body processes are then

$$
\begin{aligned}
\frac{d\sigma_{\psi N\to \bar{D}\Lambda_c}}{dt} &= \frac{1}{64\pi s p_i^2}|M_{4a}+M_{4b}|^2, \\
\frac{d\sigma_{\psi N\to \bar{D}^*\Lambda_c}}{dt} &= \frac{1}{64\pi s p_i^2}|M_{5a}+M_{5b}|^2,
\end{aligned}
\tag{3.11}
$$

where $|M_{4a}+M_{4b}|^2$ and $|M_{5a}+M_{5b}|^2$ can be evaluated using the software package FORM [47].

In evaluating the amplitudes, we have again introduces monopole form factors of Eq. (3.6) at the vertices with the cutoff parameter $\Lambda = 1$ GeV. The resulting cross sections for $\psi N \to \bar{D}\Lambda_c$ and $\psi N \to \bar{D}^*\Lambda_c$ are shown in Fig. 4 by the dashed and
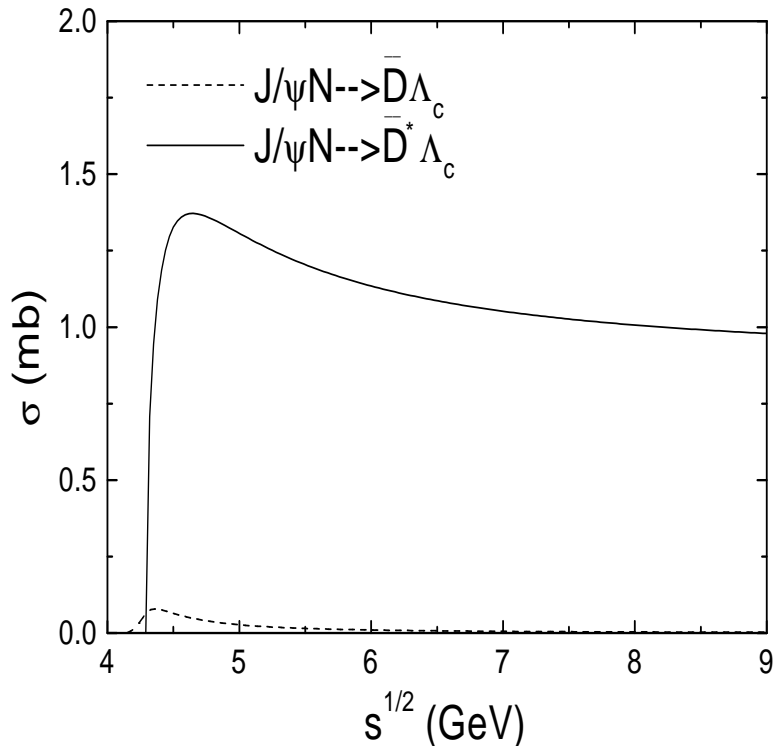
Fig. 4. Cross section for $J/\psi$ absorption by nucleon due to charmed hadron exchange as a function of center-of-mass energy.

solid curves, respectively. Their values are seen to be less than 1 mb. Furthermore, $\sigma_{J/\psi N \to \bar{D}^* \Lambda_c}$ is much larger than $\sigma_{J/\psi N \to \bar{D}\Lambda_c}$ due to the three vector mesons coupling, which has been shown to increase significantly the $J/\psi - \pi$ absorption cross section as well [23].

In Ref. [46], only diagram (4a) in Fig. 3 has been studied, and the result there is about a factor of 4 larger than our cross section for $J/\psi N \to \bar{D}\Lambda_c$, which includes also diagram (4b). The larger cross section in Ref. [46] is again due to both a larger cutoff parameter of 2 GeV versus 1 GeV used here and the use of four momentum instead of three momentum transfer in the form factors. Our total $J/\psi - N$ absorption cross section due to charmed hadron exchange is, however, larger as we have also included

the more important processes shown by diagrams (5a) and (5b).

C.   Anomalous parity interactions
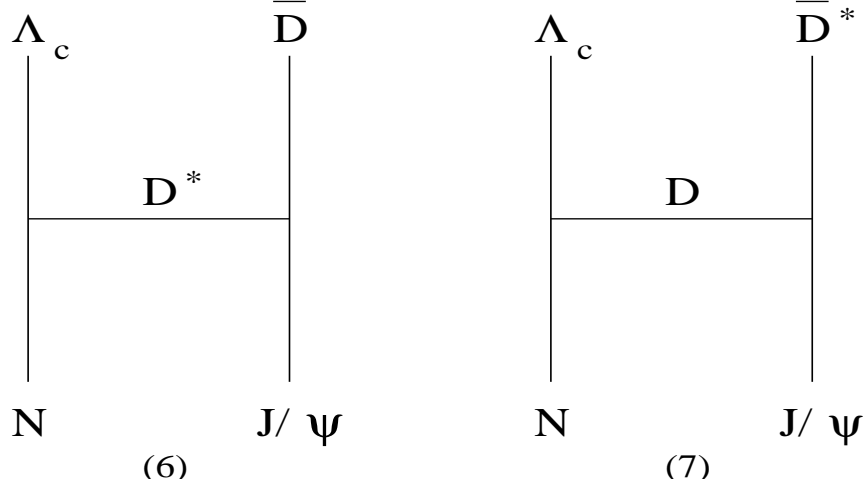


Fig. 5. $J/\psi$ absorption by nucleon via charmed meson exchange through the anomalous parity interactions.

There are also anomalous parity interactions of $J/\psi$ with charmed mesons [45], i.e.,

$$\mathcal{L}_{\psi D^* D} = g_{\psi D^* D} \varepsilon_{\alpha\beta\mu\nu}(\partial^\alpha \psi^\beta)[(\partial^\mu \bar{D}^{*\nu})D + \bar{D}(\partial^\mu D^{*\nu})], \qquad (3.12)$$

which not only introduces additional diagrams for the processes shown in Fig. 1 but also leads to the reactions $J/\psi N \to \bar{D}\Lambda_c$ via $D^*$ exchange and $J/\psi N \to \bar{D}^*\Lambda_c$ via $D$ exchange shown by the diagrams in Fig. 5.

The amplitudes for the process $J/\psi N \to \bar{D}\Lambda_c$ and $J/\psi N \to \bar{D}^*\Lambda_c$ are given by

$$M_6 = M_6^\mu \varepsilon_{2\mu}, \quad M_7 = M_7^{\mu\nu} \varepsilon_{2\mu}\varepsilon_{4\nu}, \qquad (3.13)$$

with $\varepsilon_{2\mu}$ and $\varepsilon_{4\nu}$ again being the polarization vectors of $J/\psi$ and $D^*$, respectively,

and

$$M_6^\mu = -g_{\psi D^* D} g_{D^* N \Lambda_c} \frac{1}{t - m_{D^*}^2} \varepsilon^{\mu\nu\alpha\beta} p_{2\alpha}(p_1 - p_3)_\beta \bar{\Lambda}_c(p_3)\gamma_\nu N(p_1),$$

$$M_7^{\mu\nu} = ig_{\psi D^* D} g_{D N \Lambda_c} \frac{1}{t - m_D^2} \varepsilon^{\mu\nu\alpha\beta} p_{2\alpha} p_{4\beta} \bar{\Lambda}_c(p_3)\gamma_5 N(p_1). \tag{3.14}$$

Because of the anomalous parity in the $\Psi D^* D$ vertex, the process $J/\Psi N \to \bar{D}\Lambda_c$ via $D^*$ exchange does not interfere with the similar process via $D$ exchange shown in Fig. 3. The differential cross sections for the two anomalous processes in Fig. 5 are given by similar expressions as Eqs. (3.11) and (3.11) with

$$\begin{aligned}
|M_6|^2 &= \frac{g_{\psi D^* D}^2 g_{D^* N \Lambda_c}^2}{12} \frac{1}{(t - m_{D^*}^2)^2} \left\{ 4m_\psi^2[2(m_N^2 + m_{\Lambda_c}^2)t - t^2 - (m_{\Lambda_c}^2 - m_N^2)^2] \right. \\
&+ 2(m_{\Lambda_c}^2 - m_N^2)[(m_\psi^2 + m_{\Lambda_c}^2 - u)^2 - (s - m_N^2 - m_\psi^2)^2] \\
&- [2(m_N^2 + m_{\Lambda_c}^2) - t](2m_\psi^2 + m_{\Lambda_c}^2 + m_N^2 - u - s)^2 \\
&- t(m_{\Lambda_c}^2 - m_N^2 + s - u)^2 \\
&\left. - 2[(m_N - m_{\Lambda_c})^2 - t][4m_\psi^2 t - (2m_\psi^2 + m_N^2 + m_{\Lambda_c}^2 - u - s)^2] \right\}, \tag{3.15}
\end{aligned}$$

and

$$\begin{aligned}
|M_7|^2 &= \frac{g_{\Psi D^* D}^2 g_{D N \Lambda_c}^2}{6} \frac{1}{(t - m_D^2)^2}[(m_N - m_{\Lambda_c})^2 - t] \\
&\times [(m_\psi^2 + M_{D^*}^2 - t)^2 - m_\psi^2 m_{D^*}^2], \tag{3.16}
\end{aligned}$$

where $u = (p_1 - p_4)^2$.

The coupling constant in the anomalous parity interaction has been determined to be $g_{\psi D D^*} = 8.61$ GeV$^{-1}$ from the radiative decay of $D^*$ to $D$ using the vector dominance model [45]. With a monopole form factor similar to Eq. (3.6) at the $D^* N \Lambda_c$ vertex and a cutoff parameter of 1 GeV, the cross sections for the reactions $J/\psi N \to D\Lambda_c$ due to $D^*$ exchange and $J/\psi N \to D^*\Lambda_c$ due to $D$ exchange are shown
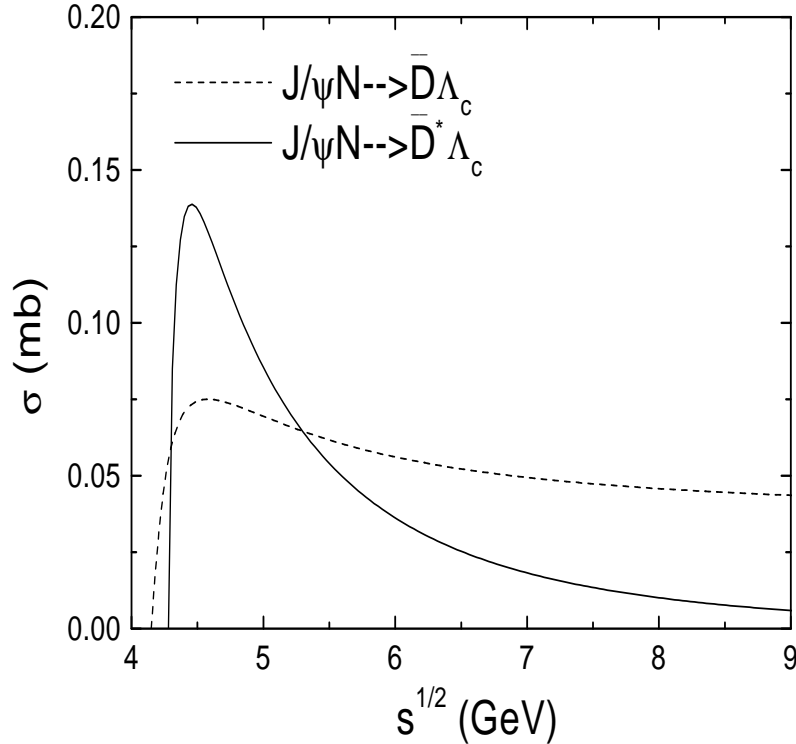
Fig. 6. Contribution of anomalous interactions to the cross section for $J/\psi$ absorption by nucleon as a function of center-of-mass energy.

in Fig. 6. Their values are seen to be less than 0.15 mb, which is negligible compared to the contributions from the normal interactions studied in A and B of this chapter.

We note that the two processes in Fig. 5 due to the anomalous interaction have also been studied in Ref. [46]. Their coupling constant is related to ours by $g_{\psi DD^*}/m_{J/\psi}$, where $m_{J/\psi}$ is the mass of $J/\psi$. Since they assume that $g_{\psi DD^*} = g_{\psi DD} = 7.64$ based on an incorrect quotation from Ref. [23], the strength of the anomalous coupling constant in their study is only 2.47 GeV$^{-1}$ and is about a factor of 3 smaller than that used here. However, they have used a much larger value for $g_{D^*N\Lambda_c} = -19$ than that given by the SU(4) relation. As a result, their cross section for diagram (7) in Fig. 5 should have a similar magnitude as ours while that of diagram (6) should be

larger than our value. Because of the larger value of cutoff parameter of 2 GeV and the use of four momentum transfer in the form factor, the results in Ref.[46] from the anomalous interaction turn out to be order-of-magnitude larger than ours.

We have not included additional diagrams due to the anomalous parity interactions in processes involving three-body final states shown in Fig. 1. As shown in Ref. [45], the anomalous interaction is not important for $J/\psi - \rho$ absorption and increases the $J/\psi - \pi$ absorption cross section by only about 50%. Thus, inclusions of processes will probably increase the $J/\psi - N$ absorption cross section calculated here by less than 50%.

D.   Total $J/\psi$ absorption cross section by nucleon

The total $J/\psi$ absorption cross section by nucleon, obtained by adding the contributions shown in Figs. 2 and 6 is given in Fig. 7. At low center-of-mass energies, the cross section is dominated by the process $J/\psi N \to \bar{D}^*\Lambda_c$ while at high center-of-mass energies, the processes $J/\psi N \to D^*\bar{D}N$ and $J/\psi N \to \bar{D}^*DN$ due to the virtual pion cloud of the nucleon are most important. The total $J/\psi$ absorption cross section is at most 5 mb and is consistent with that extracted from $J/\psi$ production in photo-nucleus and proton-nucleus reactions.

E.   Discussion

Our results are not much affected if we use the coupling constants $g_{DN\Lambda_c} \sim 6.7 - 7.9$ and $g_{D^*N\Lambda_c} \sim -7.5$ determined from the QCD sum rules [48] instead from the SU(4) symmetry. With these values, $\sigma_{\psi N \to \bar{D}\Lambda_c}$ will be even smaller while $\sigma_{\psi N \to \bar{D}^*\Lambda_c}$ will be about a factor of two larger than those shown in Fig. 4. In this case, the $J/\psi - N$ absorption cross section is only increased by about 1 mb. On the other hand, if the
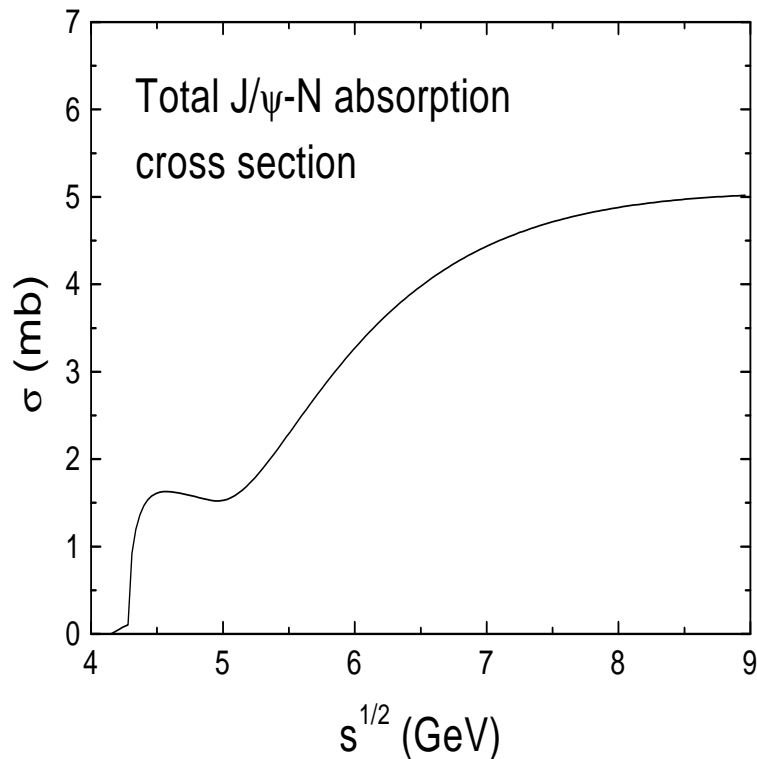
Fig. 7. Total cross section for $J/\psi$ absorption by nucleon as a function of center-of-mass energy.

cutoff parameter is taken to be $\Lambda = 2$ GeV at vertices involving charmed hadrons as suggested by QCD sum rules [48], then the total $J/\psi - N$ absorption cross section increases to about 10 mb, which is about a factor of two larger than the empirical value from $J/\psi$ production in photo-nucleus and proton-nucleus reactions. With this cutoff parameter, the $J/\psi - \pi$ absorption cross section is also about 10 mb as shown in Ref.[23]. Since the meson-exchange model is based on effective hadronic Lagrangians, one can either fit the empirical $J/\psi - N$ absorption cross section by treating the cutoff parameter as a phenomenological parameter, or use the cutoff parameter from the QCD sum rules but with a different effective Lagrangian. In the former case, a cutoff parameter of 1 GeV is required at the interaction vertices involving charmed

hadrons in order to have the correct $J/\psi_N$ absorption cross section. The meson-exchange model of Ref.[23] then gives a $J/\psi - \pi$ absorption cross section of about 3 mb, which is also consistent with that used in the comover model for $J/\psi$ suppression in heavy ion collisions [9, 24]. In the latter case, one may follow the suggestion of Ref.[49] to drop the nongradient pion couplings in the effective Lagrangians, as they breaks the chiral $SU(2) \times SU(2)$ symmetry. As shown in Ref. [49], neglecting these terms reduces the $J/\psi - \pi$ absorption cross section by about a factor of two, leading again to a $J/\psi - \pi$ absorption cross section similar to that in the comover model. The $J/\psi - N$ absorption cross section obtained with such an effective Lagrangian is expected to be reduced as well.

CHAPTER IV

CHARMED HADRON PRODUCTION IN HADRONIC REACTIONS

The effective Lagrangian introduced in Chapter II also allows us to study charmed hadron production in meson-nucleon and nucleon-nucleon reactions. These reactions are relevant to charm production in relativistic heavy ion collisions at both SPS and RHIC.

A. Charmed hadron production in meson-nucleon reactions*
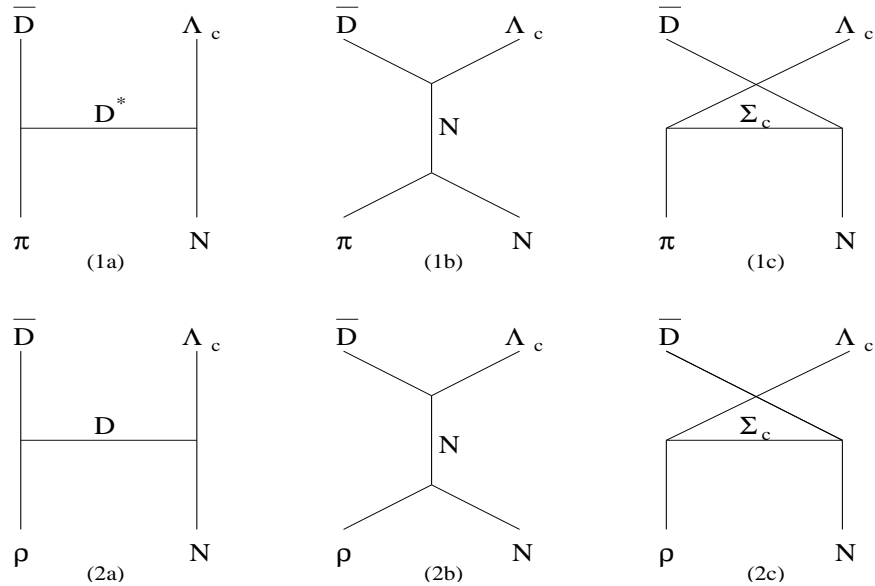


Fig. 8. Charmed meson production from meson-nucleon scattering.

Possible processes for charmed meson production from meson-nucleon scattering are $\pi N \rightarrow \bar{D} \Lambda_c$ and $\rho N \rightarrow \bar{D} \Lambda_c$ as shown by the diagrams in Fig. 8. For both pion-nucleon and rho-nucleon reactions, there are $t$ channel charmed meson exchange

---

*Reprinted with permission from "Charm meson production from meson nucleon scattering" by W. Liu and C. M. Ko, 2002. Physics Letter B533, 259-264. 2004 by Elsevier. Available at doi:10.1016/S0370-2693(02)01661-1.

diagrams, $s$ channel nucleon pole diagrams, and $u$ channel charmed baryon pole diagrams.

Besides those interaction Lagrangians already given in Eqs.(3.1) and (3.8), other interaction Lagrangian densities that are relevant to these processes are given as follows:

$$
\begin{aligned}
\mathcal{L}_{\pi\Sigma_c\Lambda_c} &= \frac{f_{\pi\Sigma_c\Lambda_c}}{m_\pi}\bar{\Lambda}_c\gamma^5\gamma^\mu\vec{\Sigma}_c\cdot\partial_\mu\vec{\pi} + \text{H.c.}, \\
\mathcal{L}_{\rho\Sigma_c\Lambda_c} &= g_{\rho\Sigma_c\Lambda_c}\bar{\Lambda}_c\gamma^\mu\vec{\Sigma}_c\cdot\vec{\rho}_\mu + \text{H.c.}, \\
\mathcal{L}_{DN\Sigma_c} &= \frac{f_{DN\Sigma_c}}{m_D}(\bar{N}\gamma_5\gamma^\mu\vec{\tau}\cdot\vec{\Sigma}_c\partial_\mu\bar{D} + \vec{\tau}\cdot\bar{\vec{\Sigma}}_c\gamma_5\gamma^\mu N\partial_\mu D).
\end{aligned}
\tag{4.1}
$$

The coupling constants in the above interaction Lagrangians are not known empirically, and we determine them according to the following SU(4) relations [31, 32]:

$$
\begin{aligned}
\frac{f_{DN\Lambda_c}}{m_D} &= \frac{3-2\alpha_D}{\sqrt{3}}\frac{f_{\pi NN}}{m_\pi} \simeq \frac{f_{\pi NN}}{m_\pi} = 7.18\ \text{GeV}^{-1}, \\
\frac{f_{\pi\Sigma_c\Lambda_c}}{m_\pi} &= 2\frac{\alpha_D}{\sqrt{3}}\frac{f_{DN\Lambda_c}}{m_D} \simeq 2.66\ \text{GeV}^{-1}, \\
\frac{f_{DN\Sigma_c}}{m_D} &= (2\alpha_D - 1)\frac{f_{DN\Lambda_c}}{m_D} = 2.01\ \text{GeV}^{-1}, \\
g_{\rho\Sigma_c\Lambda_c} &= \frac{2}{\sqrt{3}}g_{\rho NN} \simeq 3.75.
\end{aligned}
\tag{4.2}
$$

In the above, $f_{\pi NN}$ and $f_{DN\Lambda_c}$ are the pseudovector coupling constants in the interaction Lagragians

$$
\begin{aligned}
\mathcal{L}_{\pi NN} &= -\frac{f_{\pi NN}}{m_\pi}\bar{N}\gamma_5\gamma^\mu\vec{\tau}N\cdot\partial_\mu\vec{\pi}, \\
\mathcal{L}_{DN\Lambda_c} &= \frac{f_{DN\Lambda_c}}{m_D}(\bar{N}\gamma_5\gamma^\mu\Lambda_c\partial_\mu D + \partial_\mu\bar{D}\bar{\Lambda}_c\gamma_5\gamma^\mu N).
\end{aligned}
\tag{4.3}
$$

The $f_{\pi NN}$ is related to the pseudoscalar coupling constant $g_{\pi NN}$ in Eq.(3.1) by

$$
f_{\pi NN} = \frac{m_\pi}{2m_N}g_{\pi NN} \simeq 1,
\tag{4.4}
$$

where $m_\pi$ and $m_N$ are the pion and nucleon masses, respectively.

The amplitudes for the two processes in Fig. 8 can be written as

$$
\begin{aligned}
\mathcal{M}_1 &= \mathcal{M}_{1a} + \mathcal{M}_{1b} + \mathcal{M}_{1c}, \\
\mathcal{M}_2 &= (\mathcal{M}_{2a}^\mu + \mathcal{M}_{2b}^\mu + \mathcal{M}_{2c}^\mu)\varepsilon_\mu,
\end{aligned}
\tag{4.5}
$$

where $\varepsilon_\mu$ is the polarization vector of rho meson. The amplitudes $\mathcal{M}_{1a}, \mathcal{M}_{1b}$ and $\mathcal{M}_{1c}$ are for the top three diagrams in Fig. 8 and are given by

$$
\begin{aligned}
\mathcal{M}_{1a} &= -g_{\pi DD^*}g_{D^*N\Lambda_c}(\tau^i)_{\alpha\beta}(p_1+p_3)^\mu \bar{\Lambda}_c(p_4)\gamma^\nu N(p_2) \\
&\quad \times \frac{1}{t-m_{D^*}^2}[g_{\mu\nu} - \frac{(p_1-p_3)_\mu (p_1-p_3)_\nu}{m_{D^*}^2}], \\
\mathcal{M}_{1b} &= \frac{f_{\pi NN}f_{DN\lambda_c}}{m_D m_\pi}(\tau^i)_{\alpha\beta}\bar{\Lambda}_c(p_4)\slashed{p}_3 \times \frac{m_N - \slashed{q}_s}{s-m_N^2}\slashed{p}_1 N(p_2), \\
\mathcal{M}_{1c} &= \frac{f_{\pi\Sigma_c\Lambda_c}f_{DN\Lambda_c}}{m_\pi m_D}(2\delta_{ij}\tau^j)_{\alpha\beta}\bar{\Lambda}_c\slashed{p}_1 \times \frac{m_{\Sigma_c} - \slashed{q}_u}{u-m_{\lambda_c}^2}\slashed{p}_3 N,
\end{aligned}
\tag{4.6}
$$

while the amplitudes $\mathcal{M}_{2a}^\mu, \mathcal{M}_{2b}^\mu$, and $\mathcal{M}_{2b}^\mu$ are for the bottom three diagrams, and they are

$$
\begin{aligned}
\mathcal{M}_{2a}^\mu &= \frac{-if_{DN\Lambda_c}g_{\rho DD}}{m_D}(\tau^i)_{\alpha\beta}(2p_3-p_1)^\mu \times \bar{\Lambda}_c\gamma_5 \frac{\slashed{p}_1 - \slashed{q}_3}{t-m_D^2}N, \\
\mathcal{M}_{2b}^\mu &= \frac{if_{DN\Lambda_c}g_{\rho NN}}{m_D}(\tau^i)_{\alpha\beta}\bar{\Lambda}_c\gamma_5\slashed{p}_3 \frac{\slashed{q}_s + m_N}{s-m_N^2}(\gamma^\mu + i\frac{k_\rho}{2m_N}\sigma^{\nu\mu}p_{1\nu})N(p_2), \\
\mathcal{M}_{2c}^\mu &= \frac{if_{DN\Sigma_c}g_{\rho\Sigma_c\Lambda_c}}{m_D}(2\delta_{ij}\tau^j)_{\alpha\beta}\bar{\Lambda}_c\gamma^\mu \times \frac{\slashed{q}_u + m_{\Sigma_c}}{u-m_{\Sigma_c}^2}\gamma_5\slashed{p}_3 N.
\end{aligned}
\tag{4.7}
$$

In the above, $p_1, p_2, p_3$ and $p_4$ denote the momenta of $\pi(\rho)$, $N$, $\bar{D}$ and $\Lambda_c$, respectively; $s = (p_1 + p_2)^2$, $t = (p_1 - p_3)^2$, and $u = (p_1 - p_4)^2$ are the Mendelstam variables; and $q_s = p_1 + p_2$ and $q_u = p_2 - p_3$.

The isospin- and spin-averaged differential cross sections for the two processes in

Fig. 8 are then

$$\frac{d\sigma_{\pi N \to \bar{D}\Lambda_c}}{dt} = \frac{1}{768\pi s p_i^2}|\mathcal{M}_1|^2,$$
$$\frac{d\sigma_{\rho N \to \bar{D}\Lambda_c}}{dt} = \frac{1}{2304\pi s p_i^2}|\mathcal{M}_2|^2. \tag{4.8}$$

The squared invariant scattering amplitudes $|\mathcal{M}_1|^2$ and $|\mathcal{M}_2|^2$, which include the summation over the spins and isospins of both initial and final particles, are again evaluated using the software package $FORM$ [47]. In evaluating these cross sections, we have introduced form factors at the interaction vertices. For three-point vertices, i.e., $\pi DD^*$, $\rho DD$, $\rho NN$, $\pi NN$, $DN\Lambda_c$, $D^*N\Lambda_c$, $DN\Sigma_c$, and $\rho\Sigma_c\Lambda_c$, they are taken to have the form [32, 33, 50]

$$f_1 = \frac{\Lambda^2}{\Lambda^2 + \mathbf{q}^2}, \quad f_2 = \frac{\Lambda^2}{\Lambda^2 + \mathbf{p}_i^2}. \tag{4.9}$$

where $f_1$ is for $t$ and $u$ channels and $f_2$ for $s$ channel with $\mathbf{q}^2$ and $\mathbf{p}_i^2$ being, respectively, the squared three momentum transfer and squared initial three momentum in the center-of-mass frame of the pion or rho meson and nucleon. In studying $J/\psi$ absorption in Chapter III and charmed meson scattering in Refs.[21, 23, 45] using the same interaction Lagrangians, values for the cutoff parameter $\Lambda$ have been taken to be 1 or 2 GeV. We use these values for the present study as well.

We first show the results obtained with a cutoff parameter $\Lambda = 1$ GeV. In Fig. 9, the cross sections for charmed meson production from meson-nucleon scattering are given as functions of center-of-mass energy. It is seen that the cross section for the reaction $\pi N \to \bar{D}\Lambda_c$ (dotted curve) has a peak value of about 0.2 mb. Although, this value is much larger than that predicted by the QGSM model [16], it is mainly due to the $s$ channel that involves a nucleon pole as shown by the dashed curve in Fig. 10, where the cross sections from individual amplitudes are shown. The contribution
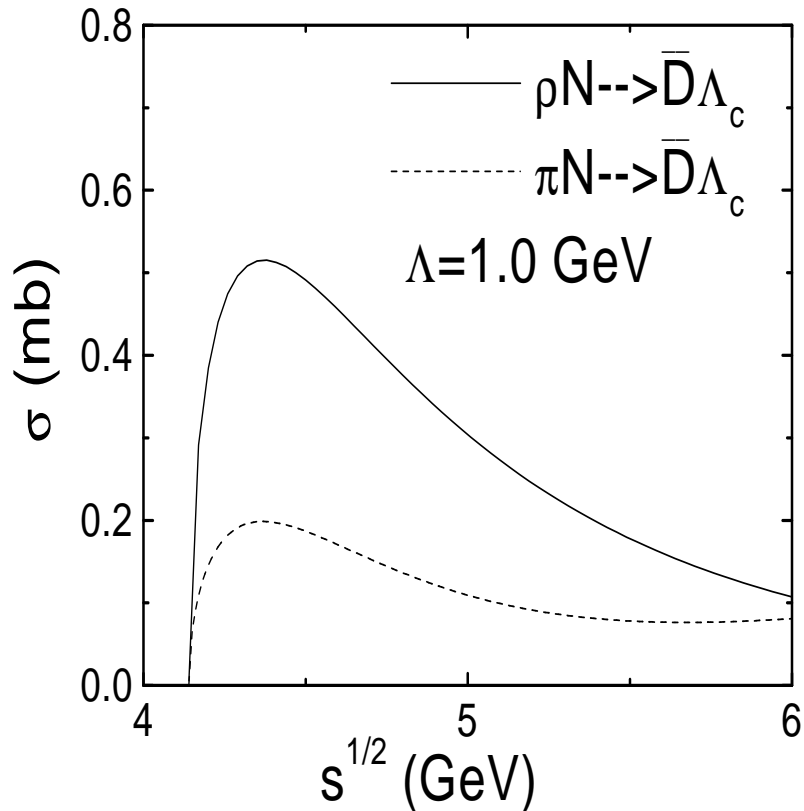
Fig. 9. Cross section for charmed meson production from meson-nucleon scattering as a function of center-of-mass energy for cutoff parameter of 1 GeV.

from the $t$ channel charmed vector meson exchange (solid curve) at low center-of-mass energy has a similar magnitude as found in QGSM, while the $u$ channel contribution (dotted curve) is indeed negligible as assumed in Ref. [16].

The cross section for the reaction $\rho N \rightarrow \bar{D}\Lambda_c$ from rho-nucleon scattering shown by the solid curve in Fig. 9 is about a factor of two larger than that from pion-nucleon scattering. The relative importance of the contributions from the $s$, $t$, and $u$ channels in this case is shown in Fig. 11. Again, the dominant contribution is from $s$ channel, while the $t$ and $u$ channel contributions are much smaller.

The magnitude of charmed meson production cross sections depends strongly on the value of the cutoff parameter. If we use a larger value of $\Lambda = 2$ GeV as
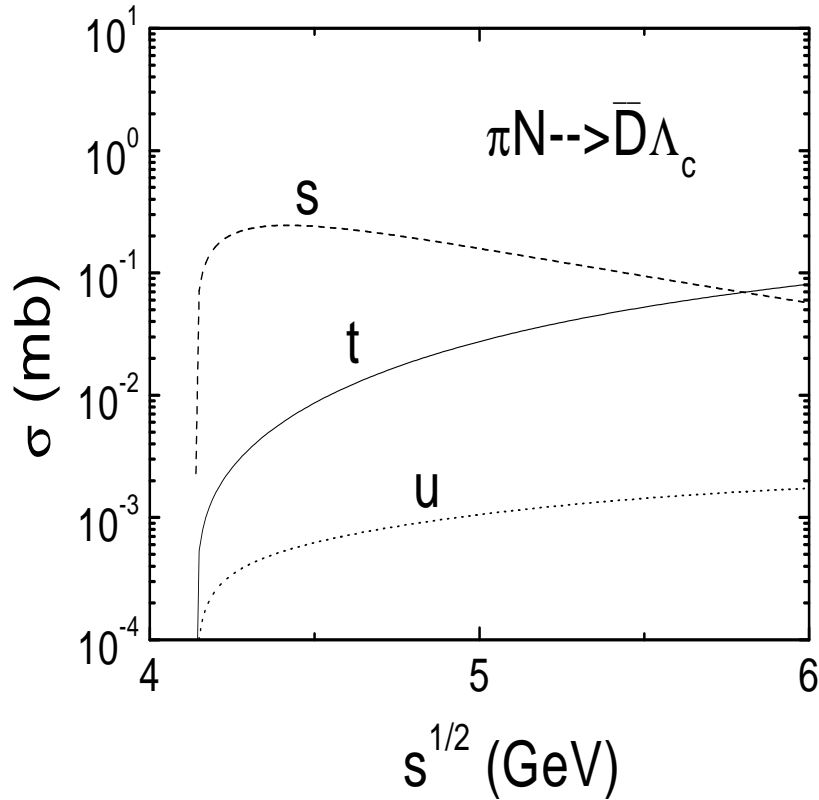
Fig. 10. Contributions from $t$, $s$, and $u$ channels to the cross section for charmed meson production from pion-nucleon scattering as functions of center-of-mass energies with cutoff parameter $\Lambda = 1$ GeV.

suggested by the QCD sum rules [48], these cross sections are increased by an order of magnitude. On the other hand, their values are reduced by more than an order of magnitude if a smaller value of $\Lambda = 0.5$ GeV is used. We note that to reproduce the empirical cross section for kaon production from pion-nucleon scattering, i.e., $\pi N \to K\Lambda$, using the same SU(4) invariant Lagrangian at the Born approximation requires $\Lambda \sim 0.4$ GeV. Because of the smaller sizes of charmed hadrons, we expect, however, that the cutoff parameter at interaction vertices involving these particles should have a larger value than at those involving strange hadrons. Using $\Lambda = 1$ GeV for charmed meson production thus seems reasonable.
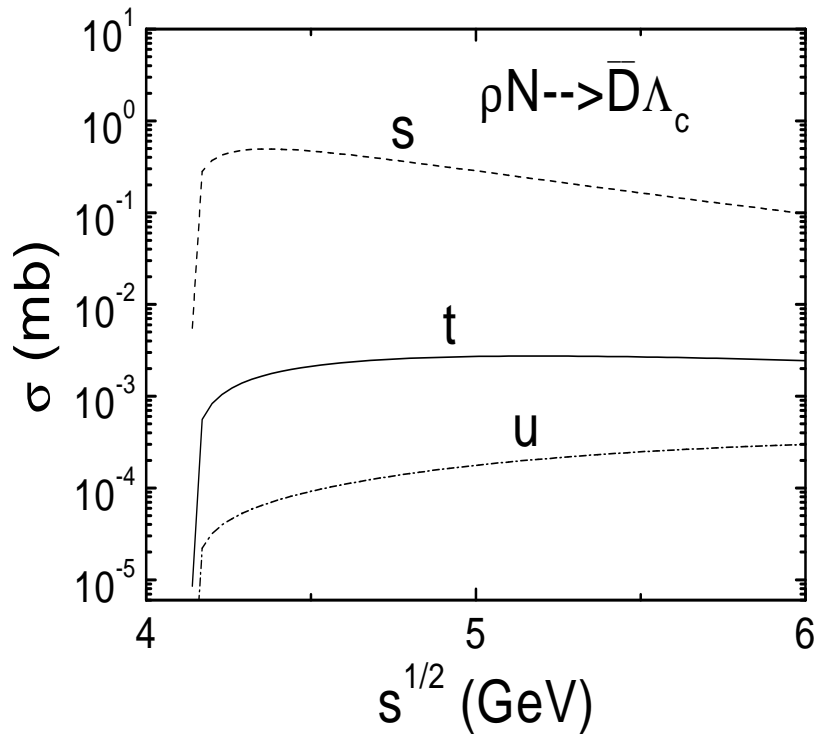
Fig. 11. Same as Fig. 10 for the cross section of charmed meson production from rho-nucleon scattering.

Since our cross sections for charmed meson production are much larger than that given by the QGSM model, they would lead to too large an enhancement of charmed meson production if used during the initial string stage of heavy ion collisions as in Ref. [16]. On the other hand, more reasonable results for charmed hadron production are expected if these cross sections are used only for collisions between mesons and baryons in the hadronic matter.

B.   Charmed hadron production in proton-proton reactions*

Possible reactions for charmed hadron production in proton-proton collisions near threshold are $pp \rightarrow \bar{D}^0 p \Lambda_c^+$ and $pp \rightarrow \bar{D}^{*0} p \Lambda_c^+$. In the following, we discuss their contributions separately.

1. $pp \rightarrow \bar{D}^0 p \Lambda_c^+$
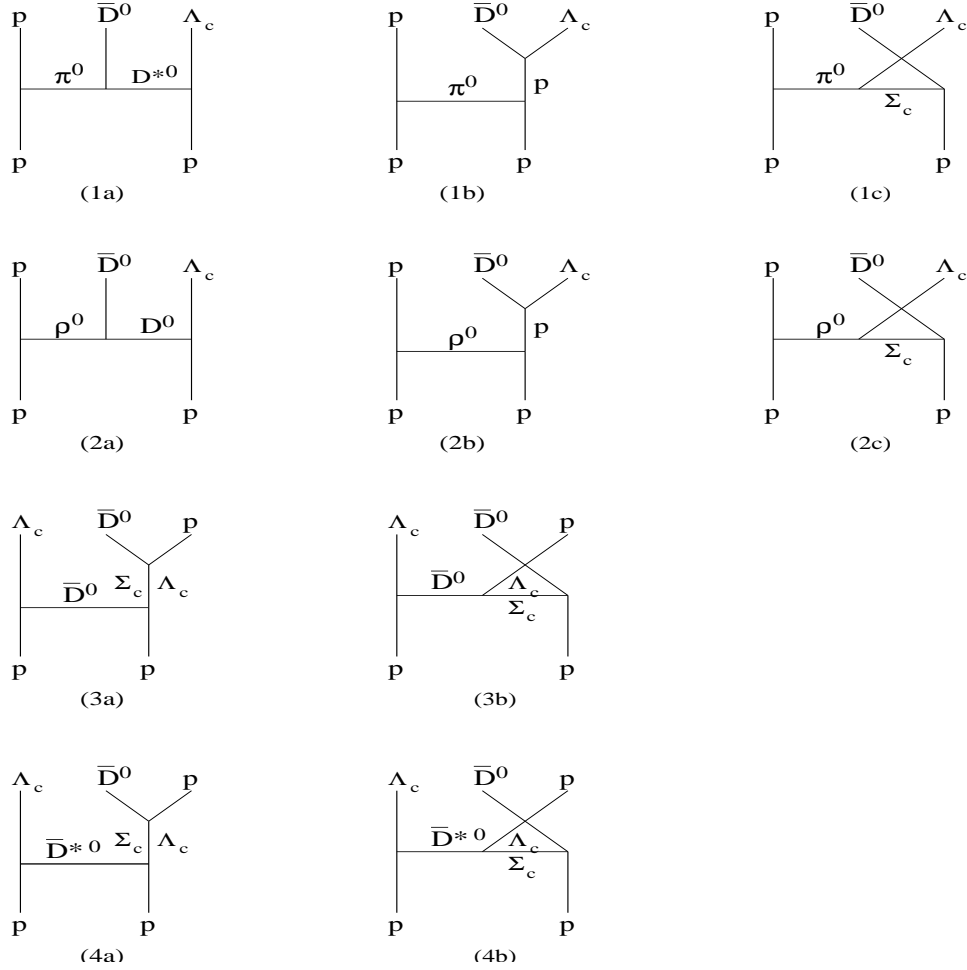


Fig. 12. Charmed hadron production from $pp \rightarrow \bar{D}^0 p \Lambda_c^+$.

Diagrams for the reaction $pp \rightarrow \bar{D}^0 p \Lambda_c^+$ are shown in Fig. 12. They involve the exchange of pion $((1a) - (1c))$, rho meson $((2a) - (2c))$, $D$ $((3a) - (3b))$, and $D^*$ $((4a) - (4b))$. With the interaction Lagrangians given in Eqs.(3.1) and (4.1), the

amplitudes for the four processes are given by

$$
\begin{aligned}
\mathcal{M}_1 &= -ig_{\pi NN}\bar{p}(p_3)\gamma_5 p(p_1)\frac{1}{t-m_\pi^2}(\mathcal{M}_{1a}+\mathcal{M}_{1b}+\mathcal{M}_{1c}), \\
\mathcal{M}_2 &= g_{\rho NN}\bar{p}(p_3)\left[\gamma^\mu + i\frac{\kappa_\rho}{2m_N}\sigma^{\alpha\mu}(p_1-p_3)_\alpha\right]p(p_1) \\
&\quad\times \left[-g_{\mu\nu} + \frac{(p_1-p_3)_\mu(p_1-p_3)_\nu}{m_\rho^2}\right]\frac{1}{t-m_\rho^2}(\mathcal{M}_{2a}^\nu+\mathcal{M}_{2b}^\nu+\mathcal{M}_{2c}^\nu), \\
\mathcal{M}_3 &= ig_{DN\Lambda_c}\bar{\Lambda}_c(p_3)\gamma_5 p(p_1)\frac{1}{t-m_D^2}(\mathcal{M}_{3a}+\mathcal{M}_{3b}), \\
\mathcal{M}_4 &= g_{D^*N\Lambda_c}\bar{\Lambda}_c(p_3)\gamma^\mu p(p_1)\left[-g_{\mu\nu}+\frac{(p_1-p_3)_\mu(p_1-p_3)_\nu}{m_{D^*}^2}\right] \\
&\quad\times \frac{1}{t-m_{D^*}^2}(\mathcal{M}_{4a}^\nu+\mathcal{M}_{4b}^\nu), \qquad\qquad (4.10)
\end{aligned}
$$

where $p_1$ and $p_3$ are, respectively, four momenta of initial and final baryons on the left side of a diagram, and $t = (p_1-p_3)^2$ is the square of nucleon momentum transfer. The amplitudes $M_{ia}$, $M_{ib}$, and $M_{ic}$ are for the subprocesses $\pi^0 p \to \bar{D}^0\Lambda_c^+$, $\rho^0 p \to \bar{D}^0\Lambda_c^+$, $\bar{D}^0 p \to \bar{D}^0 p^+$, and $\bar{D}^{*0}p \to \bar{D}^0 p$ involving exchanged virtual mesons, and they are given explicitly by

$$
\begin{aligned}
\mathcal{M}_{1a} &= -g_{\pi DD^*}g_{D^*N\Lambda_c}\frac{1}{q^2-m_{D^*}^2}(k_1+k_3)_\mu\left[g^{\mu\nu}-\frac{(k_1-k_3)^\mu(k_1-k_3)^\nu}{m_{D^*}^2}\right]\bar{\Lambda}_c\gamma_\nu p, \\
\mathcal{M}_{1b} &= g_{\pi NN}g_{DN\Lambda_c}\frac{1}{s_1-m_N^2}\bar{\Lambda}_c(m_N-\slashed{k}_1-\slashed{k}_2)p, \\
\mathcal{M}_{1c} &= g_{\pi\Lambda_c\Sigma_c}g_{DN\Sigma_c}\frac{1}{u-m_{\Sigma_c}^2}\bar{\Lambda}_c(\slashed{k}_2-\slashed{k}_3-m_{\Sigma_c})p, \\
\mathcal{M}_{2a}^\mu &= ig_{DN\Lambda_c}g_{\rho DD}\frac{1}{q^2-m_D^2}(2k_3-k_1)^\mu\bar{\Lambda}_c\gamma^5 p, \\
\mathcal{M}_{2b}^\mu &= ig_{\rho NN}g_{DN\Lambda_c}\frac{1}{s_1-m_N^2}\bar{\Lambda}_c\gamma^5(\slashed{k}_1+\slashed{k}_2+m_N)\left(\gamma^\mu+i\frac{\kappa_\rho}{2m_N}\sigma^{\beta\mu}k_{1\beta}\right)p, \\
\mathcal{M}_{2c}^\mu &= ig_{\rho\Lambda_c\Sigma_c}g_{DN\Sigma_c}\frac{1}{u-m_{\Sigma_c}^2}\bar{\Lambda}_c\gamma^\mu(\slashed{k}_2-\slashed{k}_3+m_{\Sigma_c})\gamma^5 p, \\
\mathcal{M}_{3a} &= g_{DN\Lambda_c}^2\frac{1}{s_1-m_{\Lambda_c}^2}\bar{p}(\slashed{k}_1+\slashed{k}_2-m_{\Lambda_c})p, \\
\mathcal{M}_{3b} &= g_{DN\Lambda_c}^2\frac{1}{u-m_{\Lambda_c}^2}\bar{p}(\slashed{k}_2-\slashed{k}_3-m_{\Lambda_c})p,
\end{aligned}
$$

$$\mathcal{M}_{4a}^{\mu} = ig_{D^*N\Lambda_c}g_{DN\Lambda_c}\frac{1}{s_1 - m_{\Lambda_c}^2}\bar{p}\gamma^5(\not{k}_1 + \not{k}_2 + m_{\Lambda_c})\gamma^{\mu}p,$$

$$\mathcal{M}_{4b}^{\mu} = ig_{D^*N\Lambda_c}g_{DN\Lambda_c}\frac{1}{u - m_{\Lambda_c}^2}\bar{p}\gamma^{\mu}(\not{k}_2 - \not{k}_3 + m_{\Lambda_c})\gamma^5 p. \tag{4.11}$$

Here, $k_1$ and $k_3$ are momenta of initial and final mesons, while $k_2$ and $k_4$ are momenta of initial and final baryons in the two-body subprocesses; and $q^2 = (k_1 - k_3)^2$ is the square of meson momentum transfer.

There is no interference between amplitudes involving exchange of pseudoscalar and vector mesons. Interferences between amplitudes involving exchange of pion and $D$ meson as well as those between rho meson and $D^*$ are unimportant due to the large mass difference between light and heavy mesons. Neglecting these interferences, the total cross section for the reaction $pp \to \bar{D}^0 p\Lambda_c^+$ is then given by the sum of the cross sections for the four processes in Fig. 12 and can be expressed in terms of off-shell cross sections for the subprocesses $\pi^0 p \to \bar{D}^0\Lambda_c^+$, $\rho^0 p \to \bar{D}^0\Lambda_c^+$, $\bar{D}^0 p \to \bar{D}^0 p$, and $\bar{D}^{*0} p \to \bar{D}^0 p$. Following the method of Ref. [37] for the reaction $J/\psi N \to D(D^*)\bar{D}(\bar{D}^*)N$, the spin-averaged differential cross section for the reaction $pp \to \bar{D}^0 p\Lambda_c^+$ can be written as

$$\begin{aligned}
\frac{d\sigma_{pp \to \bar{D}^0 p\Lambda_c^+}}{dt ds_1} &= \frac{g_{\pi NN}^2}{16\pi^2 sp_i^2}k\sqrt{s_1}(-t)\frac{1}{(t - m_\pi^2)^2}\sigma_{\pi^0 p \to \bar{D}^0\Lambda_c^+}(s_1, t), \\
&+ \frac{3g_{\rho NN}^2}{32\pi^2 sp_i^2}k\sqrt{s_1}\frac{1}{(t - m_\rho^2)^2}\left[4(1 + \kappa_\rho)^2(-t - 2m_N^2)\right. \\
&+ \kappa_\rho^2\frac{(4m_N^2 - t)^2}{2m_N^2} + 4(1 + \kappa_\rho)\kappa_\rho(4m_N^2 - t)\right]\sigma_{\rho^0 p \to \bar{D}^0\Lambda_c^+}(s_1, t), \\
&+ \frac{g_{DN\Lambda_c}^2}{16\pi^2 sp_i^2}k\sqrt{s_1}[-t + (m_N - m_{\Lambda_c})^2]\frac{1}{(t - m_D^2)^2}\sigma_{\bar{D}^0 p \to \bar{D}^0 p}(s_1, t) \\
&+ \frac{3g_{D^*N\Lambda_c}^2}{32\pi^2 sp_i^2}k\sqrt{s_1}\frac{1}{(t - m_{D^*}^2)^2}\left[-4t + 4(m_{\Lambda_c} - m_N)^2 - 8m_{\Lambda_c}m_N\right. \\
&+ \frac{2(m_N^2 - m_{\Lambda_c}^2 - t)(m_N^2 - m_{\Lambda_c}^2 + t)}{m_{D^*}^2}
\end{aligned}$$

$$+ \quad \frac{2((m_{\Lambda_c} - m_N)^2 + t)t}{m_{D^*}^2} \Bigg] \sigma_{\bar{D}^{*0} p \to \bar{D}^0 p}(s_1, t). \tag{4.12}$$

In the above, $p_i$ is the center-of-mass momentum of two initial protons, $t$ is the squared four momentum transfer of exchanged meson, $s$ is the squared center-of-mass energy, and $s_1$ and $k$ are, respectively, the squared invariant mass and center-of-mass momentum of exchanged meson and the nucleon in the subprocesses. We have also included a factor of two to take into account contributions from interchanging two initial protons.

Since the charmed hadron production cross sections is sensitive to the value of cutoff parameters in the form factors at interaction vertices involving virtual charmed mesons and baryons, it is necessary to constraint this cutoff parameter empirically. Without exclusive cross sections available for charmed hadron production from proton-proton scattering, we resort to strange hadron production. Using the same hadronic model for kaon production from the reaction $pp \to K^+ p \Lambda$, this reaction can be described by similar diagrams in Fig.12 for the reaction $pp \to \bar{D}^0 p \Lambda_c^+$ with $D^0$ and $\Lambda_c$ replaced by $K^+$ and $\Lambda$, respectively, in the final states. Also, the exchanged $\bar{D}^0$ in diagrams (3a) and (3b) as well as $\bar{D}^{0*}$ in diagrams (4a) and (4b) are replaced by $K$ and $K^*$, respectively, while intermediate off-shell charmed baryons are replaced by strange baryons. With empirical coupling constants $g_{\pi K K^*} = 3.25$ and $g_{\rho K K} = 3.25$, as well as others determined via SU(3) relations [51], the measured cross section can be reproduced with a cutoff parameter $\Lambda = 0.42$ GeV in the form factors $F_2(\mathbf{q}^2)$ at vertices involving virtual strange mesons and baryons, as shown in Fig.13.

Assuming that the same cutoff parameter $\Lambda = 0.42$ GeV is applicable at vertices involving virtual charmed mesons and baryons in charmed hadron production from proton-proton reactions, resulting cross sections for the reaction $pp \to \bar{D}^0 p \Lambda_c$ from the
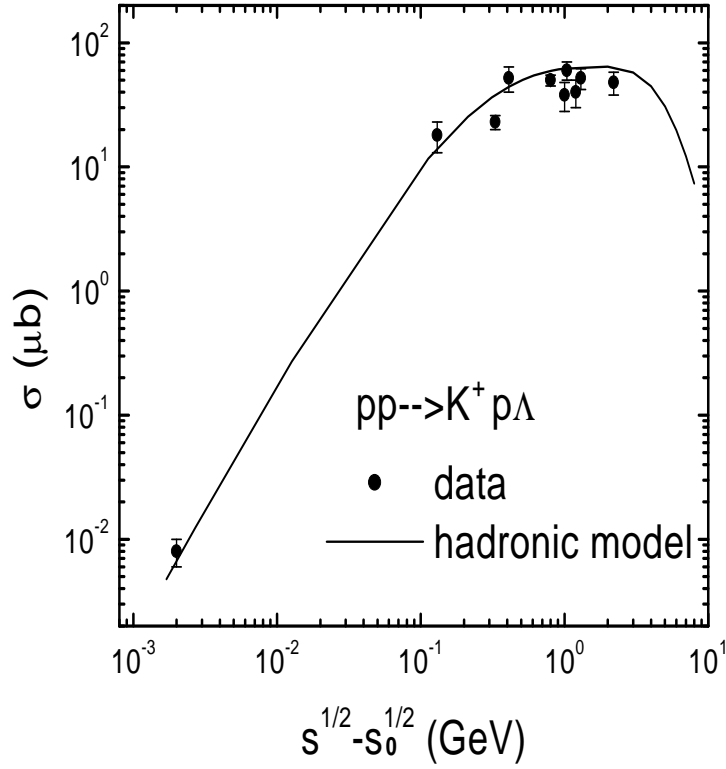
Fig. 13. Cross section for kaon production from the reaction $pp \to K^+p\Lambda$ with cutoff parameter $\Lambda = 0.42$ GeV in the form factors at interaction vertices involving exchange of strange mesons. Filled circles are experimental data taken from Ref.[52]

four possible processes of pion (solid curve), rho (dashed curve), $D$ (dotted curve), and $D^*$ (dash-dotted curve) exchanges as functions of center-of-mass energy are shown in Fig.14. It is seen that contributions from light meson exchange are more important than those from heavy meson exchange. Although we consider diagrams (1a) and (2a) in Fig.12 as exchange of pion and rho meson, respectively, they actually involve exchange of heavy $D^*$ and $D$ mesons in the subprocess $\pi^0 p \to \bar{D}^0 \Lambda_c^+$ and $\rho^0 p \to \bar{D}^0 \Lambda_c^+$, respectively. Our results that main contributions to the reaction $pp \to p\bar{D}^0 \Lambda_c^+$ are due to exchange of light mesons are not inconsistent with conclusions in Ref.[35] that

this reaction is dominated by heavy $D$ meson exchange.
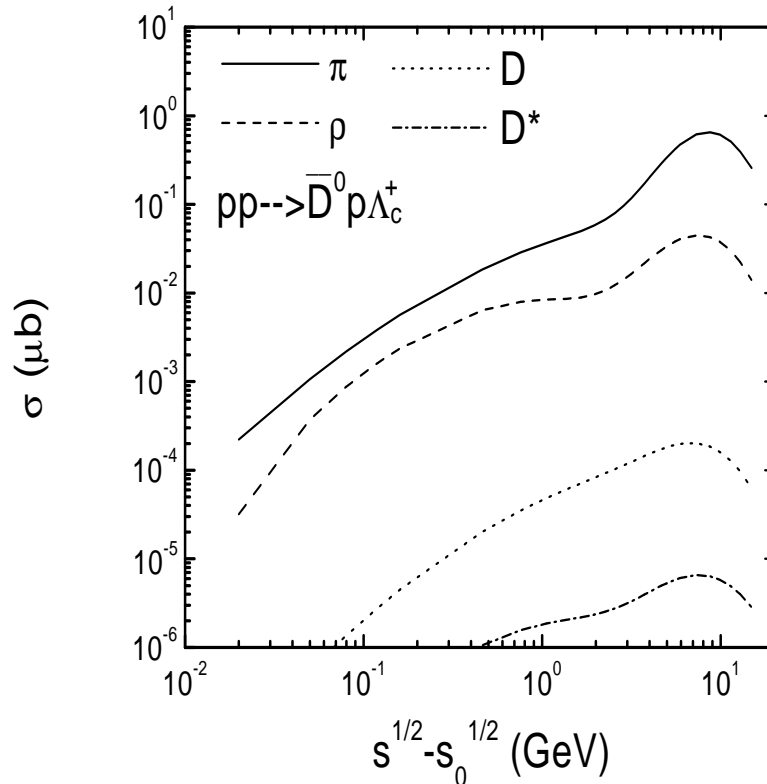


Fig. 14. Cross sections for charmed hadron production from the reaction $pp \to \bar{D}^0 p \Lambda_c^+$ due to pion (solid curve), rho meson (dashed curve), $D$ (dotted curve), and $D^*$ (dash-dotted curve).

To see the relative contributions from $s$, $t$, and $u$ channel diagrams in Fig.12, we show in Fig.15 the partial cross sections due to diagrams (1a), (1b), and (1c). It is seen that the $t$ channel diagram (1a) dominates charmed hadron production cross section at high energies while the $s$ channel diagram (1b) is most important near threshold. The contribution from the $u$ channel diagram (1c) is much smaller than those from other two diagrams. Except near threshold, our results are thus similar to those found in Ref. [35], which uses the on-shell approximation for the subprocess $\pi p \to \bar{D}^0 \Lambda_c^+$ and does not include $s$ and $u$ channel diagrams.
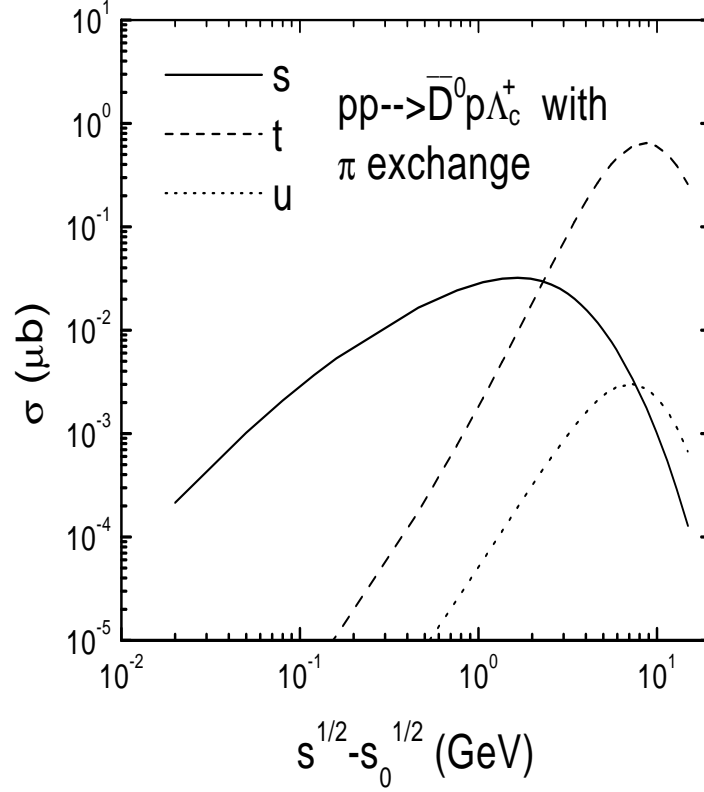
Fig. 15. Partial cross sections for $pp \to \bar{D}^0 p \Lambda_c^+$ due to contributions from different channels.

$$2. \quad pp \to \bar{D}^{*0} p \Lambda_c^+$$

For charmed hadron production from proton-proton collisions with $\bar{D}^{*0} p \Lambda_c^+$ in the final state, relevant diagrams are shown in Fig. 16. As for the reaction $pp \to \bar{D}^{*0} p \Lambda_c^+$, this reaction can proceed through pion, rho meson, $D$, and $D^*$ exchanges. Amplitudes for the four processes obtained with the interaction Lagrangians given in Eqs.(3.1) and (4.1) are given by

$$\mathcal{M}_5 = -ig_{\pi NN}\bar{p}(p_3)\gamma_5 p(p_1)\frac{1}{t - m_\pi^2}(\mathcal{M}_{5a}^\alpha + \mathcal{M}_{5b}^\alpha + \mathcal{M}_{5c}^\alpha)\epsilon_\alpha$$

$$\mathcal{M}_6 = g_{\rho NN}\bar{p}(p_3)\left[\gamma^\mu + i\frac{\kappa_\rho}{2m_N}\sigma^{\alpha\mu}(p_1 - p_3)_\alpha\right]p(p_1)$$
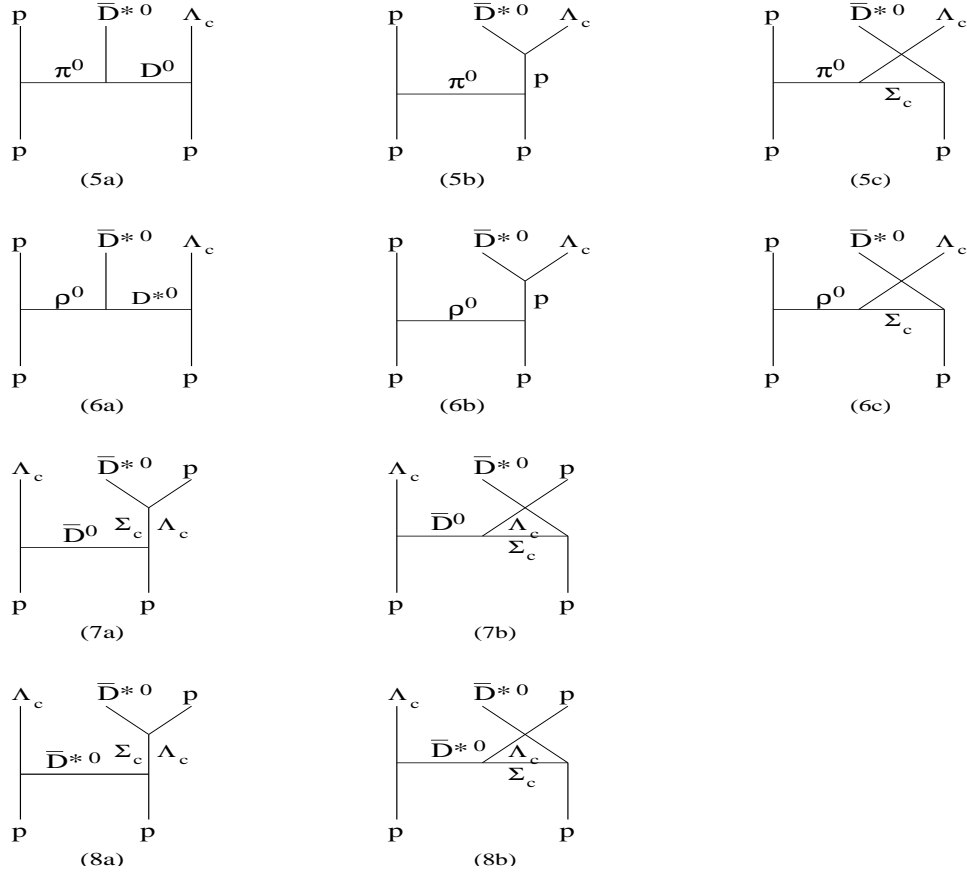
Fig. 16. Charmed hadron production from $pp \to \bar{D}^{*0}p\Lambda_c^+$.

$$\times \left[-g_{\mu\nu} + \frac{(p_1 - p_3)_\mu (p_1 - p_3)_\nu}{m_\rho^2}\right] \frac{1}{t - m_\rho^2}(\mathcal{M}_{6a}^{\nu\alpha} + \mathcal{M}_{6b}^{\nu\alpha} + \mathcal{M}_{6c}^{\nu\alpha})\epsilon_\alpha,$$

$$\mathcal{M}_7 = ig_{DN\Lambda_c}\bar{\Lambda}_c(p_3)\gamma_5 p(p_1)\frac{1}{t - m_D^2}(\mathcal{M}_{7a}^\alpha + \mathcal{M}_{7b}^\alpha)\epsilon_\alpha,$$

$$\mathcal{M}_8 = g_{D^*N\Lambda_c}\bar{\Lambda}_c(p_3)\gamma^\mu p(p_1)$$

$$\times \left[-g_{\mu\nu} + \frac{(p_1 - p_3)_\mu (p_1 - p_3)_\nu}{m_{D^*}^2}\right] \frac{1}{t - m_{D^*}^2}(\mathcal{M}_{8a}^{\nu\alpha} + \mathcal{M}_{8b}^{\nu\alpha})\epsilon_\alpha, \tag{4.13}$$

where $p_1$ and $p_3$ are again, respectively, four momenta of initial and final baryons on the left side of a diagram and $\epsilon_\alpha$ denotes the polarization vector of $D^*$ meson in final state.

Expressions for individual amplitudes can be written as follows:

$$\mathcal{M}_{5a}^{\mu} = -ig_{\pi DD^*}g_{DN\Lambda_c}\frac{1}{q^2 - m_D^2}(2k_1 - k_3)^{\mu}\bar{\Lambda}_c\gamma_5 p,$$

$$\mathcal{M}_{5b}^{\mu} = -ig_{\pi NN}g_{D^*N\Lambda_c}\frac{1}{s_1 - m_N^2}\bar{\Lambda}_c\gamma^{\mu}(\not{k}_1 + \not{k}_2 + m_N)\gamma^5 p,$$

$$\mathcal{M}_{5c}^{\mu} = ig_{\pi\Lambda_c\Sigma_c}g_{D^*N\Sigma_c}\frac{1}{u - m_{\Sigma_c}^2}\bar{\Lambda}_c\gamma^5(\not{k}_2 - \not{k}_3 + m_{\Sigma_c})\gamma^{\mu} p,$$

$$\mathcal{M}_{6a}^{\mu\nu} = g_{D^*N\Lambda_c}g_{\rho D^*D^*}\frac{1}{q^2 - m_{D^*}^2}\left[g_{\alpha\beta} - \frac{(k_1 - k_3)_{\alpha}(k_1 - k_3)_{\beta}}{m_{D^*}^2}\right]\bar{\Lambda}_c\gamma^{\alpha} p$$
$$\times \quad [2k_1^{\nu}g^{\beta\mu} - (k_1 + k_3)^{\beta}g^{\mu\nu} + 2k_3^{\mu}g^{\beta\nu}],$$

$$\mathcal{M}_{6b}^{\mu\nu} = g_{\rho NN}g_{D^*N\Lambda_c}\frac{1}{s_1 - m_N^2}\bar{\Lambda}_c\gamma^{\nu}(\not{k}_1 + \not{k}_2 + m_N)\left(\gamma^{\mu} + i\frac{\kappa_{\rho}}{2m_N}\sigma^{\beta\mu}k_{1\beta}\right) p,$$

$$\mathcal{M}_{6c}^{\mu\nu} = g_{\rho\Lambda_c\Sigma_c}g_{D^*N\Sigma_c}\frac{1}{u - m_{\Sigma_c}^2}\bar{\Lambda}_c\gamma^{\mu}(\not{k}_2 - \not{k}_3 + m_{\Sigma_c})\gamma^{\nu} p.$$

$$\mathcal{M}_{7a}^{\mu} = ig_{DN\Lambda_c}g_{D^*N\Lambda_c}\frac{1}{s_1 - m_{\Lambda_c}^2}\bar{p}\gamma^{\mu}(\not{k}_1 + \not{k}_2 + m_{\Lambda_c})\gamma^5 p,$$

$$\mathcal{M}_{7b}^{\mu} = ig_{DN\Lambda_c}g_{D^*N\Lambda_c}\frac{1}{u - m_{\Lambda_c}^2}\bar{p}\gamma^5(\not{k}_2 - \not{k}_3 + m_{\Lambda_c})\gamma^{\mu} p,$$

$$\mathcal{M}_{8a}^{\mu\nu} = g_{D^*N\Lambda_c}^2\frac{1}{s_1 - m_{\Lambda_c}^2}\bar{p}\gamma^{\nu}(\not{k}_1 + \not{k}_2 + m_{\Lambda_c})\gamma^{\mu} p,$$

$$\mathcal{M}_{8b}^{\mu\nu} = g_{D^*N\Lambda_c}^2\frac{1}{u - m_{\Lambda_c}^2}\bar{p}\gamma^{\mu}(\not{k}_2 - \not{k}_3 + m_{\Lambda_c})\gamma^{\nu} p. \tag{4.14}$$

As in the case of charmed hadron production from the reaction $pp \rightarrow \bar{D}^0 p\Lambda_c^+$, total cross section for the reaction $pp \rightarrow \bar{D}^{*0}p\Lambda_c^+$ can be expressed in terms of off-shell cross sections for the subprocesses $\pi^0 p \rightarrow \bar{D}^{*0}\Lambda_c^+$, $\rho^0 p \rightarrow \bar{D}^{*0}\Lambda_c^+$, $\bar{D}^0 p \rightarrow \bar{D}^{*0}p$, and $\bar{D}^{*0}p \rightarrow \bar{D}^{*0}p$. In this case, the spin averaged differential cross section is

$$\frac{d\sigma_{pp\rightarrow\bar{D}^0 p\Lambda_c}}{dtds_1} = \frac{g_{\pi NN}^2}{16\pi^2 sp_i^2}k\sqrt{s_1}(-t)\frac{1}{(t - m_{\pi}^2)^2}\sigma_{\pi^0 p\rightarrow\bar{D}^{*0}\Lambda_c^+}(s_1, t),$$
$$+ \quad \frac{3g_{\rho NN}^2}{32\pi^2 sp_i^2}k\sqrt{s_1}\frac{1}{(t - m_{\rho}^2)^2}\left[4(1 + \kappa_{\rho})^2(-t - 2m_N^2)\right.$$
$$+ \quad \kappa_{\rho}^2\frac{(4m_N^2 - t)^2}{2m_N^2} + 4(1 + \kappa_{\rho})\kappa_{\rho}(4m_N^2 - t)\left.\right]\sigma_{\rho^0 p\rightarrow\bar{D}^{*0}\Lambda_c^+}(s_1, t)$$
$$+ \quad \frac{g_{DN\Lambda_c}^2}{16\pi^2 sp_i^2}k\sqrt{s_1}[-t + (m_N - m_{\Lambda_c})^2]\frac{1}{(t - m_D^2)^2}\sigma_{\bar{D}^0 p\rightarrow\bar{D}^{*0}p}(s_1, t)$$

$$+ \quad \frac{3g_{D^*N\Lambda_c}^2}{32\pi^2 s p_i^2} k\sqrt{s_1} \frac{1}{(t-m_{D^*}^2)^2} \left[ -4t + 4(m_{\Lambda_c} - m_N)^2 - 8m_{\Lambda_c} m_N \right.$$

$$+ \quad \frac{2(m_N^2 - m_{\Lambda_c}^2 - t)(m_N^2 - m_{\Lambda_c}^2 + t)}{m_{D^*}^2}$$

$$+ \quad \left. \frac{2((m_{\Lambda_c} - m_N)^2 + t)t}{m_{D^*}^2} \right] \sigma_{\bar{D}^{*0}p \to \bar{D}^{*0}p}(s_1, t). \tag{4.15}$$
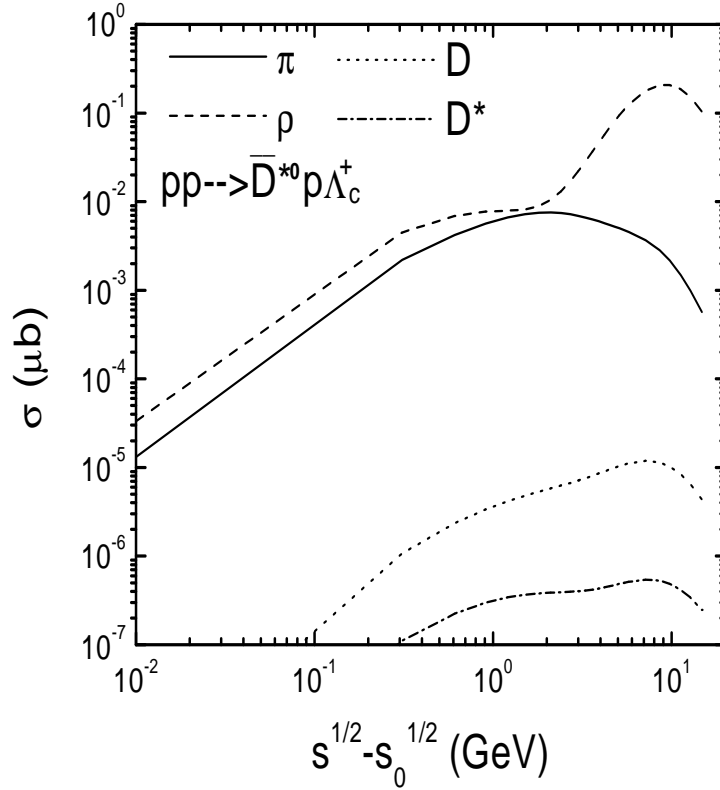


Fig. 17. Cross sections for charmed hadron production from $pp \to \bar{D}^{*0}p\Lambda_c^+$ due to pion (solid curve), rho meson (dashed curve), $D$ (dotted curve), and $D^*$ (dash-dotted curve).

Using coupling constants and cutoff parameters introduced previously, we have evaluated the cross section for the reaction $pp \to \bar{D}^{*0}p\Lambda_c^+$. In Fig. 17, we show contributions from pion (solid curve), rho meson (dashed curve), $D$ (dotted curve), and $D^*$ (dash-dotted curve) exchanges as functions of center-of-mass energy. As for

the reaction $pp \to \bar{D}^0 p \Lambda_c^+$, light meson exchanges are more important than those from heavy meson exchanges. However, the contribution from rho exchange is larger than that from pion exchange, which is opposite to that in the reaction $pp \to \bar{D}^0 \Lambda_c^+$, as a result of the couplings involving three vector mesons, which are absent in the latter reaction.

### 3. Total cross section

The total cross section for charmed hadron production from proton-proton collisions is shown in Fig.18 as a function of center-of-mass energy (solid curve). It's value at center-of-mass energy of 11.5 GeV is about 1 $\mu$b and is within the uncertainty of measured inclusive charmed hadron production cross section, which is about 2 $\mu$b as shown by solid circles with error bar [53]. The cross section decreases as energy drops and is about 1 nb at 40 MeV above threshold. Also shown in Fig.18 are the cross section for the reactions $pp \to p\bar{D}^0 \Lambda_c^+$ (dashed curve) and $pp \to p\bar{D}^{*0} \Lambda_c^+$ (dotted curve), and it is seen that the former is somewhat larger than the latter.

The cutoff parameter $\Lambda = 0.42$ GeV at interaction vertices involving virtual charmed hadrons is obtained from fitting strange hadron production with similar hadronic interaction Lagrangians and form factors. Since charmed hadrons have smaller sizes than those of strange hadrons, harder form factors with larger cutoff parameters are expected at their interaction vertices. To see how the results obtained here are affected by the cutoff parameter, we show in Fig.18 by dash-dotted curve the total cross section for charmed hadron production from proton-proton reactions using $\Lambda = 1$ GeV. It is seen that the resulting cross section is almost two order of magnitude larger than that given by $\Lambda = 0.42$ GeV and deviates strongly from the experimental data. Within our present model for charmed hadron production, a large cutoff parameter at interaction vertices involving charmed hadrons is thus excluded.

It is worthy to mention that we have not considered in the present study final states involving $\Sigma_c^+$ instead $\Lambda_c^+$ as the cross sections for such reactions are expected to be much smaller due to both larger $\Sigma_c^+$ than $\Lambda_c^+$ masses and smaller $g_{DN\Sigma_c}$ and $g_{D^*N\Sigma_c}$ coupling constants than $g_{DN\Lambda_c}$ and $g_{D^*N\Lambda_c}$ coupling constants.
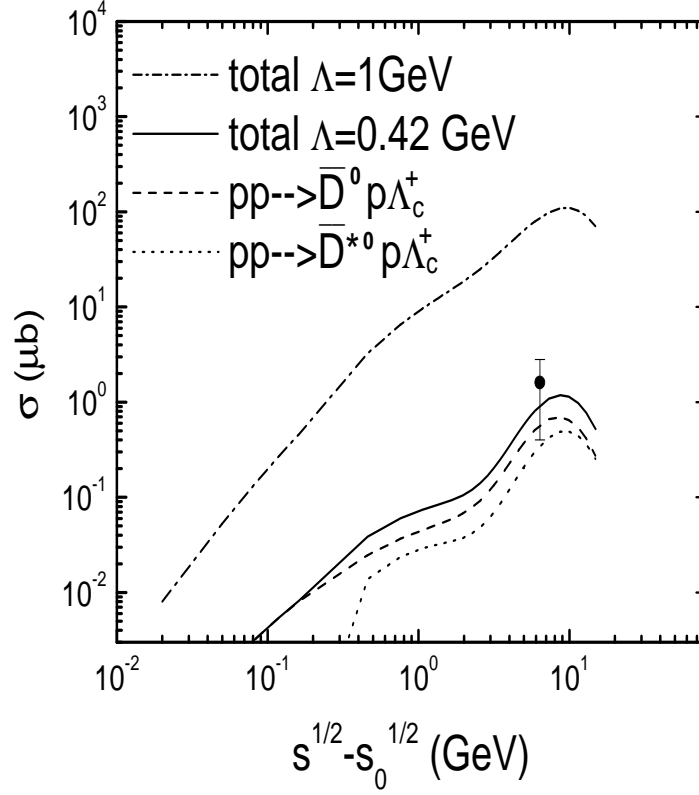


Fig. 18. Cross sections for charmed hadron production from proton-proton collisions. Dashed and dotted curves are for $pp \rightarrow p\bar{D}^0\Lambda_c^+$ and $pp \rightarrow p\bar{D}^{*0}\Lambda_c^+$, respectively, while the total cross section is shown by the solid curve. The threshold energy $s_0$ refers to that of the reaction $pp \rightarrow p\bar{D}^0\Lambda_c^+$. Experimental data are shown by filled circles [53]. Also shown by dash-dotted curve is the total cross section obtained with cutoff parameter $\Lambda = 1.0$ GeV in contrast with other curves which are based on $\Lambda = 0.42$ GeV.

CHAPTER V

CHARMED HADRON PRODUCTION FROM PHOTON-PROTON

REACTIONS*

In this chapter, the cross section for photoproduction of charmed hadrons from protons is studied using the effective Lagrangian introduced in Chapter II. Photon-hadron interactions are usually described by the vector dominance model, i.e., the photon couples to hadrons via vector mesons such as rho, omega, phi, and $J/\psi$. For a real photon, including all allowed vector mesons is equivalent to coupling the photon directly to hadrons with strengths given by their electric charges. In this study, we adopt this picture for describing production of charmed hadrons from reactions between protons and real photons. In these reactions, the final state can involve either two particles ($\bar{D}\Lambda_c$, $\bar{D}^*\Lambda_c$) or three particles ($D\bar{D}N$, $D\bar{D}^*N$, $D^*\bar{D}N$, $D^*\bar{D}^*N$). In the following, we discuss them separately and also compare the results with predictions from leading-order perturbative QCD calculations.

A. Two-body final states

For photoproduction of charmed hadrons from protons near threshold, the final states are dominated by two particles. Possible reactions are $\gamma p \to \bar{D}^0 \Lambda_c^+$ and $\gamma p \to \bar{D}^{*0} \Lambda_c^+$ as shown by diagrams in Fig. 19. Additional interaction Lagrangians needed to evaluate the cross sections for these reactions besides those given in Eq.(4.1) are:

$$\mathcal{L}_{\gamma NN} = -eA^\mu \bar{N}\gamma_\mu[(1+\tau_3)/2]N,$$
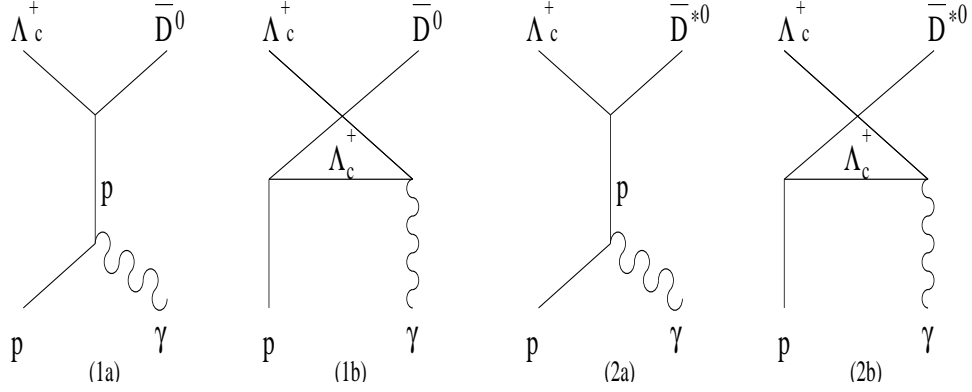
Fig. 19. Photoproduction of charmed hadrons from protons with two-body final states.

$$\mathcal{L}_{\gamma\Lambda_c\Lambda_c} \;\; = \;\; -eA^\mu\bar{\Lambda}_c\gamma_\mu\Lambda_c. \tag{5.1}$$

Amplitudes for the two reactions $\gamma p \to \bar{D}^0\Lambda_c^+$ and $\gamma p \to \bar{D}^{*0}\Lambda_c^+$ in Fig. 19 can be written, respectively, as

$$
\begin{aligned}
\mathcal{M}_1 \;\; &= \;\; (\mathcal{M}_{1a}^\mu + \mathcal{M}_{1b}^\mu)\varepsilon_{2\mu}, \\
\mathcal{M}_2 \;\; &= \;\; (\mathcal{M}_{2a}^{\mu\nu} + \mathcal{M}_{2b}^{\mu\nu})\varepsilon_{2\mu}\varepsilon_{3\nu},
\end{aligned}
\tag{5.2}
$$

where $\epsilon_{2\mu}$ and $\epsilon_{3\nu}$ are polarization vectors of $\gamma$ and $\bar{D}^{*0}$, respectively. The amplitudes $\mathcal{M}_{1a}^\mu$, $\mathcal{M}_{1b}^\mu$, $\mathcal{M}_{2a}$, and $\mathcal{M}_{2b}^\mu$ are for the four diagrams in Fig. 19, and they are given explicitly by

$$
\begin{aligned}
\mathcal{M}_{1a}^\mu \;\; &= \;\; -eg_{DN\Lambda_c}\frac{1}{s-m_N^2}\bar{\Lambda}_c(p_3)\gamma^5(\slashed{p}_1+\slashed{p}_2+m_N)\gamma^\mu N(p_1), \\
\mathcal{M}_{1b}^\mu \;\; &= \;\; -eg_{DN\Lambda_c}\frac{1}{u-m_{\Lambda_c}^2}\bar{\Lambda}_c(p_3)\gamma^\mu(\slashed{p}_1-\slashed{p}_4+m_{\Lambda_c})\gamma^5 N(p_1), \\
\mathcal{M}_{2a}^{\mu\nu} \;\; &= \;\; ieg_{D^*N\Lambda_c}\frac{1}{s-m_N^2}\bar{\Lambda}_c(p_3)\gamma^\nu(\slashed{p}_1+\slashed{p}_2+m_N)\gamma^\mu N(p_1), \\
\mathcal{M}_{2b}^{\mu\nu} \;\; &= \;\; ieg_{D^*N\Lambda_c}\frac{1}{u-m_{\Lambda_c}^2}\bar{\Lambda}_c(p_3)\gamma^\mu(\slashed{p}_1-\slashed{p}_4+m_{\Lambda_c})\gamma^\nu N(p_1).
\end{aligned}
\tag{5.3}
$$

In the above, $p_1$, $p_2$, $p_3$, and $p_4$ denote the four momenta of $p$, $\gamma$, $\Lambda_c^+$, and $\bar{D}^0(\bar{D}^{*0})$, respectively, while $s = (p_1 + p_2)^2$ and $u = (p_1 - p_4)^2$.

The differential cross sections for the two reactions are then

$$\frac{d\sigma_i}{dt} = \frac{1}{256\pi s p_{\mathrm{cm}}^2}|\mathcal{M}_i|^2|F_2(\mathbf{q}^2)|^2, \tag{5.4}$$

with $p_{\mathrm{cm}}$ denoting the photon momentum in center-of-mass system.

To account for finite sizes of hadrons, form factors need to be introduced at strong interaction vertices. To maintain gauge invariance, we take these form factors to be the same, i.e., an overall form factor is multiplied to the total amplitude of each process, as in Ref.[54] for photoproduction of pion on the nucleon. The overall form factor is taken to have a monopole form, i.e.,

$$F_2(\mathbf{q}^2) = \frac{\Lambda^2}{\Lambda^2 + \mathbf{q}^2}, \tag{5.5}$$

with $\mathbf{q}$ denoting the three momentum of photon in center-of-mass system. This is different from the one used in Ref.[54], where the center-of-mass momentum of produced pion is used in the form factor. Because of the large threshold for photoproduction of charmed hadrons, the off-shellness of $p$ in the $s$-channel or $\Lambda_c^+$ in the $u$-channel is thus proportional to the photon momentum rather than the momentum of produced charmed meson. We choose the cutoff parameter $\Lambda = 0.75$ GeV to reproduce the measured cross section for photoproduction of charmed hadrons from protons at center-of-mass energy of 6 GeV [55], as shown below.

Cross sections for the reactions $\gamma p \to \bar{D}^0 \Lambda_c^+$ (solid curve) and $\gamma p \to \bar{D}^{*0} \Lambda_c^+$ (dashed curve) are shown in Fig. 20 as functions of total center-of-mass energy. It is seen that they have similar magnitude with a peak value of about 19 nb for $\gamma p \to \bar{D}^0 \Lambda_c^+$ and about 23 nb for $\gamma p \to \bar{D}^{*0} \Lambda_c^+$.
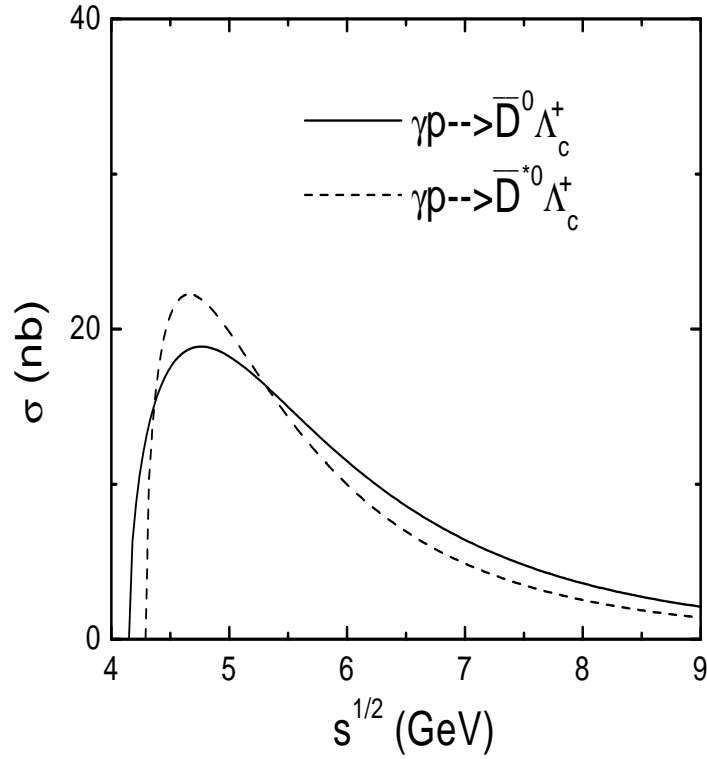
Fig. 20. Cross sections for photoproduction of charmed hadrons from protons as functions of center-of-mass energy: $\gamma p \to \bar{D}^0 \Lambda_c^+$ (solid curve) and $\gamma p \to \bar{D}^{*0} \Lambda_c^+$ (dashed curve).

B.   Three-body final states

As energy increases, three-body final states become important for charmed hadron production from photon-proton reactions, and the possible reactions are $\gamma p \to D^+ D^{*-} p$, $\gamma p \to D^- D^{*+} p$, $\gamma p \to D^+ \bar{D}^{*0} n$, $\gamma p \to \bar{D}^0 D^{*+} n$, $\gamma p \to D^+ D^- p$, $\gamma p \to D^+ \bar{D}^0 n$, $\gamma p \to D^{*+} D^{*-} p$, and $\gamma p \to D^{*+} \bar{D}^{*0} n$. The lowest-order diagrams for the first four reactions are shown in Fig. 21. These involve charmed vector and pseudoscalar mesons in final states and the exchange of pion in intermediate states. Shown in Figs. 22 and 23 are the lowest order diagrams for the other four reactions, which involve two
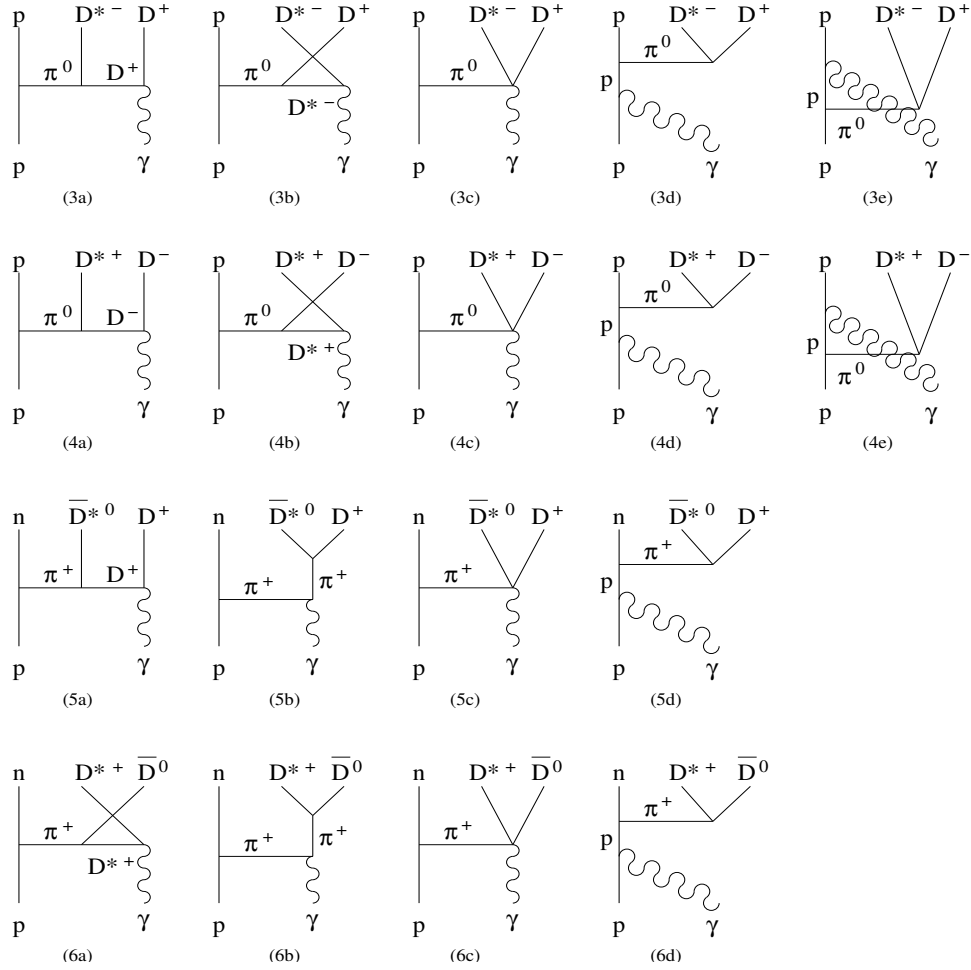
Fig. 21. Photoproduction of charmed hadrons ($D^*\bar{D}$ or $D\bar{D}^*$) from protons involving pion exchange.

charmed pseudoscalar mesons or two charmed vector mesons in final states and the exchange of rho mesons in intermediate states.

To evaluate the cross sections for these reactions, we need the following interactions Lagrangians besides those given in Eqs.(3.1), (3.8), and (4.1):

$$\mathcal{L}_{\gamma DD} = ieA^\mu[DQ\partial_\mu\bar{D} - (\partial_\mu D)Q\bar{D}],$$

$$\mathcal{L}_{\gamma D^*D^*} = ie[A^\mu(\partial_\mu D^{*\nu}Q\bar{D}^*_\nu - D^{*\nu}Q\partial_\mu\bar{D}^*_\nu)$$

$$+ (\partial_\mu A^\nu D^*_\nu - A^\nu\partial_\mu D^*_\nu)Q\bar{D}^{*\mu} + D^{*\mu}Q(A^\nu\partial_\mu D^*_\nu - \partial_\mu A^\nu\bar{D}^*_\nu],$$
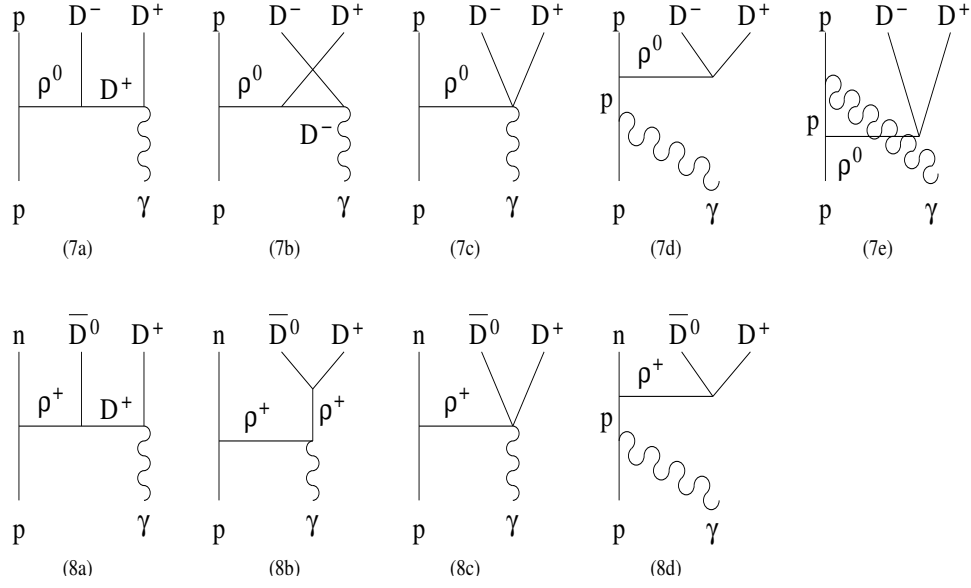
Fig. 22. Photoproduction of charmed hadrons $(D\bar{D})$ from protons involving rho meson exchange.

$$\mathcal{L}_{\pi\gamma DD^*} = -eg_{\pi DD^*}A^\mu(D^*_\mu(2\vec{\tau}Q - Q\vec{\tau})\bar{D} + D(2Q\vec{\tau} - \vec{\tau}Q)\bar{D}^*_\mu)\cdot\vec{\pi},$$

$$\mathcal{L}_{\rho\gamma DD} = eg_{\rho DD}A^\mu D(\vec{\tau}Q + Q\vec{\tau})\bar{D}\cdot\vec{\rho}_\mu,$$

$$\mathcal{L}_{\rho\gamma D^*D^*} = eg_{\rho D^*D^*}(A^\nu D^*_\nu(2\vec{\tau}Q - Q\vec{\tau})\bar{D}^*_\mu$$

$$+ A^\nu D^*_\mu(2\vec{\tau}Q - Q\vec{\tau})\bar{D}^*_\nu - A_\mu D^{*\nu}(2\vec{\tau}Q - Q\vec{\tau})\bar{D}^*_\nu)\cdot\vec{\rho}^\mu. \tag{5.6}$$

In the above, $Q$ is the diagonal charge operator with diagonal elements equal to 0 and -1.

Diagrams in Figs. 21, 22, and 23 can be separated into two types; one in which the photon is coupled to mesons such as the first three diagrams (denoted by (ia) to (ic) with i=3 to 10), and the other in which the photon is coupled directly to either the incoming or outgoing proton. As shown in Section E of this Chapter, contributions from the latter type are much smaller than those from the first type of diagrams and are neglected in following calculations. As a result, results obtained
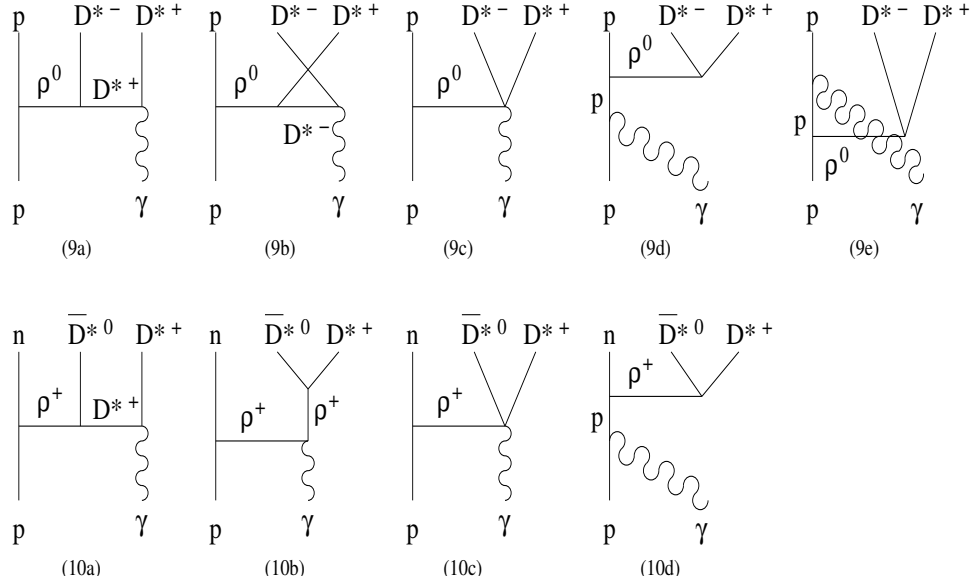
Fig. 23. Photoproduction of charmed hadrons $(D^*\bar{D}^*)$ from protons involving rho meson exchange.

in present study for charmed production with three-body final states violate slightly the gauge invariance. We note that diagrams of first type are similar to those for $J/\psi$ absorption by nucleons, which can be interpreted as absorption by virtual pions and rho mesons from nucleons. Here, they can be considered as charmed hadron production from interactions of photons with virtual mesons from the proton.

The amplitudes for the four reactions in Fig. 21 are given by

$$\mathcal{M}_i = -iag_{\pi NN}\bar{N}(p_3)\gamma_5 N(p_1)\frac{1}{t - m_\pi^2}(M_{ia} + M_{ib} + M_{ic}), \qquad (5.7)$$

with $i = 3$ to 6, while amplitudes for the four reactions in Figs. 22 and 23 can be written as

$$\mathcal{M}_j = ag_{\rho NN}\bar{N}(p_3)\left[\gamma^\mu + i\frac{\kappa_\rho}{2m_N}\sigma^{\alpha\mu}(p_1 - p_3)_\alpha\right] N(p_1)\frac{1}{t - m_\rho^2}$$

$$\times \left[-g_{\mu\nu} + \frac{(p_1 - p_3)_\mu(p_1 - p_3)_\nu}{m_\rho^2}\right](M_{ja}^\nu + M_{jb}^\nu + M_{jc}^\nu), \qquad (5.8)$$

with $j = 7$ to 10. In the above, $p_1$ and $p_3$ are four momenta of initial and final nucleons, respectively; and $t = (p_1 - p_3)^2$. The coefficient $a$ is 1 and $\sqrt{2}$, respectively, for neutral and charged pion or rho meson couplings to protons.

The three amplitudes $M_{ia}$, $M_{ib}$, and $M_{ic}$ represent the subprocess $\gamma\pi \to D^*\bar{D}$ in Fig. 21. Explicitly, they are:

$$
\begin{aligned}
\mathcal{M}_{3a} &= \mathcal{M}_{4a} \\
&= eg_{\pi DD^*}(-2k_1 + k_3)^\mu \frac{1}{t - m_D^2}(k_1 - k_3 + k_4)^\nu \varepsilon_{3\mu}\varepsilon_{2\nu}, \\
\mathcal{M}_{3b} &= \mathcal{M}_{4b} \\
&= -eg_{\pi DD^*}(-k_1 - k_4)^\alpha \frac{1}{u - m_{D^*}^2}\left[g_{\alpha\beta} - \frac{(k_1 - k_4)_\alpha(k_1 - k_4)_\beta}{m_{D^*}^2}\right] \\
&\times \ [(-k_2 - k_3)^\beta g^{\mu\nu} + (-k_1 + k_2 + k_4)^\nu g^{\beta\mu} + (k_1 + k_3 - k_4)^\mu g^{\beta\nu}]\varepsilon_{3\mu}\varepsilon_{2\nu}, \\
\mathcal{M}_{3c} &= \mathcal{M}_{4c} \\
&= eg_{\pi DD^*}g^{\mu\nu}\varepsilon_{3\mu}\varepsilon_{2\nu}, \\
\mathcal{M}_{5a} &= \sqrt{2}eg_{\pi DD^*}(-2k_1 + k_3)^\mu \frac{1}{t - m_D^2}(k_1 - k_3 + k_4)^\nu \varepsilon_{3\mu}\varepsilon_{2\nu}, \\
\mathcal{M}_{5b} &= -\sqrt{2}eg_{\pi DD^*}(2k_1 + k_2)^\nu \frac{1}{s - m_\pi^2}(k_1 + k_2 + k_4)^\mu \varepsilon_{3\mu}\varepsilon_{2\nu}, \\
\mathcal{M}_{5c} &= 2\sqrt{2}eg_{\pi DD^*}g^{\mu\nu}\varepsilon_{3\mu}\varepsilon_{2\nu}, \\
\mathcal{M}_{6a} &= -\sqrt{2}eg_{\pi DD^*}(-k_1 - k_4)^\alpha \frac{1}{u - m_{D^*}^2}\left[g_{\alpha\beta} - \frac{(k_1 - k_4)_\alpha(k_1 - k_4)_\beta}{m_{D^*}^2}\right] \\
&\times \ [(-k_2 - k_3)^\beta g^{\mu\nu} + (-k_1 + k_2 + k_4)^\nu g^{\beta\mu} + (k_1 + k_3 - k_4)^\mu g^{\beta\nu}]\varepsilon_{3\mu}\varepsilon_{2\nu}, \\
\mathcal{M}_{6b} &= \sqrt{2}eg_{\pi DD^*}(2k_1 + k_2)^\nu \frac{1}{s - m_\pi^2}(k_1 + k_2 + k_4)^\mu \varepsilon_{3\mu}\varepsilon_{2\nu}, \\
\mathcal{M}_{6c} &= -\sqrt{2}eg_{\pi DD^*}g^{\mu\nu}\varepsilon_{3\mu}\varepsilon_{2\nu}, \quad\quad\quad\quad (5.9)
\end{aligned}
$$

where $k_i$ denotes the momentum of particle $i$ of each subprocess, and $\varepsilon_\mu$ and $\varepsilon_\nu$ are polarization vectors of $D^*$ and $\gamma$, respectively. We choose the convention that particles 1 and 2 represent initial-state particles while particles 3 and 4 represent final-state ones on the left and right sides of a diagram.

Although the $\pi DD^*$ interaction Lagrangian in Eq.(5.6) breaks chiral symmetry due to nonderivative pion coupling, the sum $M_{ia} + M_{ib} + M_{ic}$ fulfills the chiral constraint for processes 3, 4, and 6 in Fig. 21, i.e., it vanishes at the soft pion limit. This is due to cancellations between non-chiral contributions from diagrams involving $D^*$ exchange and contributions from diagrams involving $\pi DD^*\gamma$ four point interactions as shown in Appendix B. Such effect was first found in studying $J/\psi$ absorption by pions [49]. Using the equation of motion for $D^*$ meson, it was shown that the non-chiral piece of $\pi DD^*$ interaction Lagrangian leads to an effective $\pi DD^* J/\psi$ four point interaction, which cancels the $\pi DD^* J/\psi$ four point interaction in the Lagrangian when $m_{J/\psi} \to 0$ (see Appendix C). Unfortunately, the chiral constraint is not satisfied for process 5 in Fig. 21 as it does not involve $D^*$-exchange. It thus remains a challenge to construct an effective Lagrangian for the interactions between heavy mesons and pions, that has the correct soft pion limit.

The amplitudes $M_{ja}^\nu$, $M_{jb}^\nu$, and $M_{jc}^\nu$ are those for the subprocesses $\gamma\rho \to D\bar{D}$ and $\gamma\rho \to D^*\bar{D}^*$ in Figs. 22 and 23, and they are given explicitly by

$$
\begin{aligned}
\mathcal{M}_{7a}^\mu &= -eg_{\rho DD}(k_1 - 2k_3)^\mu \frac{1}{t - m_D^2}(k_1 - k_3 + k_4)^\nu \varepsilon_{2\nu}, \\
\mathcal{M}_{7b}^\mu &= -eg_{\rho DD}(-k_1 + 2k_4)^\mu \frac{1}{u - m_D^2}(-k_1 - k_3 + k_4)^\nu \varepsilon_{2\nu}, \\
\mathcal{M}_{7c}^\mu &= 2eg_{\rho DD}g^{\mu\nu}\varepsilon_{2\nu}, \\
\mathcal{M}_{8a}^\mu &= \sqrt{2}eg_{\rho DD}(k_1 - 2k_3)^\mu \frac{1}{t - m_D^2}(k_1 - k_3 + k_4)^\nu \varepsilon_{2\nu}, \\
\mathcal{M}_{8b}^\mu &= \sqrt{2}eg_{\rho DD}[(-2k_1 - k_2)^\nu g^{\mu\alpha} + (k_1 + 2k_2)^\mu g^{\alpha\nu} + (k_1 - k_2)^\alpha g^{\mu\nu}]\frac{1}{s - m_\rho^2} \\
&\quad \times \left[ g_{\alpha\beta} - \frac{(k_1 + k_2)_\alpha (k_1 + k_2)_\beta}{m_\rho^2} \right] (k_3 - k_4)^\beta \varepsilon_{2\nu}, \\
\mathcal{M}_{8c}^\mu &= -\sqrt{2}eg_{\rho DD}g^{\mu\nu}\varepsilon_{2\nu}, \\
\mathcal{M}_{9a}^\mu &= eg_{\rho D^*D^*}[(-k_1 - k_3)^\alpha g^{\mu\lambda} + (2k_1 - k_3)^\lambda g^{\alpha\mu} + (2k_3 - k_1)^\mu g^{\alpha\lambda}]\frac{1}{t - m_{D^*}^2}
\end{aligned}
$$

$$\times \quad \left[g_{\alpha\beta} - \frac{(k_1 - k_3)_\alpha (k_1 - k_3)_\beta}{m_{D^*}^2}\right][-2k_2^\omega g^{\beta\nu} + (k_2 + k_4)^\beta g^{\nu\omega} - 2k_4^\nu g^{\beta\omega}]$$

$$\times \quad \varepsilon_{2\nu}\varepsilon_{3\lambda}\varepsilon_{4\omega},$$

$$\mathcal{M}_{9b}^\mu = eg_{\rho D^* D^*}[(-2k_1 + k_4)^\omega g^{\alpha\mu} + (k_1 + k_4)^\alpha g^{\mu\omega} + (k_1 - 2k_4)^\mu g^{\alpha\omega}]\frac{1}{u - m_{D^*}^2}$$

$$\times \quad \left[g_{\alpha\beta} - \frac{(k_1 - k_4)_\alpha (k_1 - k_4)_\beta}{m_{D^*}^2}\right][(-k_2 - k_3)^\beta g^{\nu\lambda} + 2k_2^\lambda g^{\beta\nu} + 2k_3^\nu g^{\beta\lambda}]$$

$$\times \quad \varepsilon_{2\nu}\varepsilon_{3\lambda}\varepsilon_{4\omega},$$

$$\mathcal{M}_{9c}^\mu = eg_{\rho D^* D^*}(g^{\mu\lambda}g^{\nu\omega} + g^{\mu\omega}g^{\nu\lambda} - 2g^{\mu\nu}g^{\lambda\omega})\varepsilon_{2\nu}$$

$$\times \quad \varepsilon_{3\lambda}\varepsilon_{4\omega},$$

$$\mathcal{M}_{10a}^\mu = \sqrt{2}eg_{\rho D^* D^*}[(-k_1 - k_3)^\alpha g^{\mu\lambda} + (2k_1 - k_3)^\lambda g^{\alpha\mu} + (2k_3 - k_1)^\mu g^{\alpha\lambda}]\frac{1}{t - m_{D^*}^2}$$

$$\times \quad \left[g_{\alpha\beta} - \frac{(k_1 - k_3)_\alpha (k_1 - k_3)_\beta}{m_{D^*}^2}\right][-2k_2^\omega g^{\beta\nu} + (k_2 + k_4)^\beta g^{\nu\omega} - 2k_4^\nu g^{\beta\omega}]$$

$$\times \quad \varepsilon_{2\nu}\varepsilon_{3\lambda}\varepsilon_{4\omega},$$

$$\mathcal{M}_{10b}^\mu = - \sqrt{2}eg_{\rho D^* D^*}[(-2k_1 - k_2)^\nu g^{\mu\alpha} + (k_1 + 2k_2)^\mu g^{\alpha\nu} + (k_1 - k_2)^\alpha g^{\mu\nu}]\frac{1}{s - m_\rho^2}$$

$$\times \quad \left[g_{\alpha\beta} - \frac{(k_1 + k_2)_\alpha (k_1 + k_2)_\beta}{m_\rho^2}\right][-2k_4^\lambda g^{\beta\omega} + 2k_3^\omega g^{\beta\lambda} + (k_4 - k_3)^\beta g^{\lambda\omega}]$$

$$\times \quad \varepsilon_{2\nu}\varepsilon_{3\lambda}\varepsilon_{4\omega},$$

$$\mathcal{M}_{10c}^\mu = -\sqrt{2}eg_{\rho D^* D^*}(g^{\mu\lambda}g^{\nu\omega} - 2g^{\mu\omega}g^{\nu\lambda} + g^{\mu\nu}g^{\lambda\omega})$$

$$\times \quad \varepsilon_{2\nu}\varepsilon_{3\lambda}\varepsilon_{4\omega}. \tag{5.10}$$

The cross sections for reactions with three particles in the final state can be expressed in terms of the off-shell cross sections for subprocesses involving two particles in the final state. Following the method of Ref. [44] for studying the reaction $pp \to p\Lambda K^+$, differential cross sections for the four reactions $\gamma p \to D^* \bar{D}(D\bar{D}^*)N$ in Fig. 21 can be written as

$$\frac{d\sigma_{\gamma p \to D^* \bar{D}(D\bar{D}^*)N}}{dt ds_1} = \frac{ag_{\pi NN}^2}{32\pi^2 s p_{cm}^2}k\sqrt{s_1}(-t)\frac{|F(t)|^2}{(t - m_\pi^2)^2}\sigma_{\gamma\pi \to D^* \bar{D}(D\bar{D}^*)}(s_1, t), \tag{5.11}$$

while those for the two reactions $\gamma p \to D\bar{D}N$ in Fig. 22 are

$$
\begin{aligned}
\frac{d\sigma_{\gamma p \to D\bar{D}N}}{dt ds_1} &= \frac{3ag_{\rho NN}^2}{64\pi^2 sp_{\text{cm}}^2} k\sqrt{s_1} \frac{|F(t)|^2}{(t-m_\rho^2)^2} \Big[ 4(1+\kappa_\rho)^2(-t-2m_N^2) \\
&+ \kappa_\rho^2 \frac{(4m_N^2-t)^2}{2m_N^2} + 4(1+\kappa_\rho)\kappa_\rho(4m_N^2-t) \Big] \sigma_{\gamma\rho \to D\bar{D}}(s_1,t). \quad (5.12)
\end{aligned}
$$

In the above, $s_1$ and $k$ are, respectively, squared invariant mass and center-of-mass momentum of $\pi$ and $\gamma$ in the subprocess $\gamma\pi \to D^*\bar{D}(\bar{D}^*D)$ or of $\rho$ and $\gamma$ in the subprocesses $\gamma\rho \to D\bar{D}$ and $\gamma\rho \to D^*\bar{D}^*$. Cross sections for these subprocesses are obtained from the amplitudes in Eqs.(5.9) and (5.10) using the software package FORM [47] to evaluate the summation over polarizations of both initial and final particles. The differential cross sections for the two reactions $\gamma p \to D^*\bar{D}^*N$ in Fig. 23 are similar to those for $\gamma p \to D\bar{D}N$ with $\sigma_{\gamma\rho \to D\bar{D}}(s_1,t)$ replaced by $\sigma_{\gamma\rho \to D^*\bar{D}^*}(s_1,t)$.

We have introduced in Eqs.(5.11) and (5.12) form factors $F_{\pi NN}$ and $F_{\rho NN}$ at $\pi NN$ and $\rho NN$ vertices, respectively, to take into account finite sizes of hadrons. As in Chapter III and Ref.[31], both are taken to have the following monopole form:

$$
F(t) = \frac{\Lambda^2 - m^2}{\Lambda^2 - t}, \quad (5.13)
$$

where $m$ is the mass of exchanged pion or rho meson, and $\Lambda$ is a cutoff parameter with values $\Lambda_{\pi NN} = 1.3$ GeV and $\Lambda_{\rho NN} = 1.4$ GeV. We have also introduced an overall dipole form factor for the two-body subprocesses $\gamma\pi \to D^*\bar{D}(D\bar{D}^*)$, $\gamma\rho \to D\bar{D}$, and $\gamma\rho \to D^*\bar{D}^*$ as in Section A for the reactions $\gamma p \to \bar{D}^0\Lambda_c^+$ and $\gamma p \to \bar{D}^{*0}\Lambda_c^+$. The same cutoff parameter $\Lambda = 0.75$ GeV is used in this form factor for evaluating the cross sections for charmed hadron production from photon-proton reactions with three-body final states.

The cross section for the reaction $\gamma p \to D^*\bar{D}(D\bar{D}^*)N$ is given by the sum of the cross sections for the four processes in Fig. 21, which are obtained by integrating
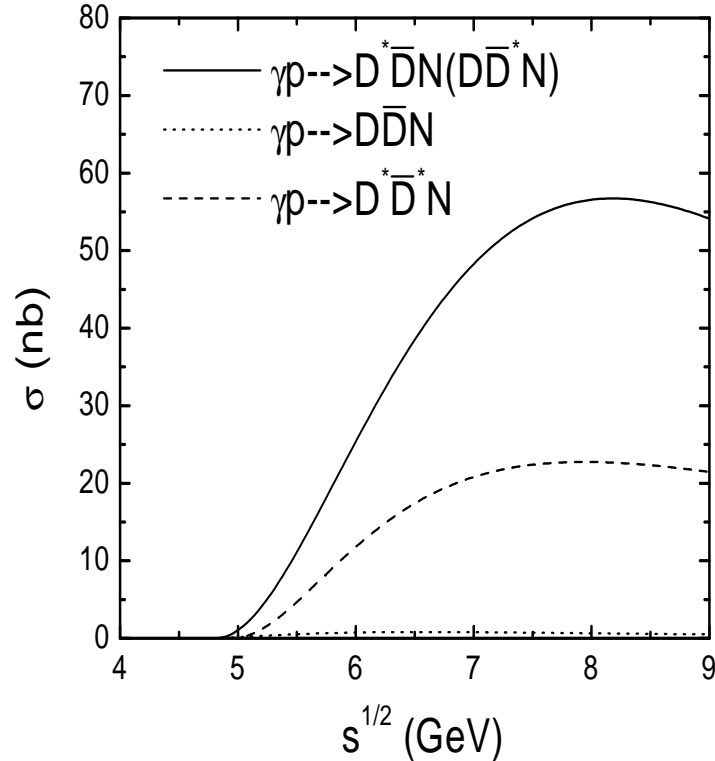
Fig. 24. Cross sections for photoproduction of charmed hadrons from protons with three particles in the final states: $\gamma p \rightarrow D^* \bar{D} N (D \bar{D}^* N)$ (solid curve), $\gamma p \rightarrow D \bar{D} N$ (dotted curve), and $\gamma p \rightarrow D^* \bar{D}^* N$ (dashed curve).

Eq.(5.11) over $t$ and $s_1$. Similarly, one can obtain from Eq.(5.12) the cross sections for the reactions $\gamma p \rightarrow D \bar{D} N$ and $\gamma p \rightarrow D^* \bar{D}^* N$, shown respectively, in Figs. 22 and 23. Results for these cross sections are shown in Fig. 24 by the solid, dotted, and dashed curves, respectively, for the reactions $\gamma p \rightarrow D^* \bar{D} N (D \bar{D}^* N)$, $\gamma p \rightarrow D \bar{D} N$, and $\gamma p \rightarrow D^* \bar{D}^* N$. It is seen that the reaction $\gamma p \rightarrow D^* \bar{D} N (D \bar{D}^* N)$ has the largest cross section with a peak value of about 57 nb, while the reaction $\gamma p \rightarrow D \bar{D} N$ has the smallest cross section of only about 1 nb. The larger cross sections for reactions with charmed vector meson in the final state is due to presence of interaction vertices involving three vector mesons, which have a stronger momentum dependence than

vertices with fewer number of vector mesons, leading thus to a larger strength at high energies.

C.   Total cross section
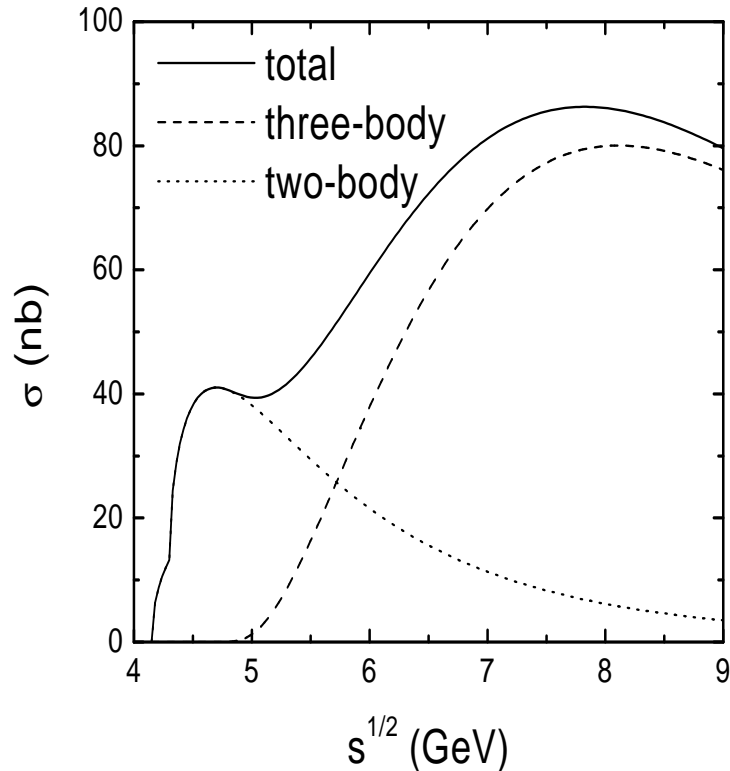


Fig. 25. Total (solid curve) and partial (dotted curve for two-body final states and dashed curve for three-body final states) cross sections for charmed hadron production in photon-proton reactions as functions of center-of-mass energy.

The total cross section for photoproduction of charmed hadrons from protons is given by the sum of the cross sections for two-body and three-body final states. In Fig. 25, we show the total cross section (solid curve) together with those for two-body final states (dotted curve) and three-body final states (dashed curve). It is seen that two-body final states involving $\Lambda_c$ and charmed meson dominate at low energy,

while three-body final states involving nucleon as well as charmed and anticharmed meson pair are more important at high energies. The two have comparable magnitude around center-of-mass energy of about 5.7 GeV. As in the experimental data at 6 GeV [55], two-body final states constitute about 33% of the total cross section.

## D. Charm photoproduction from protons in perturbative QCD

Charm production from photon-proton reactions can also be estimated using the leading-order perturbative QCD [56, 57, 58]. As shown in Appendix D, the cross section in this approach is given by

$$\sigma^{\gamma p}(\nu) = \int_{2m_c^2/\nu}^{1} dx \ \sigma^{\gamma g}(\nu x) g(x), \tag{5.14}$$

where $m_c$ is the charm quark mass, $g(x)$ is the gluon distribution function in protons, and $\nu = p \cdot p_\gamma$ with $p$ and $p_\gamma$ being the momenta of incoming proton and photon. The cross section $\sigma^{\gamma g}(\omega)$ is for charm-anticharm quark production from leading order photon-gluon scattering, i.e.,

$$\begin{aligned}
\sigma^{\gamma g \to \bar{c}c}(\omega) &= \frac{2\pi\alpha_s\alpha}{9}\frac{4}{\omega^2}\Bigg[\left(1 + \frac{4m^2}{\omega^2} - \frac{8m_c^2}{\omega^4}\right)\log\frac{1 - \sqrt{1 - \frac{4m_c^2}{\omega^2}}}{1 + \sqrt{1 - \frac{4m_c^2}{\omega^2}}} \\
&\quad - \left(1 + \frac{4m_c^2}{\omega^2}\right)\sqrt{1 - \frac{4m_c^2}{\omega^2}}\Bigg],
\end{aligned} \tag{5.15}$$

where $\omega^2 = 2p_g \cdot p_\gamma$ with the gluon momentum denoted by $p_g$.

Using $m_c = 1.3$ GeV and the leading order MRST 2001 parameterization of the gluon distribution function in protons [59], we have calculated the cross section for charm photoproduction from protons using the LO QCD formula, and the result is shown by the dashed curve in Fig. 26. Also shown are the cross section from the hadronic model (solid curve) and available experimental data (open circles) [55]. We see that the LO QCD result reproduces the data at 6 GeV and at higher energies.
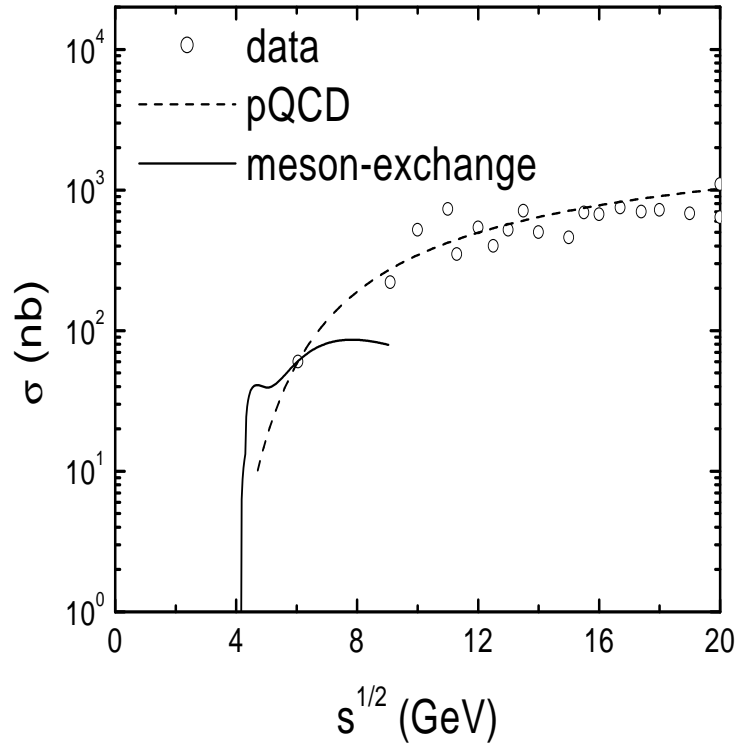
Fig. 26. Cross sections for charm production from photon-proton reactions in the hadronic model (solid curve) and the pQCD approach (dashed curve). The experimental data [55] are shown by open circles.

The QCD prediction below 6 GeV falls well below that from the effective hadronic model. It is known that the QCD formula for photoproduction of heavy quarks works best when momenta involved in the process are larger than the heavy quark mass $m_c$. Below this momentum and near threshold energy, large logarithms appear in the perturbative QCD approach and spoil its convergence [60]. At low energies, our phenomenological hadronic approach is expected to be more reliable as the cross section is dominated by two-body final states with no additional contribution to cause any large correction. On the other hand, results from the hadronic model at higher energies fall short of experimental data. This is expected because contributions from

four-body final states and from exchange of heavier mesons become important as energy increases. For higher energies, perturbative QCD calculations should be a more efficient way for determining the cross section for charm photoproduction than adding more complicated processes to the phenomenological hadronic model.

E.    Contributions from photon-proton couplings
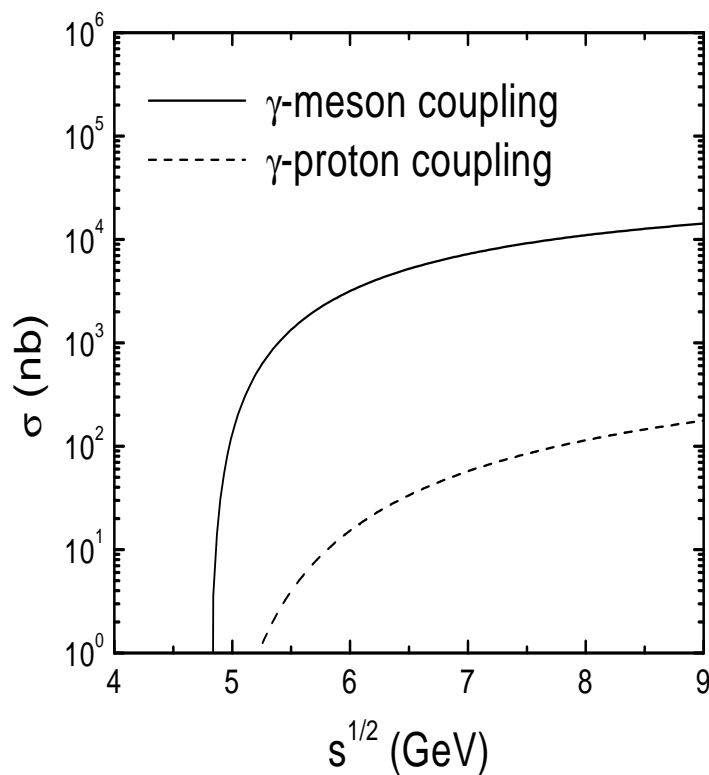


Fig. 27. Cross sections for charmed hadron production in photoproton reactions due to photon coupling directly to protons (diagram (3d) in Fig. 21, dashed curve) and to mesons (diagrams (3a)-(3c) in Fig. 21, solid curve). No form factors are included in these results.

In the present study, the cross sections for charmed hadron production from photon-proton reactions with three particles in the final state are obtained without

contributions from diagrams involving photons coupled directly to external protons. These diagrams are needed to preserve gauge invariance in each process. Their contributions are small compared to those from diagrams with photons coupled only to mesons. This is due to the $s$-channel nucleon propagator $(1/(s - m_N^2))$ in these diagrams, which suppresses their amplitudes more than the $t$-channel heavy meson propagator in other diagrams as a result of the large photon energy needed to produce the charmed and anticharmed meson pair. In the following, we demonstrate this effect by comparing the contribution from diagram (3d) with that from diagrams (3a)-(3c) in Fig. 21.

The amplitude for diagram (3d) in Fig. 21 can be written as

$$
\begin{aligned}
\mathcal{M} &= i2eg_{\pi NN}g_{\pi DD^*}\frac{1}{(s - m_N^2)(t - m_\pi^2)}\bar{p}(p_3)\gamma_5(\not{p}_1 + \not{p}_2 + m_N)\gamma^\mu p(p_1)\varepsilon_\mu p_5^\nu \varepsilon_\nu \\
&\equiv 2g_{\pi DD^*}M_2 p_5^\nu \varepsilon_\nu, \tag{5.16}
\end{aligned}
$$

where $p_1$, $p_3$, $p_2$, and $p_5$ are the momenta of initial and final nucleons, photon, and charmed meson, respectively. The cross section due to this diagram alone is given by

$$
\frac{d\sigma}{dtds_1} = \frac{\sqrt{s_1}}{256\pi^2 sp_{\text{cm}}^2}|\mathcal{M}_2|^2\Gamma(s_1), \tag{5.17}
$$

where $s_1$ is the invariant mass of $D^+ D^{*-}$ pair, and $\Gamma(s_1)$ is the decay width of the off-shell pion to $D^+$ and $D^{*-}$.

The cross section due to the $s-$channel diagram (3d) in Fig. 21 involving photon coupling directly to protons is shown by the dashed curve in Fig. 27 together with that due to photon coupling to mesons (diagrams (3a)-(3c) in Fig. 21) shown by the solid curve. Form factors are neglected in these results as we are only interested in their relative magnitude. It is seen that contributions from diagrams with direct photon-proton couplings are more than two orders of magnitude smaller than those

from diagrams with photon coupled to mesons. These diagrams can thus be safely neglected in calculating the cross section for charmed hadron production from photon-proton reactions.

CHAPTER VI

SUMMARY

In this dissertation, we have introduced an effective Lagrangian based on the SU(4) flavor symmetry. To take into account the symmetry breaking effects due to the larger masses of hadrons consisting of charm quarks, we have used the empirical hadron masses and coupling constants. For coupling constants that are unknown empirically, their values are, however, determined from the known ones using the SU(4) relations. We have also included form factors at the strong interaction vertices to take in to account the finite sizes of hadrons. This model has been used to evaluate the cross sections for a number of reactions involving charmed hadrons production, such as $J/\psi$ absorption by nucleon, charmed hadron production in meson-nucleon and proton-proton reactions, and photoproduction of charmed hadrons from protons. The cross section for charmonium absorption by nucleon is found to be about 5 mb, which is consistent with that extracted from $J/\psi$ production in photo-nucleus and proton-nucleus reactions and comparable with other theoretical approaches or models. The cross sections for charmed hadron production are about a few hundred $\mu$b in meson-nucleon reactions and about $1\mu b$ in proton-proton reactions at center-of-mass energy of 11.5 GeV. The latter is comparable to available experimental data. Including photon as a U(1) gauge particle, the effective Lagrangian has been used to evaluate the cross section for charmed hadron photoproduction on protons, and its value is about 70 nb at center-of-mass energy of 5.7 GeV with two-body final states constituting about 33% of the total cross section as in experimental data. Knowledge on the cross sections for charmonium absorption and charmed hadron production are useful for understanding the mechanism of observed charmonium suppression and for studying charm production in relativistic heavy ion collisions.

Although an effective Lagrangian similar to ours can be obtained from an SU(4) chiral Lagrangian, our effective Lagrangian violates chiral symmetry due to the terms with derivative operator acting on heavy meson fields instead of the pion field. Also, the heavy quark symmetry reflected in the approximately degenerate masses of pseudoscalar ($D$, $B$) and vector ($B$, $B^*$) heavy mesons has been shown to be useful for studying the decays of heavy hadrons and their interactions [61]. It will be of interest to improve our effective Lagrangian approach by including both the chiral symmetry and the heavy quark symmetry.

The effective Lagrangians used in our dissertation can be extended to study the production of exotic pentaquark baryons, which have recently attracted much attention as a result of the experimental discovery of the $\Theta^+(1540)$ particle from the invariant mass spectrum of $K^+n$ or $K^0p$ in nuclear reactions induced by photons [62, 63] or kaons [64]. The extracted mass of about 1.54 GeV and width of less than 21-25 MeV are consistent with those of the pentaquark baryon $\Theta^+$ consisting of $uudd\bar{s}$ quarks predicted in the chiral soliton model [65]. Its existence has also been verified recently in the constituent quark model [66, 67] and the QCD sum rules [68]. Although the spin and isospin of $\Theta^+$ are predicted to be 1/2 and 0, respectively, those of the one detected in experiments are not yet determined. Studies have therefore been carried out to predict its decay branching ratios based on different assignments of its spin and isospin [69, 70]. Including the coupling of $\Theta^+$ with both $KN$ and $K^*N$ in our effective Lagrangians, one can then evaluate the cross sections for the production of exotic pentaquark $\Theta^+$ and/or other exotic pentaquark baryons $\Xi_5^+$ ($uuss\bar{d}$)and $\Xi_5^{--}$ ($ddss\bar{u}$) in reactions induced by photons [71, 72, 73], nucleons, pions, and kaons [74] on nucleon targets. One can also determine their yield in relativistic heavy ion collisions by taking into account their production from the initial quark-gluon plasma and the effects due to subsequent hadronic absorption and regeneration [75].

These studies will be useful in understanding not only the production mechanism of pentaquark baryons but also their properties. They may also provide the possibility of understanding the dynamics of hadronization of the quark-gluon plasma.

REFERENCES

[1] T. Matsui and H. Satz, Phys. Lett. B **178**, 416 (1986).

[2] M. C. Abreu *et al.*, NA38 Collaboration, Z. Phys. C **38**, 117 (1988); C. Baglin *et al.*, Phys. Lett. B **220**, 471 (1989).

[3] C. Baglin *et al.*, Phys. Lett. B **270**, 105 (1991);   **345**, 617 (1995).

[4] M. Gonin *et al.*, NA50 Collaboration, Nucl. Phys. **A610**, 404c (1996); M. C. Abreu *et al.*, NA50 Collaboration, Phys. Lett. B **450**, 456 (1999).

[5] D. Kharzeev, C. Lourenço, M. Nardi, and H. Satz, Z. Phys. C **74**, 307 (1997).

[6] R. Vogt, Phys. Rep. **310**, 197 (1999) and references therein.

[7] J.-P. Blaizot and J.-Y. Ollitrault, Phys. Rev. Lett. **77**, 1703 (1996).

[8] C.-Y. Wong, Nucl. Phys. **A630**, 487 (1998).

[9] W. Cassing and C. M. Ko, Phys. Lett. B **396**, 39 (1997); W. Cassing and E. L. Bratkovskaya, Nucl. Phys. **A623**, 570 (1997).

[10] N. Armesto and A. Capella, Phys. Lett. B **430**, 23 (1998).

[11] C. M. Ko, X.-N. Wang, B. Zhang, and X. F. Zhang, Phys. Lett. B **444**, 237 (1998).

[12] P. Braun-Munzinger and K. Redlich, Nucl. Phys. **A661**, 546 (1999).

[13] E. V. Shuryak, Phys. Rep. **61**, 71 (1980).

[14] E. Scomparin *et al.* NA50 Collaboration, Nucl. Phys. **A610**, 331c (1996); M.C. Abreu *et al.* (NA38/NA50 Collaborations), Nucl. Phys. **A661**, 538 (1999); N. Masera for the HELIOS-3 Collaboration, Nucl. Phys. **A590**, 93c (1995).

[15] Z. Lin and X.-N. Wang, Phys. Lett. B **444**, 245 (1998).

[16] W. Cassing, L. A. Kondratyuk, G. I. Lykasov, and M. V. Rzjanin, Phys. Lett. B **513**, 1 (2001).

[17] K. Martins, D. Blaschke, and E. Quack, Phys. Rev. C **51**, 2723 (1995).

[18] C.-Y. Wong, E. S. Swanson, and T. Barnes, hep-ph/9912431.

[19] D. Kharzeev and H. Satz, Phys. Lett. B **334**, 155 (1994).

[20] S. G. Matinyan and B. Müller, Phys. Rev. C **58**, 2994 (1998).

[21] K. L. Haglin, Phys. Rev. C **61**, 031902 (2000); K. L. Haglin, Phys. Rev. C **63**, 065201 (2001).

[22] F. S. Navarra, M. Nielsen, R. S. Marques de Carvalho, and G. Krein, Phys. Lett. B **529**, 87 (2002).

[23] Z. W. Lin and C. M. Ko, Phys. Rev. C **62**, 034903 (2000).

[24] S. Gavin, Nucl. Phys. **A566**, 287c (1994); R. Vogt, Phys. Rep. **310**, 197 (1999).

[25] R. L. Anderson *et al.*, Phys. Rev. Lett. **38**, 263 (1977).

[26] Z. Lin and M. Gyulassy, Phys. Rev. C **51**, 2177 (1995).

[27] Z. Lin, R. Vogt, and X. N. Wang, Phys. Rev. C **57**, 899 (1998).

[28] W. Cassing and E. L. Bratkovskaya, Phys. Rep. **308**, 68 (1999).

[29] A. B. Kaidalov, Z. Phys. C **12**, 63 (1982).

[30] M. C. Abreu *et al.*, NA50 Collaboration, Eur. Phys. J. C **14**, 443 (2000).

[31] W. Liu, C. M. Ko, and Z. Lin, Phys. Rev. C **65**, 015203 (2001).

[32] Z. W. Lin, T. G. Di, and C. M. Ko, Nucl. Phys. **A689**, 965 (2001).

[33] Z. Lin, C. M. Ko, and B. Zhang, Phys. Rev. C **61**, 024904 (2000).

[34] See the website of GSI at http://www.gsi.de/forschung/kp/kp3/index_e.html for details.

[35] A. M. Gasparyan, V. Y. Grishina, L. A. Kondratyuk, W. Cassing, and J. Speth, nucl-th/0210018.

[36] M. P. Rekalo and E. Tomasi-Gustafsson, Eur. Phys. Jour. A **16**, 575 (2003).

[37] W. Liu, S. H. Lee, and C. M. Ko, Nucl. Phys. **A724**, 375 (2003).

[38] K. Abe *et al.*, Phys. Rev. D **30**, 1 (1984).

[39] See the website of J-PARC at http://jkj.tokai.jaeri.go.jp/Home.files/AccSci.html for details.

[40] R. A. Adelseck and B. Saghai, Phys. Rev. C **42**, 108 (1990).

[41] S. Okubo, Phys. Rev. D **11**, 3261 (1975).

[42] B. Holzenkamp, K. Holinde, and J. Speth, Nucl. Phys. **A500**, 485 (1989); G. Janssen, J.W. Durso, K. Holinde, B. C. Pearce, and J. Speth, Phys. Rev. Lett. **71**, 1978 (1993).

[43] G. Janssen, K. Holinde, and J. Speth, Phys. Rev. C **54**, 2218 (1996).

[44] T. Yao, Phys. Rev. **125**, 1048 (1961).

[45] Y. Oh, T. Song, and S. H. Lee, Phys. Rev. C **62**, 034901 (2001).

[46] A. Sibertsev, K. Tsushima, and A. W. Thomas, Phys. Rev. C **63**, 044906 (2001)

[47] J. Vermaseren, computer code FORM, 1989. The free version of the software is available on the internet at ftp://hep.itp.tuwien.ac.at/pub/Form/PC/.

[48] F. S. Navarra and M. Nielsen, Phys. Lett. B **443**, 285 (1998); F. O. Durães, F. S. Navarra and M. Nielsen, Phys. Lett. B **498**, 169 (2001).

[49] F. S. Navarra, M. Nielsen, and M. R. Robilotta, Phys. Rev. C 64, 021901 (2001).

[50] K. Tsushima, S. W. Huang, and A. Faessler, Phys. Lett. B **337**, 245 (1994); E. L. Bratkovskaya and C. M. Ko, Phys. Lett. B **445**, 265 (1999).

[51] C. H. Li and C. M. Ko, Nucl. Phys. **A712**, 110 (2002).

[52] G. Q. Li, C.-H. Lee and G. E. Brown, Nucl. Phys. A **625**, 372 (1997).

[53] N. S. Amaglobeli *et al.*, SVD Collaboration, Phys. At. Nucl. **64**, 891 (2001).

[54] S. Nozawa, B. Blankleider, T.-S. H.Lee, Nucl. Phys. **A513**, 459 (1990).

[55] F. Abe *et al.*, CDF collaboration, Phys. Rev. Lett. **70**, 713 (1993).

[56] M. A. Shifman, A. I. Vainstein, V. I. Zakharov, Phys. Lett. B **65**, 255 (1976); Nucl. Phys. B **136**, 125 (1978).

[57] H. Fritzsch and K. H. Streng, Phys. Lett. B **72**, 385 (1978).

[58] R. K. Ellis and P. Nason, Nucl. Phys. B **312**, 551 (1989).

[59] See the website of 2003 NLO and NNLO 'conservative' parton distributions at http://durpdg.dur.ac.uk/hepdata/mrs.html for details.

[60] S. Frixione, Nucl. Phys. Proc. Suppl. **79**, 399 (1999).

[61] T. M. Yan, H. Y. Cheng, C. Y. Cheung, G. L. Lin, Y. C. Lin, and H. L. Yu, Phys. Rev. D **46**, 1148 (1992).

[62] T. Nakano *et al.*, Phys. Rev. Lett. **91**, 012002 (2003).

[63] S. Stepanyan *et al.*, CLAS Collaboration, Phys. Rev. Lett. **91**, 252001 (2003).

[64] V.V. Barmin *et al.*, Phys. Atom. Nucl. **66**, 1715 (2003), Yad. Fiz. **66**, 1763 (2003).

[65] D. Diakonov, V. Petrov, and M. Poliakov, Z. Phys. **A359**, 305 (1997).

[66] Fl. Stancu and D. O. Riska, Phys. Lett. B **575**, 242 (2003).

[67] M. Karliner and H.J. Lipkin, hep-th/0307243.

[68] S. L. Zhu, Phys. Rev. Lett. **91**, 232002 (2003).

[69] C.E. Carlson, C. D. Carone, H. J. Kwee, and V. Nazaaryan, Phys. Lett. B **573**, 101 (2003).

[70] X. Chen, Y. Mao, and B. Q. Ma, hep-ph/0307381.

[71] C. M. Ko, W. Liu, V. Kubarovsky, Phys. Rev. C **69**, 025202 (2004).

[72] C. M. Ko and W. Liu, Phys. Rev. C **69**, 045204 (2004).

[73] C. M. Ko and W. Liu, Nucl. Phys. **A741**, 215 (2004).

[74] C. M. Ko and W. Liu, Phys. Rev. C **68**, 045203 (2003).

[75] L.W. Chen, V. Greco, C.M. Ko, S.H. Lee, and W. Liu, Phys. Lett. B **601**, 34 (2004).

[76] F. Klingle, N. Kaiser, and W. Weise, Z. Phys. A **356**, 193 (1996).

APPENDIX A

VECTOR MESON DOMINANCE MODEL

For some coupling constants in our effective Lagrangians, their values can be determined from the Vector Meson Dominance (VMD) model. In this model, the virtual photon in the process $e^- D^+ \to e^- D^+$ is coupled to vector mesons $\rho$, $\omega$, and $J/\psi$, which are then coupled to the charmed meson. At zero momentum transfer, the following relation holds:

$$\sum_{V=\rho,\omega,\psi} \frac{\gamma_V \ g_{VD^+D^-}}{m_V^2} = e. \tag{A.1}$$

In the above, $\gamma_V$ is the photon-vector-meson mixing amplitude and can be determined from the vector meson partial decay width to $e^+e^-$, i.e.,

$$\Gamma_{Vee} = \frac{\alpha \gamma_V^2}{3 m_V^3}, \tag{A.2}$$

with the fine structure constant $\alpha = e^2/4\pi$. The relative signs of $\gamma_V$'s can be determined from the hadronic electromagnetic current expressed in terms of quark currents [76]. Since the virtual photon sees the charge of charm quark in the charmed meson through the $\psi DD$ coupling, we have the following relations:

$$\frac{\gamma_\psi g_{\psi D^+ D^-}}{m_\psi^2} = \frac{2}{3}e, \quad \frac{\gamma_\rho g_{\rho D^+ D^-}}{m_\rho^2} + \frac{\gamma_\omega g_{\omega D^+ D^-}}{m_\omega^2} = \frac{1}{3}e. \tag{A.3}$$

Similarly, one has, from the process $e^- D^0 \to e^- D^0$,

$$\frac{\gamma_\psi g_{\psi D^0 \bar{D}^0}}{m_\psi^2} = \frac{2}{3}e, \quad \frac{\gamma_\rho g_{\rho D^0 \bar{D}^0}}{m_\rho^2} + \frac{\gamma_\omega g_{\omega D^0 \bar{D}^0}}{m_\omega^2} = -\frac{2}{3}e. \tag{A.4}$$

Using $g_{\rho D^+ D^-} = -g_{\rho D^0 \bar{D}^0} = g_{\rho DD}$, $g_{\omega D^+ D^-} = g_{\omega D^0 \bar{D}^0} = g_{\omega DD}$, and $g_{\psi D^+ D^-} =$

$g_{\psi D^0 \bar{D}^0} = g_{\psi DD}$ from isospin symmetry, we then have

$$\frac{\gamma_\psi g_{\psi DD}}{m_\psi^2} = \frac{2}{3}e, \quad \frac{\gamma_\rho g_{\rho DD}}{m_\rho^2} + \frac{\gamma_\omega g_{\omega DD}}{m_\omega^2} = \frac{1}{3}e, \quad -\frac{\gamma_\rho g_{\rho DD}}{m_\rho^2} + \frac{\gamma_\omega g_{\omega DD}}{m_\omega^2} = -\frac{2}{3}e. \quad (A.5)$$

¿From the above equations, we obtain the following coupling constants:

$$g_{\rho DD} = 2.52 \ , \ g_{\omega DD} = -2.84 \ , \ g_{\psi DD} = 7.64 \ . \quad (A.6)$$

We note that in Ref.[20] the same VMD relations for $g_{\rho DD}$ and $g_{\psi DD}$ as our Eq. (A.5) are used but slightly different values, i.e., $g_{\rho DD} = 2.8$ and $g_{\psi DD} = 7.7$, are obtained.

Equations similar to Eq. (A.5) can be written for kaons and pions in order to obtain $g_{VKK}$ and $g_{V\pi\pi}$. The resulting coupling constants, multiplied by the corresponding prefactors in the following SU(4) relations, are given in the parentheses for comparison:

$$g_{\rho\pi\pi}(5.04) = 2g_{\rho KK}(5.04) = 2g_{\rho DD}(5.04) = \frac{\sqrt{6}}{2}g_{\psi DD}(9.36) \ . \quad (A.7)$$

We note that $|g_{\rho\pi\pi}|$ is 6.06 if it is determined from the $\rho$ meson decay width to two pions. It is seen that the predicted values differ only slightly from the above SU(4) relation except the coupling constant $g_{\psi DD}$. This may indicate a sizable uncertainty in the $\psi DD$ coupling.

## APPENDIX B

## CHIRAL SYMMETRY CONSTRAINT

In this appendix, we give an example on how the chiral symmetry constraint is fulfilled in the process $\gamma p \rightarrow D^{*-}D^+ p$. For diagrams (3a)-(3c) in Fig.21, their amplitudes are

$$
\begin{aligned}
\mathcal{M}_{3a} &= eg_{\pi DD^*}(-2k_1 + k_3)^\mu \frac{1}{t - m_D^2}(k_1 - k_3 + k_4)^\nu \varepsilon_{3\mu}\varepsilon_{2\nu}, \\
\mathcal{M}_{3b} &= -eg_{\pi DD^*}(-k_1 - k_4)^\alpha \frac{1}{u - m_{D^*}^2}\left[g_{\alpha\beta} - \frac{(k_1 - k_4)_\alpha (k_1 - k_4)_\beta}{m_{D^*}^2}\right] \\
&\times \quad [(-k_2 - k_3)^\beta g^{\mu\nu} + (-k_1 + k_2 + k_4)^\nu g^{\beta\mu}(k_1 + k_3 - k_4)^\mu g^{\beta\nu}]\varepsilon_{3\mu}\varepsilon_{2\nu}, \\
\mathcal{M}_{3c} &= eg_{\pi DD^*}g^{\mu\nu}\varepsilon_{3\mu}\varepsilon_{2\nu}. \quad\quad\quad\quad (B.1)
\end{aligned}
$$

In soft pion limit, i.e., $k_1^\mu = 0$, we have

$$
\begin{aligned}
\mathcal{M}_{3a} &= eg_{\pi DD^*}(-2k_1)^\mu \frac{1}{t - m_D^2}(k_1 + k_4)^\nu \varepsilon_{3\mu}\varepsilon_{2\nu} = 0, \\
\mathcal{M}_{3b} &= eg_{\pi DD^*}k_4^\alpha \frac{1}{u - m_{D^*}^2}\left[g_{\alpha\beta} - \frac{(k_1 - k_4)_\alpha (k_1 - k)4_\beta}{m_{D^*}^2}\right] \\
&\times \quad [(-k_2 - k_3)^\beta g^{\mu\nu} + k_4^\nu g^{\beta\mu} - k_4^\mu g^{\beta\nu}]\varepsilon_{3\mu}\varepsilon_{2\nu}, \\
&= -eg_{\pi DD^*}\frac{1}{u - m_{D^*}^2}[(k_4 - k_1)_\beta - \frac{(k_4 - k_1)^2(k_4 - k_1)_\beta}{m_{D^*}^2}] \\
&\times \quad (k_2 + k_3)^\beta g^{\mu\nu}\varepsilon_{3\mu}\varepsilon_{2\nu} \\
&= eg_{\pi DD^*}\frac{(k_4 - k_1)_\beta (k_2 + k_3)^\beta}{m_{D^*}^2}g^{\mu\nu}\varepsilon_{3\mu}\varepsilon_{2\nu} \\
&= eg_{\pi DD^*}\frac{m_2^2 - m_3^2}{m_{D^*}^2}g^{\mu\nu}\varepsilon_{3\mu}\varepsilon_{2\nu} = -eg_{\pi DD^*}g^{\mu\nu}\varepsilon_{3\mu}\varepsilon_{2\nu} \\
\mathcal{M}_{3c} &= eg_{\pi DD^*}g^{\mu\nu}\varepsilon_{3\mu}\varepsilon_{2\nu}. \quad\quad\quad\quad (B.2)
\end{aligned}
$$

It is thus easy to see that $\mathcal{M}_{3a} + \mathcal{M}_{3b} + \mathcal{M}_{3c} = 0$ in the chiral limit although the Lagrangian $\mathcal{L}_{\pi DD^*}$ we used in calculation violates chiral symmetry due to the term coupled to non-gradient pion field.

APPENDIX C

CHIRAL SYMMETRY

The SU(4) flavor symmetric effective Lagrangian in our model contains terms with nongradient pion couplings that violate chiral symmetry as first pointed out in Ref.[49]. This can be seen as follows.

For the $\pi D D^*$ coupling, we have two alternative forms, i.e.,

$$
\begin{aligned}
\mathcal{L}_{\pi D D^*}^{(I)} &= \frac{i}{2} g_{\pi D D^*} \left[ \left( \bar{D} \vec{\tau} D^{*\mu} - \bar{D}^{*\mu} \vec{\tau} D \right) \cdot \partial_\mu \vec{\pi} \right. \\
&\left. - \left( \partial_\mu \bar{D} \vec{\tau} D^{*\mu} - \bar{D}^{*\mu} \vec{\tau} \partial_\mu D \right) \cdot \vec{\pi} \right],
\end{aligned}
\tag{C.1}
$$

and

$$
\mathcal{L}_{\pi D D^*}^{(II)} = i g_{\pi D D^*} \left( \bar{D} \vec{\tau} D^{*\mu} - \bar{D}^{*\mu} \vec{\tau} D \right) \cdot \partial_\mu \vec{\pi} ,
\tag{C.2}
$$

with the first one violating chiral symmetry. The Lagrangians in Eqs. (C.1) and (C.2) can be related by performing an integration by parts in the last term in Eq.(C.1), i.e.,

$$
\mathcal{L}_{\pi D D^*}^{(I)} = \mathcal{L}_{\pi D D^*}^{(II)} + \frac{i}{2} g_{\pi D D^*} \left( \bar{D} \vec{\tau} \partial_\mu D^{*\mu} - \partial_\mu \bar{D}^{*\mu} \vec{\tau} D \right) \cdot \vec{\pi} .
\tag{C.3}
$$

The above result indicates that the two forms of the $\pi D D^*$ coupling would be equivalent if the condition $\partial_\mu D^{*\mu} = \partial_\mu \bar{D}^{*\mu} = 0$ holds, which is the case for on-mass shell vector mesons. However, this condition is not valid in the presence of interactions, and hence that Eqs. (C.1) and (C.2) correspond to different dynamical hypotheses. The difference can, however, be absorbed by an effective contact term that is proportional to $g_{\pi D D^*} g_{\phi D^* D^*} (m_\phi^2 / m_{D^*}^2 - 1)$ and vanishes in the SU(4) limit.

APPENDIX D

LEADING-ORDER PQCD CROSS SECTION FOR $\gamma P \rightarrow C\bar{C}$

In this appendix, we give the details on the evaluation of the cross section for the reaction $\gamma p \rightarrow c\bar{c}$ in the leading-order perturbation QCD approach.

Based on the field equation

$$(\partial_t^2 - \nabla^2)A_\mu(x) = Q_c e(\bar{c}\gamma_\mu c), \tag{D.1}$$

the cross section for photoproton production of charm quarks can be written as

$$\sigma^{\gamma N}(\nu) \equiv \sigma_{\text{tot}}(\gamma + p \rightarrow c\bar{c}) = \frac{1}{2\nu}\text{Im}T_{i,i}, \tag{D.2}$$

where $\nu = p_p \cdot p_\gamma$ and

$$T_{i,i} = (Q_c e)^2 \frac{1}{2} \sum_{pol} \epsilon^\mu(\lambda)\Pi_{\mu\nu}\epsilon^\nu(\lambda) = -\frac{(Q_c e)^2}{2}\Pi_\mu^\mu, \tag{D.3}$$

$$\Pi_\mu^\mu = i \int d^4 x e^{iqx} \langle p|T[\bar{c}(x)\gamma_\mu c(x)\bar{c}(0)\gamma^\mu c(0)]|p\rangle. \tag{D.4}$$

Evaluating the current-current correlation function $\Pi_\mu^\mu$ in above equation using the operator product expansion (OPE), i.e.,

$$\Pi_\mu^\mu(p, q) = \sum C_n A_n \nu^n + \text{Higher dim. op}, \tag{D.5}$$

leads to the dispersion relation

$$\int_{\nu_0}^\infty \frac{d\nu}{\nu^n}\sigma^{\gamma N}(\nu) = I(n)A_n, \tag{D.6}$$

with $\nu_0 = \frac{1}{2}((m_D + m_{\Lambda_c})^2 - m_N^2)$ and $I(n) = -(Q_c e)^2 \pi C_n/4$.

In Eq.(D.5), $C_n's$ are the Wilson coefficients and $A_n's$ are the matrix elements

defined by

$$i^{n-2}\langle p|F^a_{\alpha\mu_1}D_{\mu_2}\cdots F^a_{\mu_n\alpha}|p\rangle = (p_{\mu_1}p_{\mu_2}\cdots - \text{Trace terms})A_n, \tag{D.7}$$

with $F^a_{\mu\nu}$ denoting the gluon field strength tensor. The $A_n$ can be expressed in terms of the gluon distribution function inside the nucleon $G(x, Q^2_{\text{eff}})$, i.e.,

$$A_n = 2\int \frac{dx}{x}x^n G(x, Q^2_{eff}). \tag{D.8}$$

The Wilson coefficients can be determined by considering the process $\gamma g \to c\bar{c}$. In this case, $|p\rangle$ in Eq.(D.7) is replaced by a gluon state with momentum $q$ and color $a$, i.e., $|g(q), a\rangle$. This leads to $A_n = 2$ and the following relation between the Wilson coefficients and the cross section for the reaction $\gamma g \to c\bar{c}$:

$$I(n) = \frac{1}{2}\int_{\nu_g}^{\infty} \frac{d\nu}{\nu^n}\sigma^{\gamma g}(\nu), \tag{D.9}$$

with $\nu_g = 2m^2$. The cross section $\sigma^{\gamma g}(\nu)$ can be calculated in pQCD as given in Eq.(5.15).

In terms of the Mellin and inverse Mellin transformations

$$\begin{aligned}\bar{F}(n) &= \int_0^1 \frac{dx}{x}x^n F(x),\\ F(x) &= \frac{1}{2\pi i}\int_{a-i\infty}^{a+i\infty} dn\bar{F}(n)x^{-n},\end{aligned} \tag{D.10}$$

one can further derive the generalized convolution relations

$$\begin{aligned}\bar{F}(n) &= r^n \bar{G}(n)\bar{H}(n)\\ F(x) &= \int_{x/r}^1 \frac{dz}{z}G\left(\frac{x}{rz}\right)H(z).\end{aligned} \tag{D.11}$$

This can be shown as follows:

$$F(x) = \frac{1}{2\pi i}\int_{a-i\infty}^{a+i\infty} \bar{F}(n)x^{-n}dn$$

$$= \frac{1}{2\pi i} \int_{a-i\infty}^{a+i\infty} dn x^{-n} \int_0^1 \frac{dy}{y} y^n G(y) \int_0^1 \frac{dz}{z} z^n H(z)$$

$$= \frac{1}{2\pi i} \int_{a-i\infty}^{a+i\infty} dn \int_0^1 dy \int_0^1 dz \left(\frac{yz}{x}\right)^n \frac{1}{zy} G(y) H(z)$$

$$= \frac{1}{2\pi} \int_{-\infty}^{\infty} db \int_0^1 dy \int_0^1 dz \left(\frac{yz}{x}\right)^a \frac{1}{zy} \exp\left[ib\ln\left(\frac{yz}{x}\right)\right] G(y) H(z)$$

$$= \int_0^1 dy \int_0^1 dz \frac{1}{z} \delta\left(y - \frac{x}{z}\right) G(y) H(z)$$

$$= \int_0^1 dz \frac{1}{z} G\left(\frac{x}{z}\right) H(z)$$

$$= \int_x^1 dz \frac{1}{z} G\left(\frac{x}{z}\right) H(z). \tag{D.12}$$

In the above, we have used the following relations: $n = a + ib$, $\delta\left[\ln\left(\frac{yz}{z}\right)\right] = y\delta(y - \frac{x}{z})$, and $0 < y = \frac{x}{z} < 1$.

Let $\nu = \nu_0/y$ and $\nu_g/z$ on the left and right hand sides of Eq.(D.6), respectively, we then have

$$\frac{1}{\nu_0^{n-1}} \int_0^1 dy y^{n-2} \sigma^{\gamma N}\left(\frac{\nu_0}{y}\right) = \frac{1}{\nu_g^{n-1}} \int_0^1 dz z^{n-2} \sigma^{\gamma g}\left(\frac{\nu_g}{z}\right) \int_0^1 \frac{dx}{x} x^n G(x). \tag{D.13}$$

Changing $n - 1$ to $n$ gives

$$\int_0^1 dy y^{n-1} \sigma^{\gamma N}\left(\frac{\nu_0}{y}\right) = \left(\frac{\nu_0}{\nu_g}\right)^n \int_0^1 dz z^{n-1} \sigma^{\gamma g}\left(\frac{\nu_g}{z}\right) \int_0^1 \frac{dx}{x} x^{n+1} G(x). \tag{D.14}$$

Applying Eq.(D.11), we have

$$\sigma^{\gamma N}\left(\frac{\nu_0}{y}\right) = \int_{y\nu_g/\nu_0}^1 \frac{dx}{x} \sigma^{\gamma g}\left(\frac{\nu_0 x}{y}\right) G(x) x, \tag{D.15}$$

which can be rewritten as

$$\sigma^{\gamma N}(\nu) = \int_{\nu_g/\nu}^1 dx \sigma^{\gamma g}(\nu x) G(x). \tag{D.16}$$

Finally, setting $\nu_g = 2m_c^2$ and we get

$$\sigma^{\gamma N}(\nu) = \int_{2m_c^2/\nu}^1 dx \sigma^{\gamma g}(\nu x) G(x). \tag{D.17}$$

VITA

Wei Liu was born in Hengyang, Hunan province, P.R.China in 1971. He attended Railway's First High School in Hengyang, Hunan province, P.R.China before attending Tongji University, Shanghai, P.R. China in 1989. He graduated from Tongji University in 1993 with a B.S. in engineering, and proceeded to work as an engineer for a railway company in Hunan province. Three years later he passed the entrance exam and started his graduate study at Peking University where he graduated in 1999 with a M.S in physics. After that he came to Texas A&M University in 1999 to pursue his Ph.D. in physics. He can be reached at Physics Department Peking University, Beijing 100871, P.R.China.